



University of Kentucky  
UKnowledge

---

Theses and Dissertations--Chemical and  
Materials Engineering

Chemical and Materials Engineering

---

2018

## COMBINATORIAL SCREENING APPROACH IN DEVELOPING NON-EQUIATOMIC HIGH ENTROPY ALLOYS

Azin Akbari

University of Kentucky, [azin.akbari@uky.edu](mailto:azin.akbari@uky.edu)

Digital Object Identifier: <https://doi.org/10.13023/etd.2018.407>

[Right click to open a feedback form in a new tab to let us know how this document benefits you.](#)

---

### Recommended Citation

Akbari, Azin, "COMBINATORIAL SCREENING APPROACH IN DEVELOPING NON-EQUIATOMIC HIGH ENTROPY ALLOYS" (2018). *Theses and Dissertations--Chemical and Materials Engineering*. 87. [https://uknowledge.uky.edu/cme\\_etds/87](https://uknowledge.uky.edu/cme_etds/87)

This Doctoral Dissertation is brought to you for free and open access by the Chemical and Materials Engineering at UKnowledge. It has been accepted for inclusion in Theses and Dissertations--Chemical and Materials Engineering by an authorized administrator of UKnowledge. For more information, please contact [UKnowledge@lsv.uky.edu](mailto:UKnowledge@lsv.uky.edu).

## **STUDENT AGREEMENT:**

I represent that my thesis or dissertation and abstract are my original work. Proper attribution has been given to all outside sources. I understand that I am solely responsible for obtaining any needed copyright permissions. I have obtained needed written permission statement(s) from the owner(s) of each third-party copyrighted matter to be included in my work, allowing electronic distribution (if such use is not permitted by the fair use doctrine) which will be submitted to UKnowledge as Additional File.

I hereby grant to The University of Kentucky and its agents the irrevocable, non-exclusive, and royalty-free license to archive and make accessible my work in whole or in part in all forms of media, now or hereafter known. I agree that the document mentioned above may be made available immediately for worldwide access unless an embargo applies.

I retain all other ownership rights to the copyright of my work. I also retain the right to use in future works (such as articles or books) all or part of my work. I understand that I am free to register the copyright to my work.

## **REVIEW, APPROVAL AND ACCEPTANCE**

The document mentioned above has been reviewed and accepted by the student's advisor, on behalf of the advisory committee, and by the Director of Graduate Studies (DGS), on behalf of the program; we verify that this is the final, approved version of the student's thesis including all changes required by the advisory committee. The undersigned agree to abide by the statements above.

Azin Akbari, Student

Dr. T. John Balk, Major Professor

Dr. Matthew J. Beck, Director of Graduate Studies

COMBINATORIAL SCREENING APPROACH IN DEVELOPING NON-  
EQUIATOMIC HIGH ENTROPY ALLOYS

---

DISSERTATION

---

A dissertation submitted in partial fulfillment of the  
requirements for the degree of Doctor of Philosophy in the  
College of Engineering at the University of Kentucky

By

Azin Akbari

Lexington, Kentucky

Director: Dr. T. John Balk, Professor of Materials Engineering

Lexington, Kentucky

2018

Copyright © Azin Akbari 2018

## ABSTRACT OF DISSERTATION

### COMBINATORIAL SCREENING APPROACH IN DEVELOPING NON-EQUIATOMIC HIGH ENTROPY ALLOYS

High entropy alloys (HEA) are a relatively new group of alloys first introduced in 2004. They usually contain 5 to 6 different principle elements. Each of these elements comprise 5-35 at. % of the chemical composition of the alloy. There is a growing interest in the research community about the development of these alloys as well as their engineering applications. Some HEAs have interesting properties that have made them well suited for higher temperature applications, particularly refractory uses, while some have been shown to maintain their mechanical properties even at cryogenic temperatures.

Initially, the HEA research was focused on developing alloys with equiatomic compositions as it was believed that the single phase HEA would only form at such composition ratios. However, further research have found multiple HEAs with non-equiatomic chemical compositions. A major question that needs to be answered at this point is how to identify these non-equiatomic single phase alloy systems. Unlike the conventional alloys, the HEAs do not have a base element as a solvent, which complicates the identification of new alloy systems via conventional development techniques. To find a potential HEA, alloy development techniques of both exploratory and computational natures are being conducted within the community. Even though multiple HEAs have been successfully identified and fabricated by these techniques, in most cases they require extensive experimental data and are relatively time consuming and expensive. This study proposes a thin film combinatorial approach as a more efficient experimental method in developing new HEA alloy systems.

In order to study HEA systems with different crystal structures, nominal HEA compositions were selected, including: CoFeMnNiCu in order to achieve face centered cubic (FCC) HEA, OsRuWMoRe to obtain hexagonal closed packed (HCP) and VNbMoTaW in an attempt to form a body centered cubic (BCC) crystal structure. Thin film samples were fabricated by simultaneous magnetron sputtering of the elements onto silicon wafer substrates. The arrangement of the sputtering targets yielded a chemical composition gradient in the films which ultimately resulted in the formation of various phases. Some of these phases exhibited the desired single-phase HEA, albeit with non-equiatomic chemical compositions. Bulk samples of the identified HEA compositions were prepared by arc melting mixtures of the metals.

Microstructure of both thin film samples and bulk samples were characterized via scanning electron microscopy (SEM), focused ion beam (FIB) and energy dispersive x-ray spectroscopy (EDX). The crystal structures of the samples were studied by X-ray diffraction (XRD) and electron backscattered diffraction (EBSD) technique. Applying nano-indentation technique, the mechanical properties of some of the samples were screened over the composition gradient as well.

By applying this combinatorial thin film approach, single-phase FCC, HCP and BCC HEAs were detected and successfully produced in bulk form. Additionally, screening the properties of the compositionally gradient thin films, as well as their chemical composition and crystal structure, provided a thorough understanding of the phase space. This experimental approach proved to be more efficient in identifying new alloy systems than conventional exploratory development methods.

**KEYWORDS:** Alloy development, multi principle element alloys, characterization

---

Azin Akbari

---

August 21<sup>st</sup> 2018

COMBINATORIAL SCREENING APPROACH IN DEVELOPING NON-  
EQUIATOMIC HIGH ENTROPY ALLOYS

By

Azin Akbari

Dr. T. John Balk

---

Director of Dissertation

Dr. Matthew J. Beck

---

Director of Graduate Studies

August 21<sup>st</sup> 2018

---

Date

*To*  
*Sima and Ali*

## ACKNOWLEDGMENTS

I would like to express the deepest appreciation to my advisor, Dr. T. John Balk, whom without his guidance and persistent help this dissertation would have not been possible. I was fortunate enough to have him as a mentor through my adventurous time in graduate school and these not-all-fun early stages of my career.

A debt of gratitude is also owed to the members of my committee Dr. Matthew Beck, Dr. Christine Trinkle and Dr. Jonathan Wenk for their time and much appreciated support.

Special thanks are in order for the Kentucky Science and Engineering Foundation for providing the financial support for this project. (KSEF-148-502-15-363)

I am grateful to all of those with whom I have the pleasure to work with (and have let's-ditch-work drinks with) in Dr. Balk's research group: Dr. Nicolas Briot, Tyler Maxwell, Michael Detisch, Xiaotao Liu and Maria Kosmidou.

In addition, a thank you to the students who collaborated with me during this project: Julia Lehmann, Sebastian Helmstetter, Lea Menken, Ben Meffert and Michael Metzger.

Great thanks to Haj Hossein Gholami, Erfan Akbari, Arianna Afshari and Alina Akbari whose love and guidance are with me in whatever I pursue. Last but not least, I would like to thank my parents, Mohammad Ali Akbari and Sima Gholami, who are my unending inspirations in life.



# TABLE OF CONTENTS

ACKNOWLEDGMENTS	iii
LIST OF FIGURES	viii
LIST OF TABLES	xiv
CHAPTER 1: INTRODUCTION	1
CHAPTER 2: BACKGROUND	5
2.1. Thermodynamics of HEA	5
2.1.1. The High Entropy Effect	6
2.1.2. Sluggish Diffusion Effect	9
2.1.3. Severe Lattice Distortion Effect	11
2.1.4. Cocktail Effect	11
2.2. Alloy Development Techniques in HEA Research	13
2.3. Thin Film Combinatorial Approach	15
CHAPTER 3: MATERIALS AND METHODS	17
3.1. Materials	17
3.2. Thin film fabrication	19

3.3. Fabrication of the Bulk Samples	21
3.4. Characterization Techniques	21
3.4.1. Scanning Electron Microscopy	22
3.4.2. Energy Dispersive Spectroscopy	26
3.4.3. X-ray Diffraction Technique	26
3.4.4. Electron Backscatter Diffraction Technique	27
3.4.5. Transmission Electron Microscopy	28
3.5. Sputtering Rate Measurement	30
3.6. Nanoindentation	31
CHAPTER 4: THIN FILM COMBINATORIAL APPROACH IN DEVELOPMENT OF A FACE CENTERED CUBIC HIGH ENTROPY ALLOY	33
4.1. Introduction	33
4.2. Experimental Methods	35
4.3. Results and Discussion	37
4.4. Conclusions	46
CHAPTER 5: THIN FILM COMBINATORIAL APPROACH IN DEVELOPMENT OF A HEXAGONAL CLOSED PACKED HIGH ENTROPY ALLOY	48
5.1. Introduction	48

5.2. Experimental Methods	49
5.3. Results and Discussion	51
5.4. Conclusions	58
CHAPTER 6: THIN FILM COMBINATORIAL APPROACH IN DEVELOPMENT OF A BODY CENTERED CUBIC HIGH ENTROPY ALLOY	59
6.1. Introduction	59
6.2. Experimental Methods	60
6.3. Results and Discussion	62
6.4. Conclusions	71
CHAPTER 7: MULTILAYER THIN FILM APPROACH IN DEVELOPMENT OF A FACE CENTERED CUBIC ALLOYS	72
7.1. Introduction	72
7.2. Experimental Methods	73
7.3. Results and Discussion:	75
7.4. Conclusions	82
CHAPTER 8: CONCLUSIONS AND CONTINUING WORK	83

APPENDIX A	88
APPENDIX B	90
APPENDIX C	91
REFERENCES	93
VITA	102

## LIST OF FIGURES

### Figure 1.1.

Materials hypertetrahedron for high entropy alloys. This figure categorizes the research areas in the high entropy alloy field<sup>1</sup> 2

### Figure 1.2.

Schematic of the 2D gradient thin film; each unit of area on this film has a different chemical composition, hence a different crystal structure and properties 4

### Figure 2.1.

Illustration of entropy of mixing for a ternary alloy system<sup>2</sup> 8

### Figure 2.2.

Diffusion coefficient of N in different FCC elements and alloys as a function of (a) inverse absolute temperature and (b) normalized inverse absolute temperature<sup>3</sup> 9

### Figure 2.3.

Schematic diagram showing large lattice distortion in a multi-component BCC lattice<sup>4</sup> 10

### Figure 2.4.

Schematic illustrating the effect of lattice distortion on x-ray diffraction data<sup>5</sup> 12

### Figure 2.5.

Changes of hardness values as a result of FCC to BCC phase transformation in the CoNiCrAl<sub>x</sub>Fe alloy system<sup>6</sup> 13

### Figure 2.6.

Phase formation diagram based on  $\delta$  and  $\Omega$ ; solid solutions form at  $\delta < 6.6\%$  and  $\Omega > 1.1$ <sup>7</sup> 14

<b>Figure 2.7.</b>	
Schematic of the sputtering set up; (a) the sputtering targets arrangement results in a	
(b) chemical composition gradient in the thin films	15
<b>Figure 3.1.</b>	
Periodic table marked with the 3 alloy system discussed in this study	18
<b>Figure 3.2.</b>	
(a) Magnetron sputtering system in Dr Balk’s research group at the University of	
Kentucky; (b) Targets, sputtering simultaneously; the unique plasma color in each	
target is due to each sputtering material’s individual properties	20
<b>Figure 3.3.</b>	
Mini arc-melting (MAM) system by Imteck, available at Dr Balk’s research group at	
the University of Kentucky	22
<b>Figure 3.4.</b>	
FEI Helios NanoLab 660; most of the characterization work in this project was	
performed using this dual beam (SEM/FIB) system. This instrument is equipped with	
multiple detectors including EDS, EBSD and STEM	24
<b>Figure 3.5.</b>	
Lift out technique: (a) both sides of the area of interest is milled; (b) the nano-	
manipulator is attached and then lifted out; the lamella (c) close to the Cu grid, (d), (e)	
welded to a Cu grid and (f) further thinning down	24
<b>Figure 3.6.</b>	
Siemens D500 XRD	27

<b>Figure 3.7.</b>	
Illustration of the EBSD detector set-up <sup>8</sup>	28
<b>Figure 3.8.</b>	
FEI Talos TEM <sup>9</sup>	29
<b>Figure 3.9.</b>	
FIB cross sectional image of a multilayer thin film sample fabricated for deposition rate measurements	30
<b>Figure 3.10.</b>	
iNano nanoindentation instrument <sup>10</sup>	32
<b>Figure 4.1.</b>	
Target arrangement in the sputtering set-up for fabrication of the thin film samples	35
<b>Figure 4.2.</b>	
XRD data collected from 9 different spots on the fabricated thin film sample; the approximate location of the spots on the Si wafer are marked in the schematic. Spot 4 on this sample exhibit a single phase FCC structure.	39
<b>Figure 4.3.</b>	
STEM image of the spot 4 on the thin film sample; the lamella, fabricated by FIB, is presented in top right corner. The higher magnification STEM image shows a columnar grain structure in spot 4 on the thin film sample	40
<b>Figure 4.4.</b>	
(a) The SEM micrograph of the as-cast bulk sample showing the dendritic structure.	
(b) The EDS maps of another region on the same sample exhibits the segregation of the elements.	41

**Figure 4.5.**

The SEM micrographs of the bulk sample after the thermomechanical processing. The uniaxial grain structure of the sample can be observed in (a) low and (b) high magnifications. 43

**Figure 4.6.**

The EBSD (a) phase and (b) orientation maps of the bulk sample post thermomechanical processing confirming the single phase structure in this sample. 45

**Figure 5.1.**

(a) Schematic of the target arrangement set up and (b) the sputtering targets flowing with the plasma 50

**Figure 5.2.**

The XRD patterns and EDS data collected from 9 different spots on the thin film sample and their approximate location on the Si wafer 52

**Figure 5.3.**

(a) FIB cross section and (b) fabricated lamella of the spot 1 on the thin film sample; (c) and (d) STEM images of film in higher magnification, taken from the same lamella, exhibiting the columnar grain structure in this spot of the film 53

**Figure 5.4.**

Microstructure of the as-cast bulk sample, exhibiting a dendritic structure 54

**Figure 5.5.**

Indexed XRD patterns of (a) spot 1 on the thin film sample and (b) the as-cast bulk sample; the peaks marked with arrows represent the second phase in the bulk sample. 55



<b>Figure 5.6.</b>	
EBSD phase map of the as-cast bulk sample showing the multi-phase nature of this sample	57
<b>Figure 6.1.</b>	
Sputtering target arrangement set-up resulting in a compositional gradient in the fabricated thin films	61
<b>Figure 6.2.</b>	
XRD data collected from 9 different spots and their approximate location on the thin film sample	63
<b>Figure 6.3.</b>	
(a) Low, (b) high magnification micrograph of the VNbMoTaW bulk sample and the EDS maps of the same region	65
<b>Figure 6.4.</b>	
(a) Low and (b) high magnification micrographs of the 2.5 g VNbMoTaW bulk sample	67
<b>Figure 6.5.</b>	
XRD data collected from (a) 5 g as-cast and (b) 2.5 g VNbMoTaW samples	66
<b>Figure 6.6.</b>	
EDS maps of the 2.5 g VNbMoTaW bulk sample	68
<b>Figure 6.7.</b>	
EDS maps of the as-cast 5 g VNbTaW sample	69
<b>Figure 6.8.</b>	
Micrographs of the VNbTaW sample	70

<b>Figure 6.9.</b>	
XRD data collected from (a) 5 g as-cast and (b) 2.5 g VNbTaW samples	71
<b>Figure 7.1.</b>	
The FIB cross section of the as-deposited layered thin film	75
<b>Figure 7.2.</b>	
FIB cross sectional images of the post annealing sample via (a) electron beam and (b) ion beam	76
<b>Figure 7.3.</b>	
Thin lamella of the annealed film and the EDS map collected by the Helios	77
<b>Figure 7.4.</b>	
Electron image and the EDS map collected from the alloyed sample by the Talos TEM	75
<b>Figure 7.5.</b>	
BF TEM image of the post annealing sample and the SDP	79
<b>Figure 7.6.</b>	
Multilayer sample (a) before and (b) after annealing	81
<b>Figure 8.1.</b>	
Illustration summarizing the combinatorial thin film approach	84
<b>Figure 8.2.</b>	
Micro specimen test set-up available in Dr. Balk's research group at the University of Kentucky <sup>11</sup>	86

## **LIST OF TABLES**

### **Table 4.1.**

The chemical composition (at. %) of the elements across the thin film sample 38

### **Table 4.2.**

Hardness values from the nanoindentation of the 9 spots on the thin film sample 44

### **Table 5.1.**

Chemical composition and crystal structure of the 2 phases observed in the bulk sample 54

### **Table 6.1.**

The chemical composition (at. %) of 9 different spots on the thin film sample 64

### **Table 7.1.**

Order of deposition in the second set of the thin film samples 74

## Chapter 1: Introduction

High entropy alloys (HEAs) are a relatively new group of alloys introduced by two different research groups at different universities in 2004<sup>6,12</sup>. The HEAs usually contain 5 to 6 principle elements. The chemical composition of each component lies in the range of 5-35 at. %. They have been also defined as alloys with configurational entropy of  $1.5R$  or higher, where  $R$  is the gas constant<sup>2</sup>. However, the definition of this group of alloys is still a topic of conversation among the research community. Yeh, et al. defined them as high entropy alloys based on the higher entropy of mixing in these alloys<sup>6</sup>, whereas Cantor, et al. differentiate these alloys from the conventional alloys by categorizing them as multiprinciple elements alloys<sup>12</sup>. The HEA terminology has been popularized in the literature, but the debate on the definition of these alloys remains<sup>13-16</sup>. No matter how we chose to define them, there is a growing interest in the field of HEA research in both theoretical alloy development aspect and engineering applications of them<sup>17</sup>.

HEAs have shown interesting properties in many different applications. Sencov, et al. introduced the first refractory HEA in 2010<sup>18</sup>. This group of HEA has shown to maintain their mechanical properties at elevated temperatures which makes them ideal candidates for refractory applications<sup>18-20</sup>. This has also initiated an ongoing research in development of high entropy super alloys which have the potential to reduce the cost of raw materials in the fabrication of turbine blades and related uses<sup>21</sup>. Interestingly, HEAs have displayed lower temperature applications as

well<sup>22,23</sup>. Gludovatz, et al. have found that some HEAs show exceptional damage tolerance and higher fracture toughness at cryogenic temperatures<sup>24</sup>. The research in the HEA field has grown in many other directions including light HEA<sup>25</sup> and high entropy bulk metallic glasses<sup>26</sup>. Figure 1.1. represent an illustration of all these various branches of the HEA research.

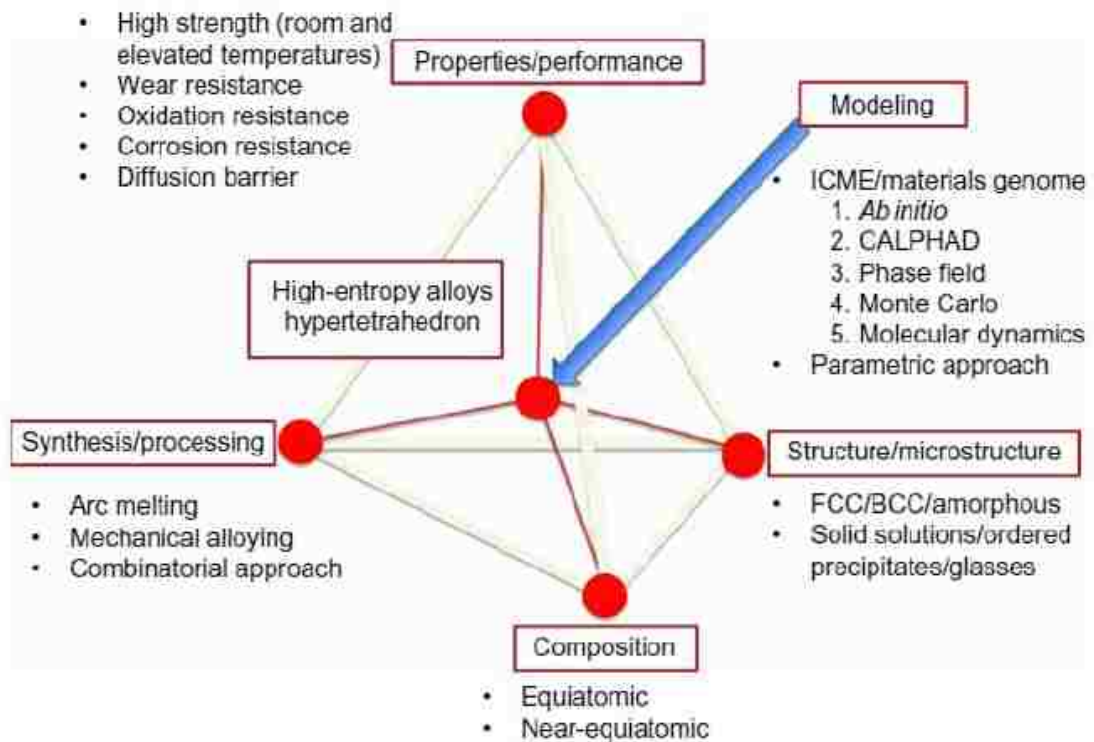


Figure 1.1. Materials hypertetrahedron for high entropy alloys. This figure categorizes the research areas in the high entropy alloy field<sup>1</sup>.

Initially HEA research was focused on developing alloys with equiatomic compositions as it was believed that a single phase HEA would only form at such composition ratio<sup>1,27-30</sup>. However, further research found multiple HEAs with non-equiatomic chemical compositions. A major question that needs to be answered at this point is how to identify these non-equiatomic single phase alloy systems. Unlike the

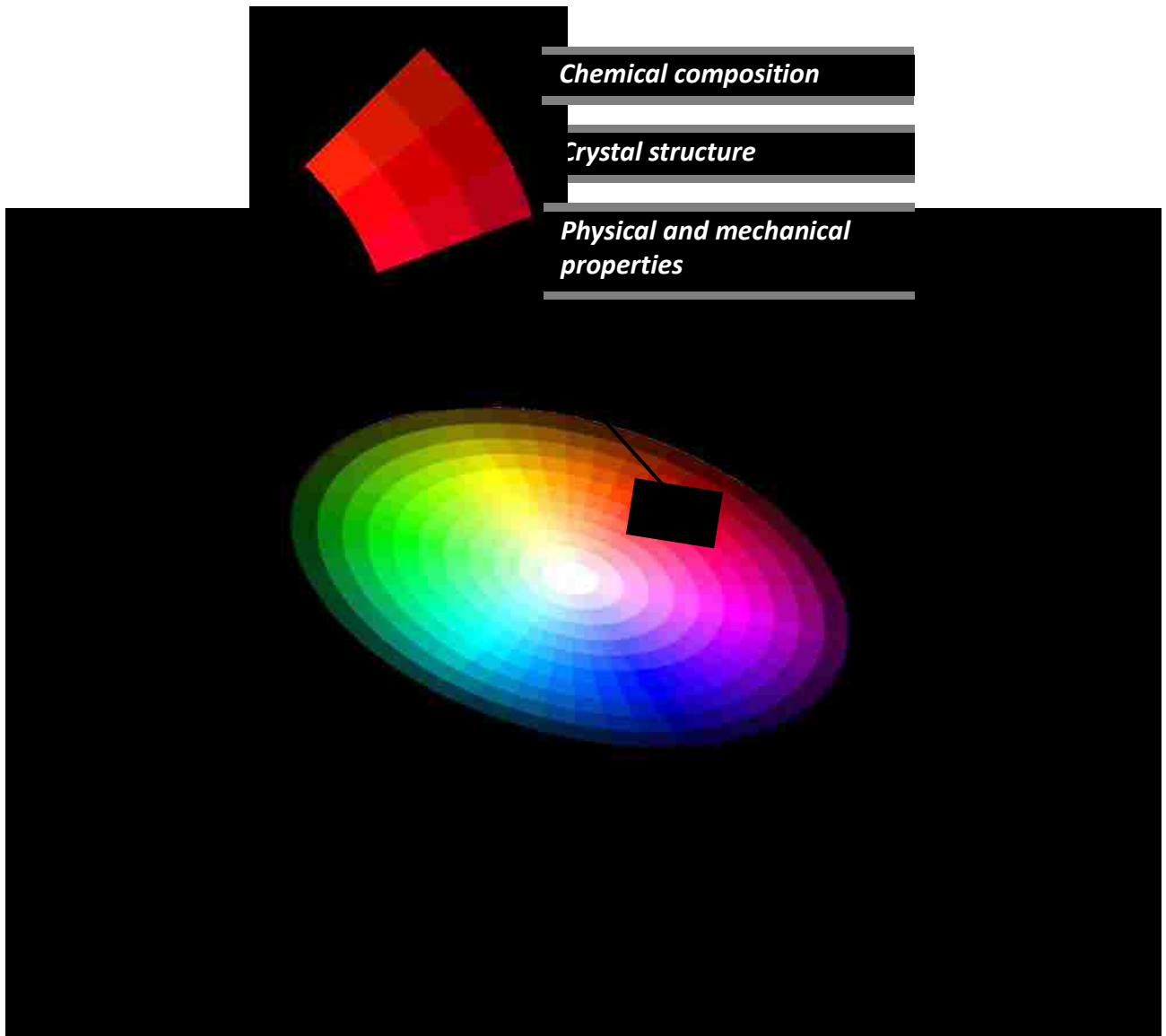
conventional alloys, the HEAs do not have a base element as a solvent, which complicates the identification of new alloy systems via conventional development techniques.

Literature suggests successful HEA developments by approaches of an exploratory nature<sup>2,17,21,31</sup>. Designing computational models is the other popular approach within the research community. These models are developed to predict the phase space of a potential HEA system<sup>17,32,33</sup>. Even though multiple HEAs have been successfully identified and fabricated by these techniques, in most cases they require extensive experimental data and are relatively time consuming and expensive.

In this study a more efficient experimental approach in developing new HEA systems is proposed. A 2D gradient of composition is created over a relatively large area. Different phases form within each unit of area on this gradient due to the variations in the chemical composition. Each of these phases exhibits a different crystal structure. Therefore screening crystal structure over this wide gradient enables us to predict which phases will form given a certain chemical composition. A thorough understanding of the phase space will be achieved by this combinatorial screening approach as illustrated in Figure 1.2.

The present work starts with a background on the field of HEAs and a summary of the ongoing research. The materials and methods chapter introduces the alloy systems studied in this project and discusses the experimental procedures. The

following chapters present the results and discussion on the development of HEAs with face centered cubic (FCC), hexagonal closed packed (HCP) and body centered cubic (BCC) crystal structures, respectively. This project concludes in the last chapter with a summary of the research and prospects for the future work.



## **Chapter 2: Background**

In this chapter the discovery process for, and importance of, high entropy alloys (HEAs) is discussed. This chapter starts with the reasoning behind the phrase “entropy” in the terminology as introduced in the initial steps of HEA discovery. Following sections present the other aspects of these alloys which have made them of interest to the research community, including the thermodynamics of HEA formation and the attractive properties which make them well suited for a variety of the applications.

### **2.1. Thermodynamics of HEA**

Historically, conventional alloys usually contain 1 or 2 principle elements, whereas HEAs have 5 or more. With most alloys, alloying elements are added to modify and/or improve their properties, but they are usually limited to a few at. %. However, in case of the HEAs, each component element comprises 5-30 at. % of the chemical composition. Conventionally for development of binary or ternary alloys, phase diagrams have been used successfully in the past. However additional components to a system, such as HEAs, complicate the phase diagram to a point that it is no longer the most efficient method for phase space predictions. Notably, the phase space becomes more complicated further away from the corners of phase diagrams (higher at. % ratios) which may results in formation of intermetallic or other undesirable phases. However, many of the known HEAs are single phase solid



solutions, even though they usually contain five or more components. The literature tries to explain this by introducing four core effects: high entropy effect, sluggish diffusion effect, severe lattice distortion effect and cocktail effect<sup>2,34</sup>.

### **2.1.1. The High Entropy Effect**

The high entropy effects, first introduced by Yeh, et al. in 2004, is the main reason for today's terminology in this field. Yeh suggests that the single phase in these multicomponent alloys is due to their higher entropy of the mixing<sup>6</sup>. The explanation is based on the thermodynamics of phase formation in alloys. This section discusses these concepts to better clarify the effect of the entropy in HEAs.

Based on Gibbs phase rule, the number of phases (P) at constant pressure and equilibrium condition is obtained by:

$$P = C - F + 1$$

in which C is the number of components and F is the degree of freedom<sup>35</sup>. Therefore, in case of a 6-component alloy we would expect the maximum number of 7 phases at a certain temperature and a constant pressure. However, in case of a single phase HEA only one of these phases is formed in a form of a solid solution. It should be noted that by definition a solid solution contains a base element, solvent, and minor addition of solutes. Whereas in this case, it will be difficult to distinguish one of the components as the solvent because the composition of the different components is usually very close.

Thermodynamics of alloys can help us investigate the formation of a solid solution with 5 or more elements in an HEA system. Configurational entropy of mixing is calculated by

$$S = k \ln W$$

Where  $k$  is the Boltzmann constant and  $W$  is the number of possible microstates of a system at certain macroscopic state<sup>35</sup>. For a random solid solution with  $N$  components the configurational entropy of mixing can be calculated with

$$\Delta S_{\text{mix}} = -R \sum c_i \ln c_i$$

where  $c_i$  concentration of the  $i^{\text{th}}$  element of a  $N$ -component system<sup>35</sup>. The term  $\Delta S_{\text{mix}}$  will be maximized when all concentrations have the same value. Which means equi-atomic concentration results in the maximum entropy value based on this equation ( $\Delta S_{\text{mix}} = R \ln N$ ). This concept is called maximum entropy production principle (MEPP)<sup>2</sup>.

Based on the definition of the Gibbs free energy the  $\Delta G_{\text{mix}}$  at the temperature  $T$  is calculated as:

$$\Delta G_{\text{mix}} = \Delta H_{\text{mix}} - T\Delta S_{\text{mix}}$$

where  $\Delta H_{\text{mix}}$  is the enthalpy and  $\Delta S_{\text{mix}}$  entropy of mixing<sup>35</sup>. The configurational entropy is one of the contributing components in the  $\Delta S_{\text{mix}}$ . Based on the MEPP,  $\Delta S_{\text{mix}}$  is maximized in equiatomic compositions. Consequently, the  $\Delta G_{\text{mix}}$  is minimized for an equiatomic solid solution. Lower Gibbs free energy in the case of multicomponent solid solution makes them the preferred phase comparing to the other phases such as

the intermetallic which have lower configurational entropy due to their ordered structures.

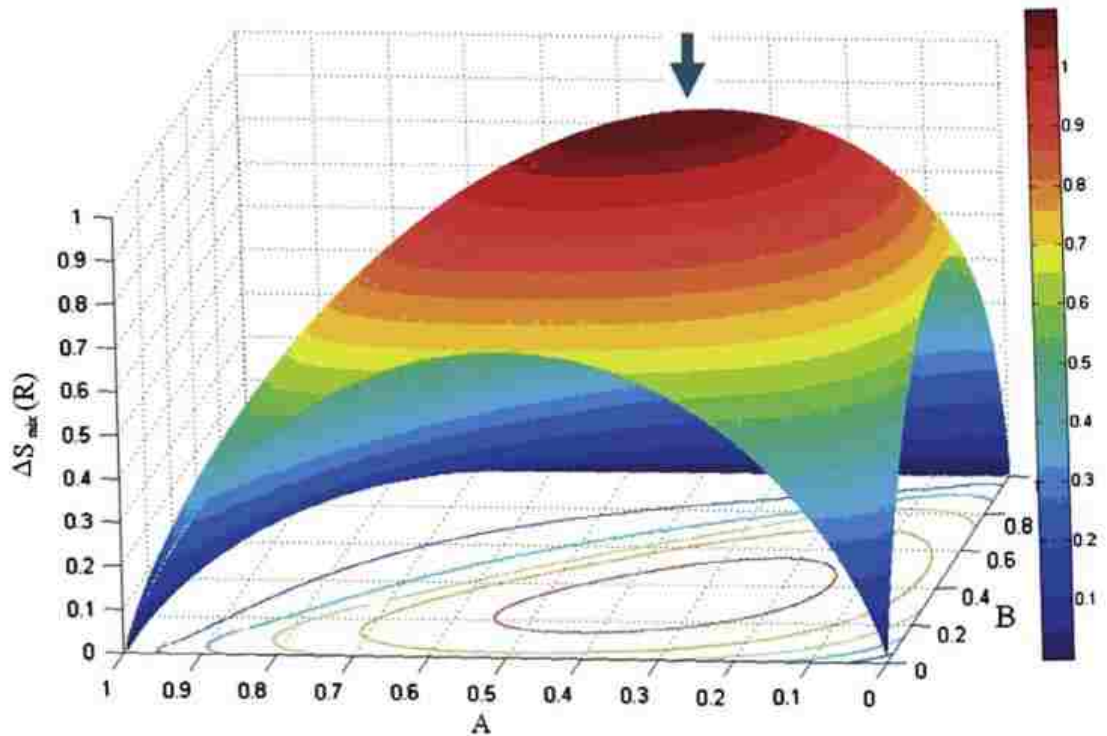


Figure 2.1. Illustration of entropy of mixing for a ternary alloy system<sup>2</sup>

Based on MEPP, the initial HEA research was focused on developing alloys with equiatomic compositions as it was believed that the single phase HEA would only form at such composition ratio. However, further research found multiple HEAs with non equiatomic chemical compositions. The literature suggests the other 3 core effects as the reasoning behind this.

### 2.1.2. Sluggish Diffusion Effect

It has been observed that the diffusion rate in HEAs is much slower than that of conventional alloys such as stainless steels<sup>36</sup>. This phenomenon is named the sluggish diffusion effect and has significant effect on the properties of HEAs. For instance, the dislocation movement within the material is hindered by the lower diffusion rate and consequently the slip systems and the deformation mechanism of the material is affected. The result is an improvement in the strength of the alloy as the mechanical properties highly depend on deformation mechanisms in crystalline materials.

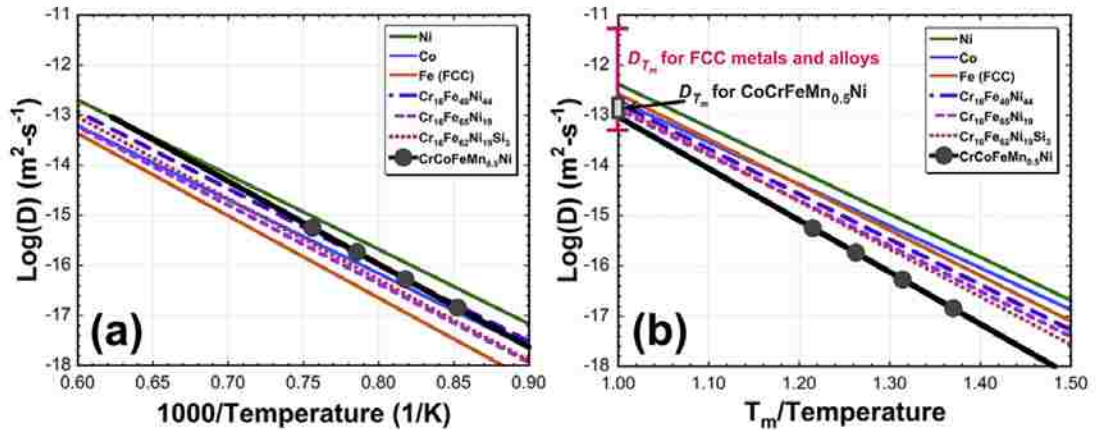
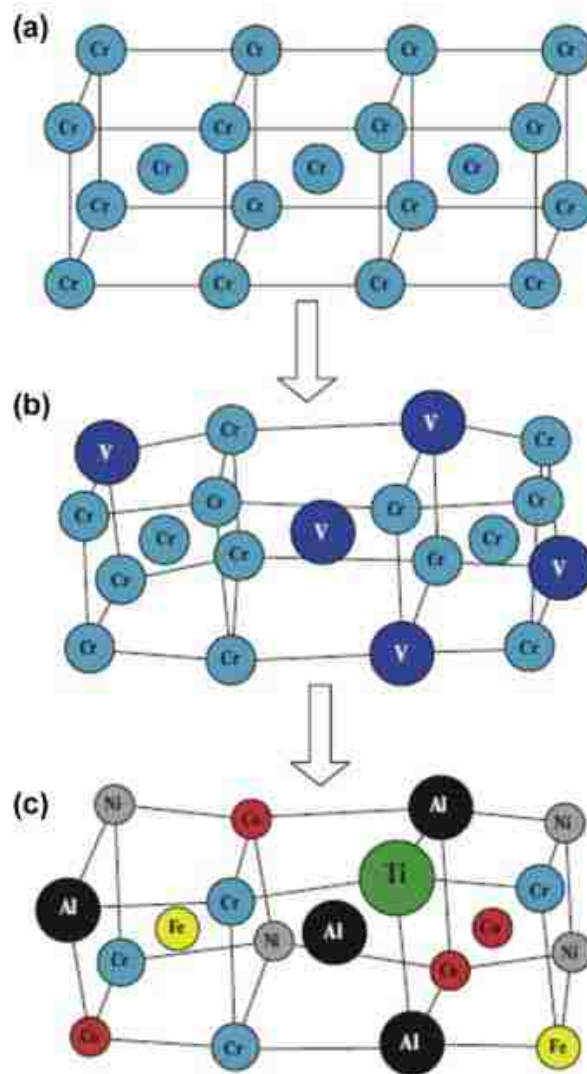


Figure 2.2. Diffusion coefficient of N in different FCC elements and alloys as a function of (a) inverse absolute temperature and (b) normalized inverse absolute temperature<sup>3</sup>

However more recent research has suggested that the diffusion rate might not be as significant of an effect<sup>3</sup> in HEAs. As shown in Figure 2.2, the diffusion rate measurements of certain HEAs were compared to that of Ni in different FCC elements

and alloys. Based on these measurements, Ni diffusion rate in the CoCrFeMn<sub>0.5</sub>Ni HEA falls in the range of other FCC alloys<sup>3</sup>. Furthermore, measuring diffusion rates is rather challenging and the reported data usually have a large error window. Considering the wide range of measured diffusion coefficient, it was concluded that the diffusion rates are not significantly different in FCC HEA compared to other FCC alloys.



*Figure 2.3. Schematic diagram showing large lattice distortion in a multi-component BCC lattice<sup>4</sup>*

### **2.1.3. Severe Lattice Distortion Effect**

In a high entropy alloy solid solution, each atom can sit in any of the lattice positions with no preferred order. Therefore, the resulted lattice is more distorted in comparison to an ordered structure due to the atomic size differences. Figure 2.3. schematically describes this effect. The lattice distortion in HEAs can be observed in the x-ray diffraction (XRD) patterns of these alloys. The severe distortion of the lattice planes affects the diffraction of the x-rays. As a result the width of the XRD peaks are widen over the diffraction angles. (Figure 2.4.) Similar to the sluggish diffusion, the severe lattice distortion can also affect the mechanical properties of the alloy due to its effects on the dislocation movement.

### **2.1.4. Cocktail Effect**

The cocktail effect first introduce by Ranganathan implies that the properties of the alloy can be modified by its chemical composition<sup>1</sup>. Addition of any alloying element can significantly affect the chemistry and structure of the base metal. Subsequently, the properties of the resulted alloy is rather different from each of the contributing components. A good example of this effect is the addition of Al in CoCrCuNiAl<sub>x</sub> which results in the transformation of the crystal structure from FCC to BCC<sup>6</sup>. (Figure 2.5.)

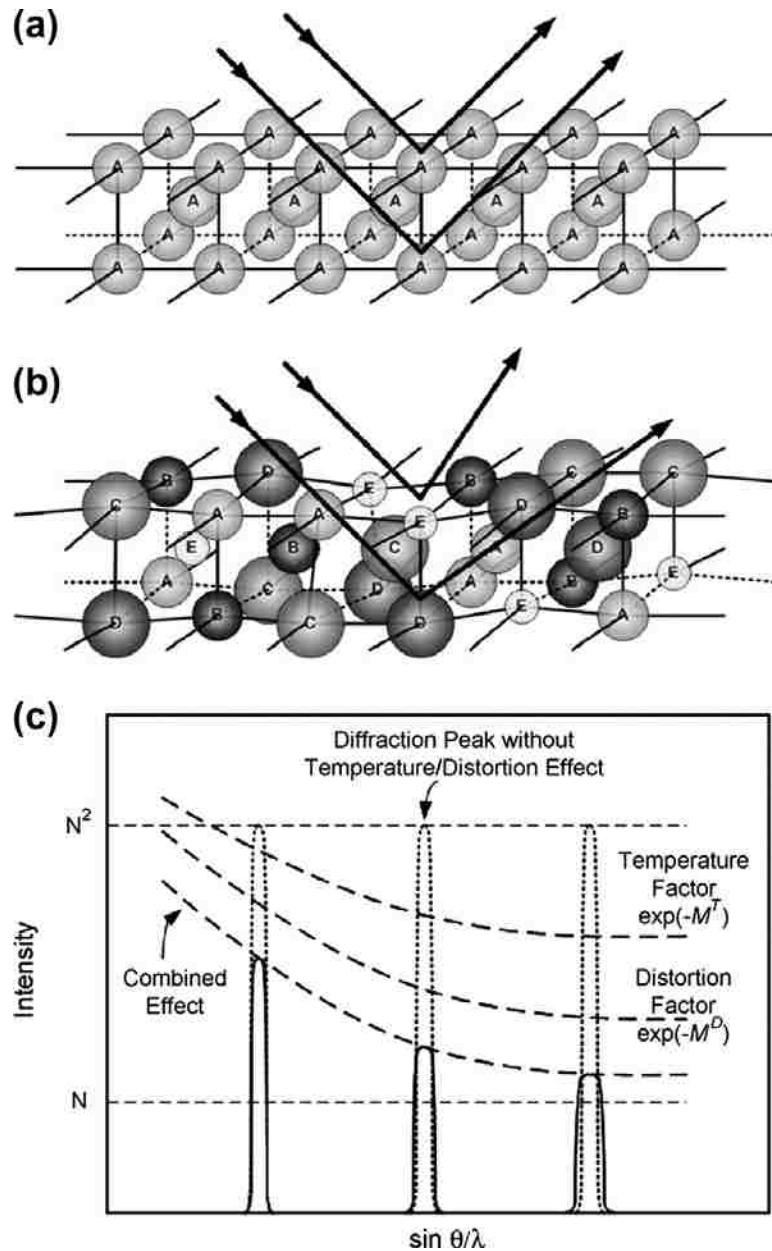


Figure 2.4. Schematic illustrating the effect of lattice distortion on x-ray diffraction data<sup>5</sup>

Jones, et al. in their 2016 review paper argue that cocktail effect is not unique to HEAs and should not be considered a core effect in the formation and thermodynamics of high entropy alloys<sup>34</sup>. They agree with Yeh, et al. that HEA

unique properties are due to the complex composition of these alloys. However based on Jones et al argument, the cocktail effect applies to all alloy systems and is the main reason for addition of alloy elements to any engineering material. They argue that the cocktail effect should be dismissed.

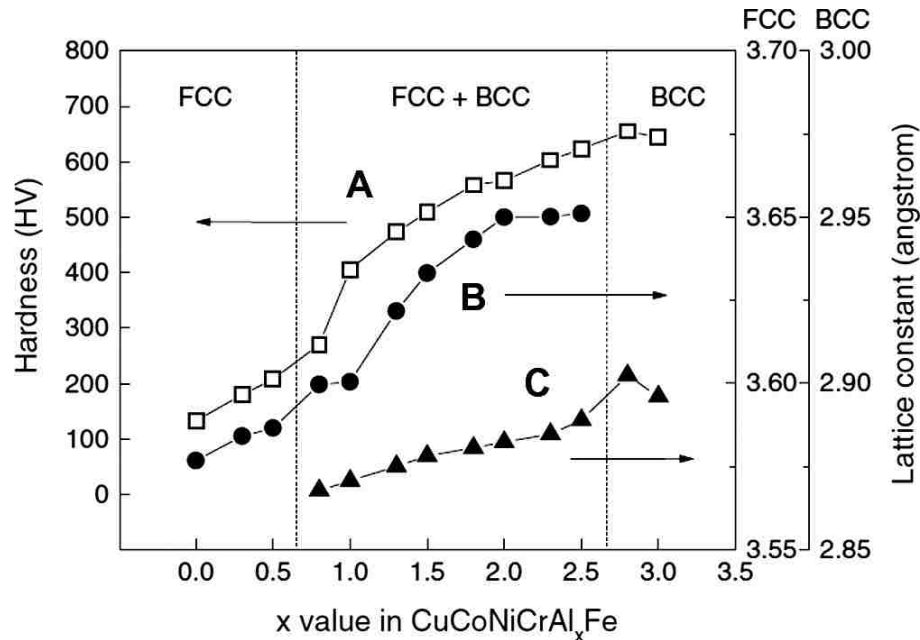


Figure 2.5. Changes of hardness values as a result of FCC to BCC phase transformation in the  $\text{CoNiCrAl}_x\text{Fe}$  alloy system<sup>6</sup>

## 2.2. Alloy Development Techniques in HEA Research

Whereas most alloys have a base element as a solvent, HEAs contain multiple principle elements. This complicates the identification of new HEAs via conventional alloy development techniques. Literature suggests successful HEA developments by approaches of an exploratory nature<sup>37-39</sup>. For instance, alloy design methods based on



the atomic size difference ( $\delta$ ) and enthalpy and entropy of mixing ratio ( $\Omega$ ) have been extensively explored<sup>17,31,40</sup>. Based on this approach, the multi component solid solutions will form at lower  $\delta$  and higher  $\Omega$  where the entropy of mixing is maximized and enthalpy is minimized to achieve lower  $\Delta G_{\text{mix}}$ <sup>7</sup>. (Figure 2.6.)

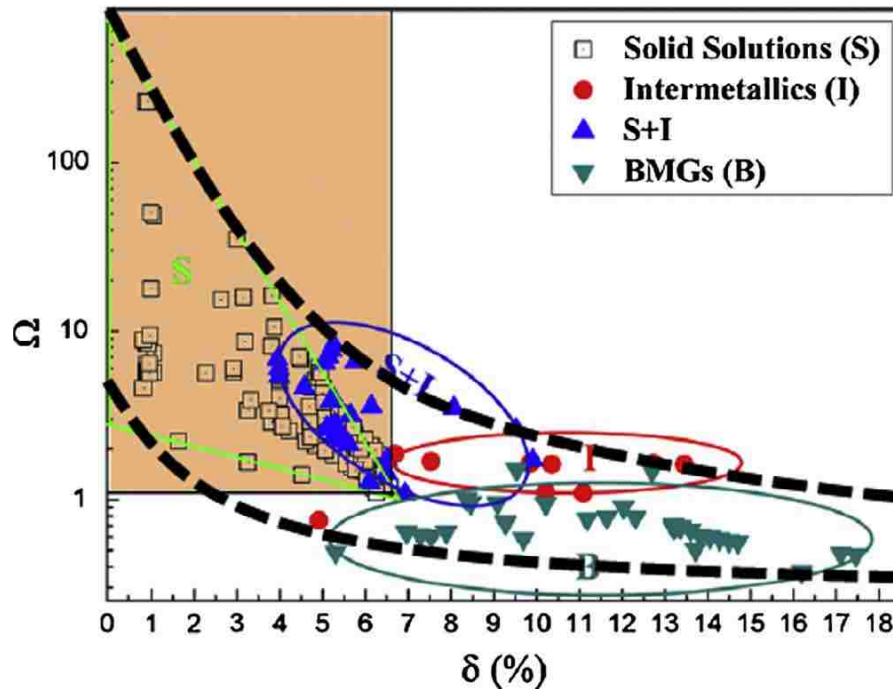
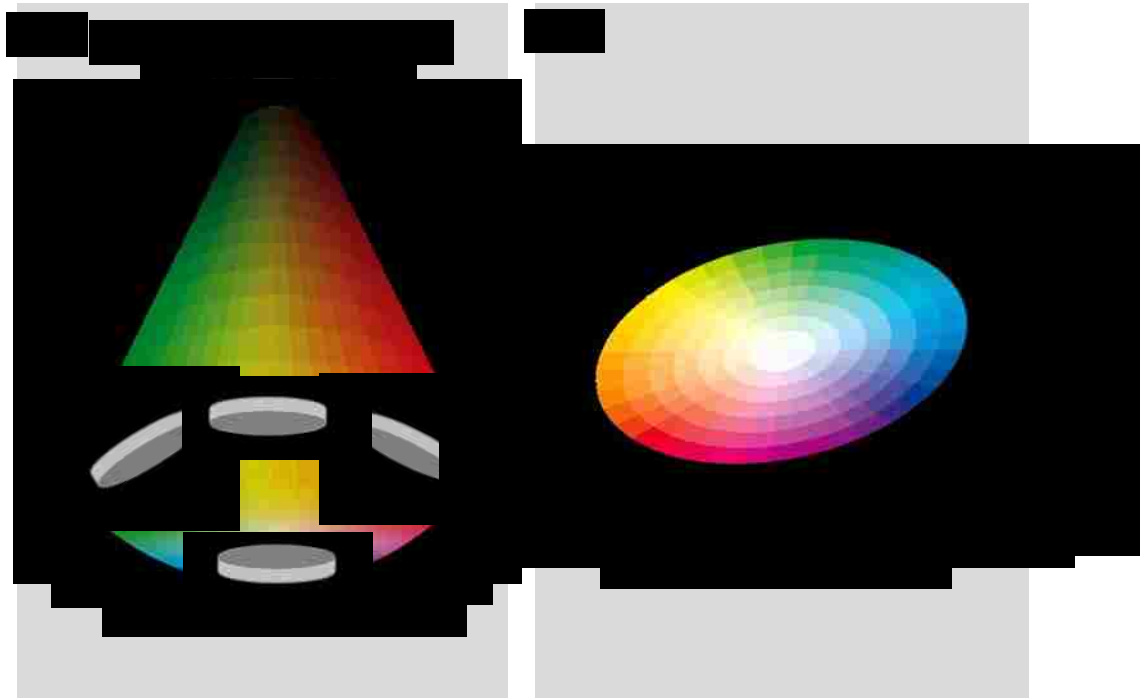


Figure 2.6. Phase formation diagram based on  $\delta$  and  $\Omega$ ; solid solutions form at  $\delta < 6.6\%$  and  $\Omega > 1.1$ <sup>7</sup>.

Designing computational models is the other popular approach within the research community. These models are developed to predict the phase space of a potential HEA system<sup>32,41-45</sup>. Even though multiple HEAs have been successfully identified and fabricated by these techniques, in most cases they require extensive experimental data to verify the models which are relatively time consuming and expensive.



*Figure 2.7. Schematic of the sputtering set up; (a) the sputtering targets arrangement results in a (b) chemical composition gradient in the thin films.*

### **2.3. Thin Film Combinatorial Approach**

In this study a more efficient experimental approach in developing new HEA systems is proposed. As schematically shown in the Figure 2.7., a 2D gradient of composition is created over a relatively large area. Different phases form within each unit of area on this gradient due to the variations in the chemical composition. Each of these phases exhibits a different crystal structure. Screening crystal structure over this wide gradient enables us to predict which phases will form given a certain chemical composition. The physical and mechanical properties of the material can be screened in a similar manner in this combinatorial approach which potentially may influence the material selection in certain applications. The screening process provides a phase

formation guide map in the 2D compositional gradient and therefore a thorough understanding of the phase space will be achieved. Based on the results of this through screening, potential HEA systems can be identified for further analysis and fabrication in bulk form.

## **Chapter 3: Materials and Methods**

In this chapter, the materials studied in this project are introduced. Several different alloy systems with different crystal structures were chosen for this study: hexagonal closed packed (HCP), face centered cubic (FCC) and body centered cubic (BCC). The wide variety of materials enabled us to have a more thorough investigation on the thin film combinatorial approach in alloy development.

As described in the introduction chapter, we applied the combinatorial thin film approach to find potential single-phase high entropy alloys (HEAs). Gradient thin films in this method provide a compositional map to identify potential HEAs. The candidate chemical compositions were later casted in bulk form to be analyzed for the crystal structure and properties.

This chapter also proposes the research plan and the implementation of it. It starts with an introduction on the fabrication method of the thin film samples and the bulk samples. Next, the details of the fabrication methods are described. The following sections focus on the characterization techniques utilized to study the samples.

### **3.1. Materials**

Several alloy systems were chosen to investigate in this project to thoroughly study the applicability of thin film combinatorial approach in alloy development. With

a focus on high entropy alloys, several potential systems were chosen, each with a different crystal structure.

The most common crystal structures in metals and alloys are face centered cubic (FCC), body centered cubic (BCC) and hexagonal closed packed (HCP). Therefore candidates of all these system were carefully chosen to cover all these crystal structures. MnFeNiCoCu, OsRuWMoRe and VNbMoTaW alloy systems represent a wide variety of the intrinsic metals in the periodic table. (Figure 3.1.) This will provide a better understanding of applicability of combinatorial thin film approach in development of alloy systems with different natures. In the following chapters, the details on development of each of these alloy systems are presented.

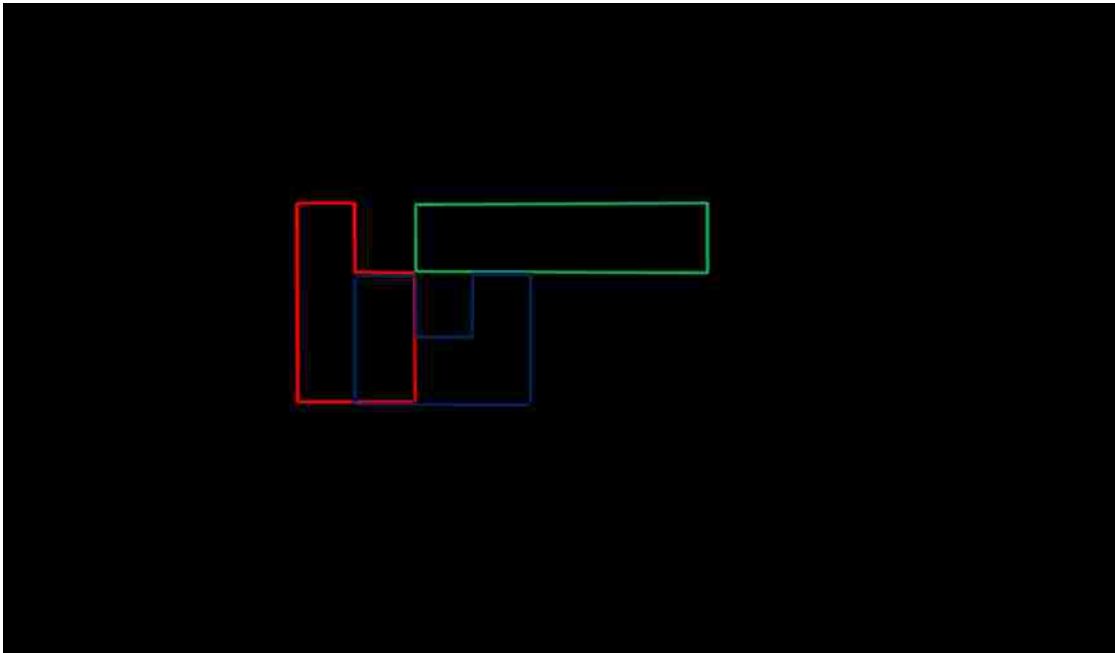


*Figure 3.1. Periodic table marked with the 3 alloy system discussed in this study*

### 3.2. Thin film fabrication

There are different deposition technologies available to fabricate films. Depending on the application, price and film thickness one may choose a different method. In this project, magnetron sputtering (ORION system, AJA International) was used to fabricate gradient thin films of the alloy system. This versatile system has been extensively used in Dr. Balk's research group in multiple projects. (Figure 3.2.a) In the magnetron sputtering technique, a gaseous plasma, in our case Ar, is generated in a high vacuum chamber ( $\sim 10^{-8}$  Torr). The material to be deposited is loaded in the system in form of a round disk and it's called the target. The high-energy ions of the plasma, erode the surface of the target, and consequently liberate the atoms from the target material. These atoms deposit onto a substrate, through the vacuum environment, to form the film. By changing the sputtering power and the duration we can control the film thickness.

The magnetron sputtering system available in our research group is equipped with 6 chimneys. This enables us to sputter from 6 different targets. These chimneys are oriented with an angle towards the substrate. Therefore, if the substrate is kept still, the resulting film would have a gradient in composition. Figure 3.2.b shows a photo of 5 of the sputtering targets in this arrangement.

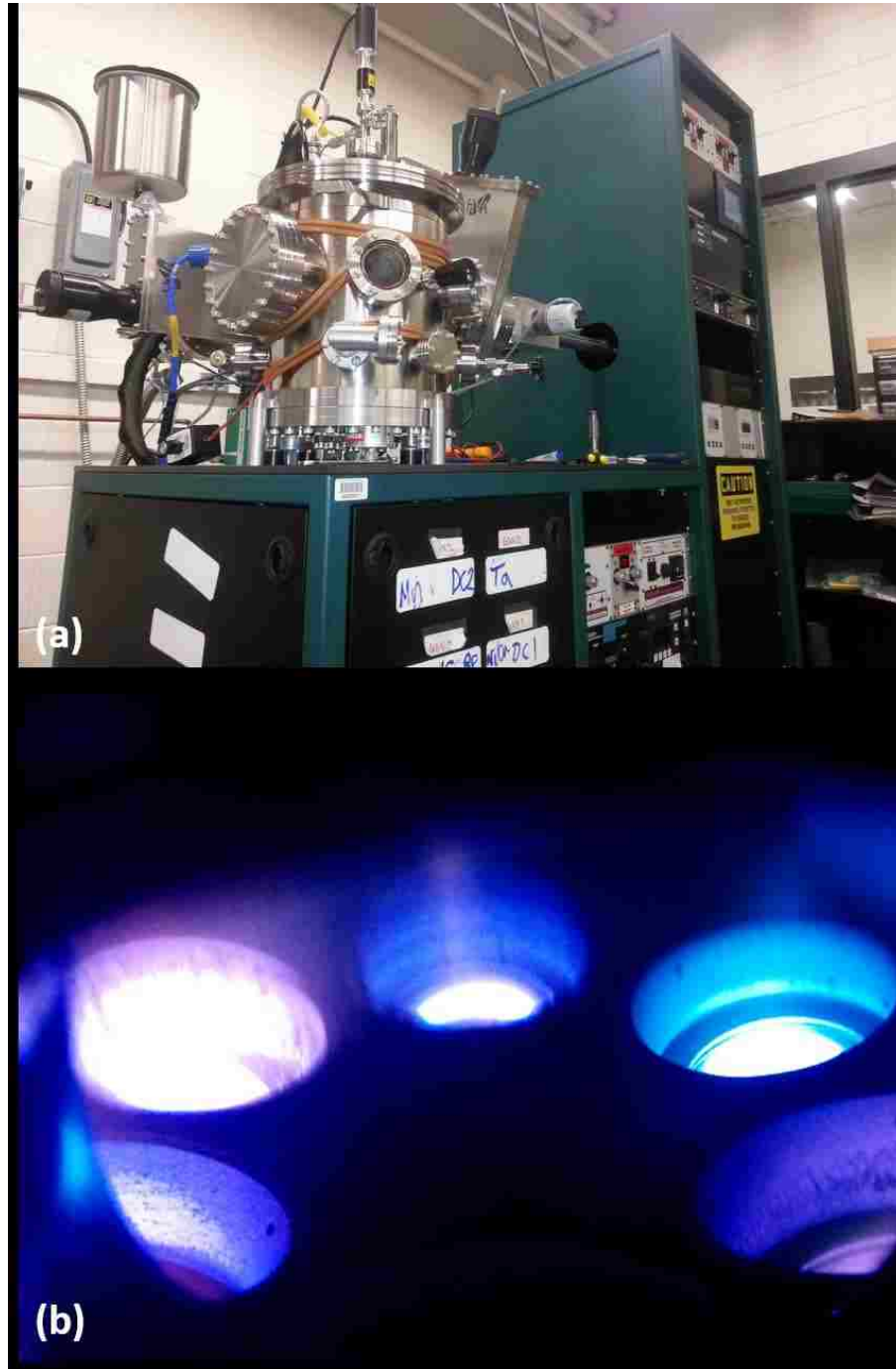


*Figure 3.2 (a) Magnetron sputtering system in Dr Balk's research group at the University of Kentucky; (b) Targets, sputtering simultaneously; the unique plasma color in each target is due to each sputtering material's individual properties.*

### **3.3. Fabrication of the Bulk Samples**

Casting is one of the oldest methods for fabrication of metals and alloys. To answer the industry's need for more specialized fabrication methods, several different casting techniques have been invented over the years. Arc-melting is one of these casting methods, which nowadays is widely used in both industry and research scale. The heat, in this technique, is generated by an electric arc between a W electrode and the material. Arc-melting is well suited for metals and alloys with higher melting points due to the higher temperature provided by the arc and the controlled atmosphere (vacuum or Ar). In this project, mini arc melting (MAM) system by Imteck was used to make the identified HEA compositions in bulk form. Figure 3.3. presents a photo of this lab-scale arc-melting system.

### **3.4. Characterization Techniques**

In this project we used scanning electron microscope (SEM) with energy dispersive spectroscopy (EDS) capabilities to screen the chemical composition of the samples, both in thin film and bulk form. In order to study the crystal structure of the materials as well, X-ray diffraction technique (XRD) and electron backscattered diffraction (EBSD) was used. A dual beam SEM with a focused ion beam (FIB) and scanning transmission electron microscopy (STEM) capabilities was used in order to further characterize the thin film structure.





*Figure 3.3. Mini arc-melting (MAM) system by Imteck, available at Dr Balk's research group at the University of Kentucky*

### **3.4.1. Scanning Electron Microscopy**

Electron microscopy is a powerful technique to characterize materials of different nature. SEMs can provide imaging in nm and  $\mu\text{m}$  scale with minimal sample preparation. Additionally, depending on the available detectors on the system, compositional and structural data can be collected from the samples. Electron microscopy is founded based on the interaction of an electron beam (high energy

accelerated electrons) with electrons of the sample material. Various signals are made as a result of these interactions. The detectors collect and interpret these signals to images and data.

Different SEMs with various capabilities are available at the University of Kentucky's electron microscopy center (EMC). They were used in this project based on the instruments availability to analyze both thin film and bulk samples.

FEI Helios NanoLab 660 is a dual beam SEM/FIB system available at the EMC. (Figure 3.4.) Most of the electron images in this study were taken using this system. Secondary and backscattered electron images as well as the STEM images were provided by this equipment. Each of these imaging modes contain different detailed information of the sample materials. Helios is also equipped with EDS and EBSD detectors which were used in this project as well.

FIB capabilities on the Helios can be used for both imaging and milling the materials. Thin lamellas, with electron beam transparency, can be made using the FIB milling. This method, known as the lift-out technique, was used in this project to fabricate lamellas for high resolution STEM imaging. Figure 3.5. summarizes the lift out steps:

- Depositing a protective layer on the area of interest usually Pt or W
- Milling both sides of the lamella using the ion beam

- Attaching the nano-manipulator to the lamella by welding and cutting the last attached part
- Lifting out and welding the lamella to a Cu grid
- Reducing the thickness even further to achieve electron beam transparency for STEM imaging or transmission electron microscopy (TEM)

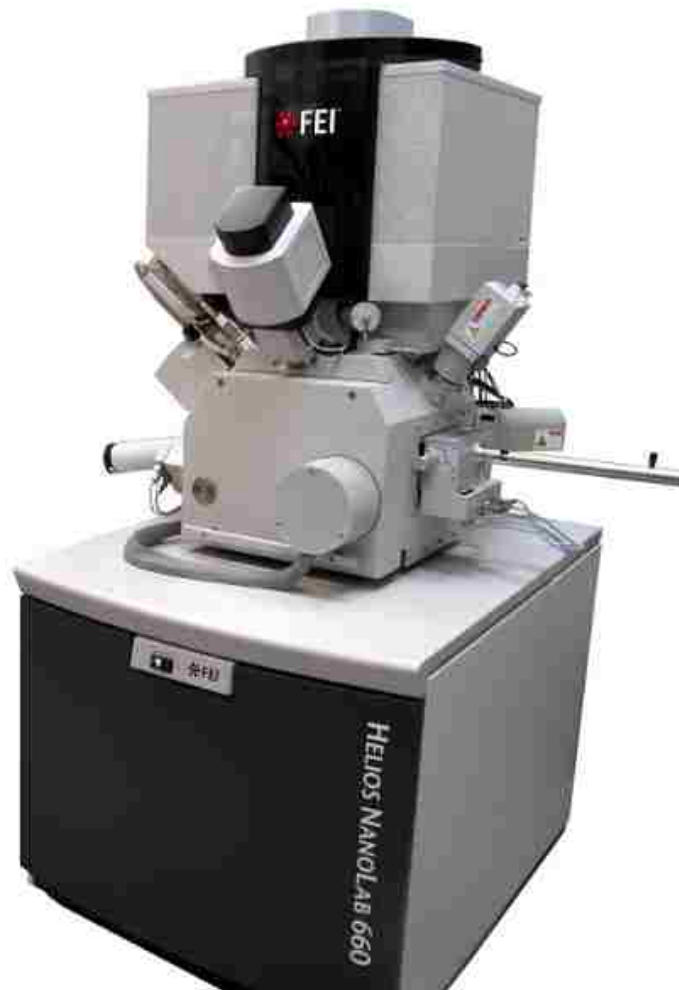


*Figure 3.4. FEI Helios NanoLab 660; most of the characterization work in this project was performed using this dual beam (SEM/FIB) system. This instrument is equipped with multiple detectors including EDS, EBSD and STEM.*

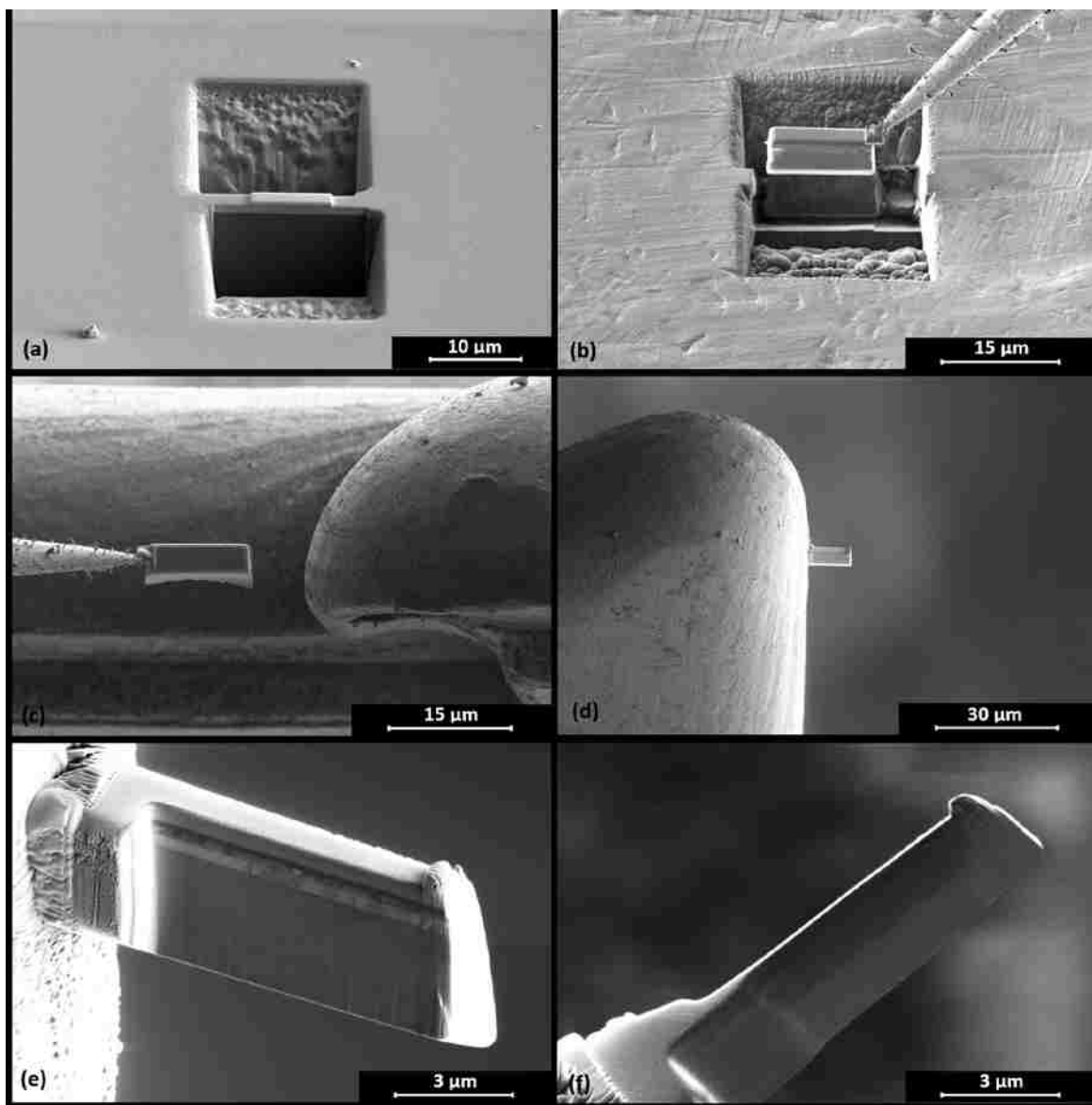


*Figure 3.5. Lift out technique: (a) both sides of the area of interest is milled; (b) the nano-manipulator is attached and then lifted out; the lamella (c) close to the Cu grid, (d), (e) welded to a Cu grid and (f) further thinning down*

### **3.4.2. Energy Dispersive Spectroscopy**

EDS is an efficient technique to analyze atomic composition of the materials with a reasonable precision for alloy development purposes (~1 at. %). The EDS detector is usually installed on an electron microscope. It collects the X-ray signal generated from the electron beam interaction with the sample material. Due to the nature of X-rays, they carry atomic information of their source. EDS detector and computing set up translate this information into atomic composition data which is accessible through a software interface.

In order to screen the chemical composition of the films across the gradient, each fabricated specimen was cut into smaller pieces of about 10 mm in size to have a more localized composition measurement. In case of the bulk samples, they were cut in half and properly prepared after several steps including: mounting in epoxy, grinding with SiC papers, polishing with fine diamond solutions and ultra-fine polishing with the Buhler Vibromet. Imaging and EDS data were collected from each of the fabricated bulk samples to confirm their chemical composition.

### **3.4.3. X-ray Diffraction Technique**

XRD is a well-established technique to investigate the crystal structure of materials base on the diffraction of the x-rays from the crystal planes of the sample

material. This technique can provide a precise identification of the crystal structure in the sample. In this study XRD (Siemens D500) was used to analyze the crystal structure of the thin film and bulk samples.



*Figure 3.6. Siemens D500 XRD*

#### **3.4.4. Electron Backscatter Diffraction Technique**

The X-ray window of the XRD equipment is about 2x2 cm, therefore for a higher resolution structural analysis of the samples, EBSD technique was proposed. EBSD detector on the SEM provides highly localized crystallographic information about the sample based on the electron diffraction rather than the x-ray diffraction in XRD. The diffracted electrons of the electron beam are generated from a nm-scale volume of the sample surface. The signal forms a unique pattern named Kikuchi after the scientist who discover it. This pattern is a characteristic of the crystal structure and

its orientation and therefore makes EBSD a useful technique to determine the crystal structure of materials. Using the Oxford EBSD detector on the Helios (Figure 3.7.), we were able to resolve the crystal structure of the bulk samples in  $\mu\text{m}$ -scale. The collected EBSD data is usually post processed to reduce the noise and convert it to more informative illustrations. In this project we used the Channel 5 software package to post process the EBSD data.

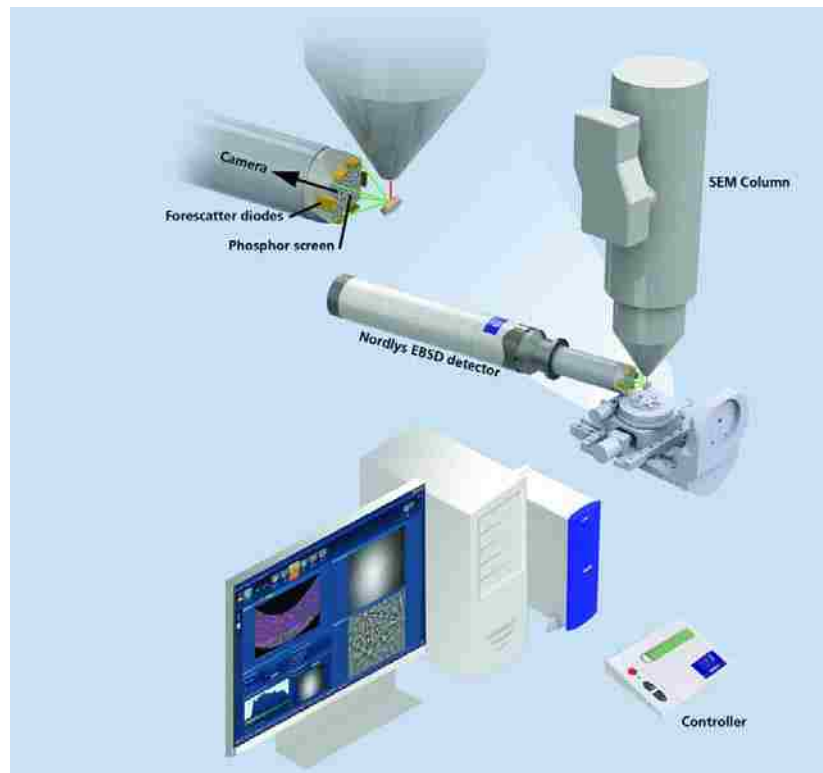


Figure 3.7. Illustration of the EBSD detector set-up<sup>8</sup>

### 3.4.5. Transmission Electron Microscopy

Transmission electron microscopy (TEM) is an advance characterization technique that can provide high resolution imaging, compositional and structural data from materials. In TEM, similar to SEM, the data is collected from the interactions of

the electron beam and the sample material. However, unlike SEM, in TEM the electron beam passes through the sample. Therefore, the sample has to be transparent to the electron beam. In this study, all the TEM samples were prepared by the lift out technique using the Helios. TEM can provide order of magnitudes higher resolution compared to SEM, therefore in many materials science studies TEM analysis is a necessity, even though sample preparation for TEM is time consuming and expensive. The TEM analysis in this project was performed at the FEI research lab using their Talos TEM. (Figure 3.8.)



*Figure 3.8. FEI Talos TEM<sup>9</sup>*



### 3.5. Sputtering Rate Measurement

As mentioned earlier, in magnetron sputtering the geometry of the target and substrate placement affects the chemical composition and the thickness of the fabricated film. The power, duration, pressure and the sputtering material are defining factors as well. The rate of the deposition can be measured and changed accordingly by changing any of these parameters. In order to control the composition of the fabricated films, rate measurement experiments are usually necessary.

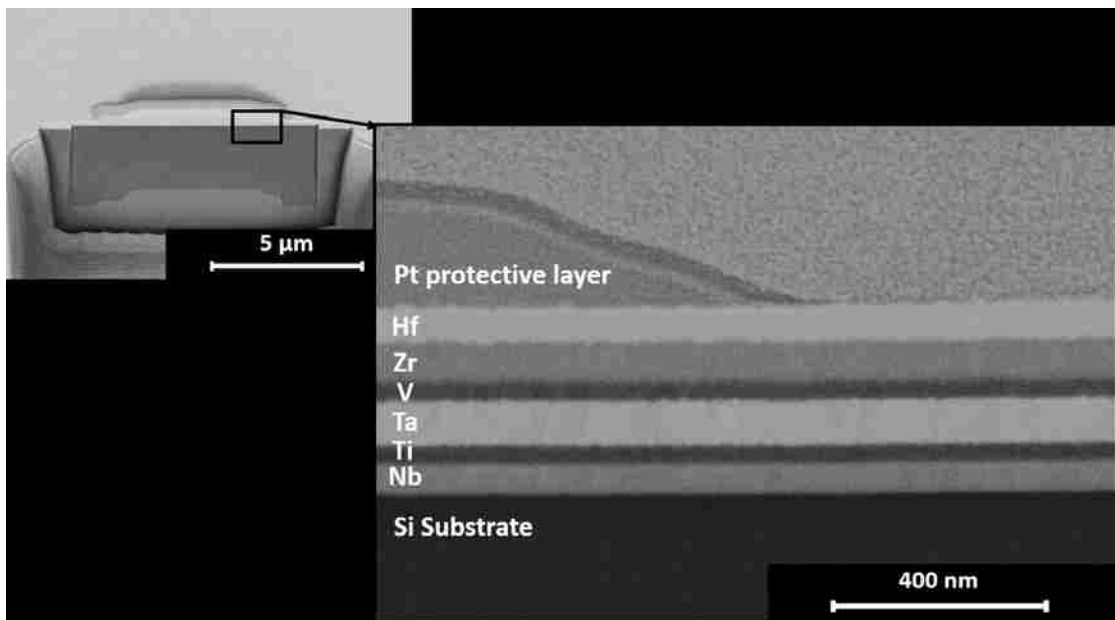


*Figure 3.9. FIB cross sectional image of a multilayer thin film sample fabricated for deposition rate measurements*

One method to measure the deposition rate for at a certain power is to deposit a film during a fixed period of time and measure the thickness afterwards. Figure 3.9. shows a FIB cross sectional image of a multilayer film of Nb, Ti, Ta, V, Zr, and Hf that

was deposited at 100 Watts for 10 mins for each element on a Si wafer. Based on the thickness of these layers, the sputtering rate of each element was calculated. However, during the film fabrication process, we observed that simultaneous deposition of the multiple elements significantly affects the deposition rate. Therefore, the sputtering rate measurement of individual elements would no longer be applicable. This difference in sputtering rate is most probably due to the interaction of the different atoms in the sputtering plasma. Therefore, for most of the film fabrication in this project, the manipulation of the chemical composition was based on the experimental approach rather than sputtering rate measurements.

### **3.6. Nanoindentation**

Nanoindentation testing was developed in the 1970s<sup>46</sup> to study the mechanical behavior of materials in small scale. This technique, as the name suggest, is based on the indentation of an indenter into the surface of the material similar to other indentation methods such as microhardness testing, however in much smaller scale. In this method, the applied load and the depth of the indentation is measured and based on the size of the area of contact, the hardness is calculated. Other information on the mechanical behavior such as modulus and yield strength of the specimen can be studied from the load-displacement curve recorded during the loading and unloading process. In this project we use the iNano system from Nano Science Instruments to measure the hardness of the thin film samples as well as the bulk samples.



*Figure 3.10. iNano nanoindentation instrument<sup>10</sup>*

## **Chapter 4: Thin Film Combinatorial Approach in Development of a Face Centered Cubic High Entropy Alloy**

### **4.1. Introduction**

High entropy alloys (HEAs) with the face centered cubic (FCC) crystal structure were among the first group of these alloys introduced in 2004<sup>12</sup>. FCC HEAs have been shown to have many different applications due to their unique properties. For instance some FCC HEAs are able to maintain their ductility and strength at cryogenic temperatures<sup>47-49</sup>. In addition to their interesting mechanical properties, their corrosion resistivity makes them ideal candidates for structural applications in more severe settings such as marine environments<sup>50-53</sup>. They usually contain five or six different principle elements of the first row of intrinsic metals in the periodic table, with chemical composition of each component in the range of 5-35 at. %.

Cantor alloys<sup>12</sup> and other FCC HEAs have been of interest within the research community since their discovery due to the extensive prior research on similar alloy systems such as super alloys<sup>2,17,22,54</sup>. FCC HEAs usually contain either 5 or 6 of the elements Mn, Fe, Ni, Co, Cu and Cr. Addition of other alloying elements such as Al or deviation of the equiatomic composition has been explored as well<sup>55-57</sup>. The variety of crystal structures can be achieved by such minor changes to the chemical compositions. Kao et al and others have studied the FCC to body centered cubic (BCC) crystal transformation by minor additions of Al to FeNiCoCr which proved to

change the mechanical properties of the alloy significantly<sup>58,59</sup>. Furthermore, relatively few studies have explored the addition of Cu to this family of alloys<sup>4,17</sup>. This study focuses on the MnFeNiCoCu alloy system in order to screen for potential non-equiatomic single phase HEAs.

As previously mentioned in Chapter 2, unlike conventional alloys, the HEAs do not have a base element as a solvent, which complicates the application of conventional development techniques to HEAs. To find potential alloy systems, one approach is to apply development techniques of an exploratory nature<sup>60,61</sup>. The other popular approach within the research community is to develop computational models to predict the formation of the single phase HEA<sup>41,42,62</sup>. However, such techniques require extensive experimental data and are relatively time consuming and expensive.

The alloy development process proposed in this project is a more efficient experimental approach in developing new HEA systems. The idea is to create a 2D gradient of composition in a relatively large area. Each unit of area on this gradient has a different composition, hence a different phase (or phases) which might have a different crystal structure. Therefore, by screening crystal structure over this wide range, one would be able to predict which phases would form at a certain chemical composition. By screening the properties in a similar manner, a thorough understanding of the composition-phase-property relations will be achieved.

## 4.2. Experimental Methods

In the present work, magnetron sputtering (ORION system, AJA International) was used to fabricate gradient thin films of the MnFeCoNiCu as a potential alloy system on single crystal Si wafers. The gradient in composition was achieved by depositing from different sputtering targets orientated at different angles towards the substrate as shown in Figure 4.1. For the deposition of the films, pure Mn, Fe and Co targets were used. However Cu/Ni target was pre-alloyed (50 at. % of each) via powder metallurgy technique in our lab. DC power supplies was used with 80, 110, 80 and 160 Watts for the Mn, Fe, Co and Cu/Ni targets respectively for 20 mins. The power was adjusted to achieve an equiatomic composition in the center of the substrate.

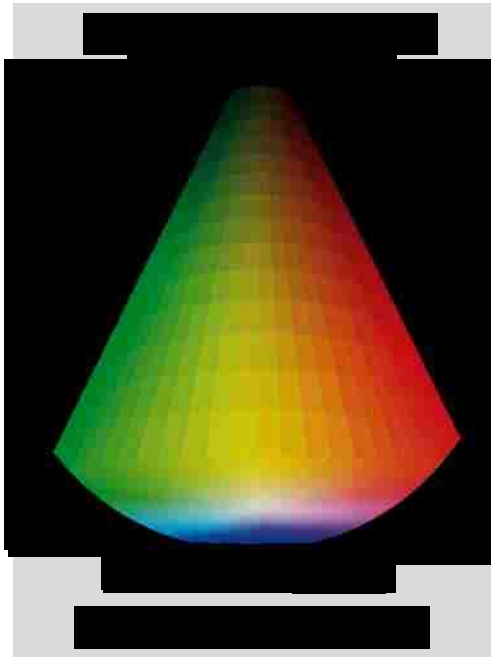


*Figure 4.1. Target arrangement in the sputtering set-up for fabrication of the thin film samples*

Each fabricated specimen was cut into smaller pieces of about 10 x10 mm in size. The chemical composition of each sample was studied by an Oxford X-Max<sup>N</sup> energy dispersive X-ray spectroscopy (EDS) detector on a FEI Helios dual-beam NanoLab 660 (SEM/FIB) at 20 kV electron beam voltage and 0.4 nA current. In order to investigate the crystal structure of each sample, X-ray diffraction (XRD) technique was used (Siemens D500).

For further investigation of the thin film structure, a thin lamella of some of the spots were made by applying the lift-out technique, using the focused ion beam (FIB) capabilities on the Helios. High resolution scanning transmission electron microscopy (STEM) images were taken from the lamella in order to observe the structure of the sample in nm scale at 30 kV.

The identified single phase compositions were cast in bulk form via Edmund Buhler compact arc-melter MAM-1. The raw material with ~99.9 purity was weighted to make a 5 g alloy sample. In order to attain a more uniform sample, the as-cast piece was flipped inside the arc-melter and remelted several times.

The fabricated bulk samples were then rolled down to 50% of the original thickness. In order to anneal the samples, they were transferred to a furnace with Ar<sub>95</sub>H<sub>5</sub> atmosphere. The temperature was raised with a rate of 5 °C/min to 900 °C and the samples were held at that temperature for 1 hour. Then with the rate of 10 °C/min

the temperature was raised to 1000 °C and the samples were held for another hour. Finally they were cooled down to room temperature while still in the furnace.

The bulk samples, before and after thermomechanical processing, were cut in half and studied with the Helios, after sample preparation steps including: mounting in epoxy, grinding with SiC papers, polishing with fine diamond solutions and ultra-fine polishing with Buehler Vibromet. The chemical composition of the samples were confirmed with the EDS technique. For further analysis of the structure of the samples, electron backscatter diffraction (EBSD) data was collected from the samples using the Oxford NordlysMax<sup>2</sup> detector on the Helios. The EBSD data was post-processed using the Channel 5 software package. Using Tango software, about 20% noise reduction was applied to the collected data. In order to have a more accurate grain size measurement the grain boundary was defined as 10° of misorientation.

Both the thin film samples and the bulk samples were further studied using the iNano nanoindentation system. The hardness value of the samples were measured over 3x3 array of spots, each 20 µm apart. The final reported hardness is an average of these measured values.

### **4.3. Results and Discussion**

The XRD and EDS data were collected from each 10x10 mm sample of the thin film. Based on the EDS data from 9 different spots on the film in Table 4.1., the



chemical composition of each element on the substrate varied around 15 at. % across the Si wafer diameter (76 mm). Figure 4.2. summarizes the data collected from these 9 different spots on the thin film over the area of around 40 mm diameter in the center of the Si wafer. Each unit has a different chemical composition and therefore different phases may have formed. The unique X-ray diffraction pattern of each spot confirms the formation of different phases with different crystal structure within that composition. Spot 4 with the chemical composition of  $\text{Mn}_{30}\text{Fe}_{20}\text{Co}_{22}\text{Ni}_{14}\text{Cu}_{14}$  (at. %) exhibits a single-phase FCC structure in the corresponding indexed XRD. This is a promising potential HEA for further investigation.

*Table 4.1. The chemical composition (at. %) of the elements across the thin film sample*

<b>Spot</b>	<b>Mn</b>	<b>Fe</b>	<b>Co</b>	<b>Ni</b>	<b>Cu</b>
<b>1</b>	20	29	16	17	18
<b>2</b>	26	30	17	14	14
<b>3</b>	30	24	19	13	14
<b>4</b>	30	20	22	14	14
<b>5</b>	26	16	23	17	16
<b>6</b>	19	16	22	21	23
<b>7</b>	16	20	19	22	24
<b>8</b>	17	27	16	20	21
<b>9</b>	23	21	2	18	19

For a better understanding of the film structure, STEM images of the thin lamella of spot 4 is presented in Figure 4.3. The top layer is the protective Pt film and

the sputtered film in observed right below that. The images suggest a columnar grain structure within the film, with grains of about 10 nm width. Such columnar structures is not uncommon in as-deposited thin films, fabricated via physical vapor deposition techniques<sup>63</sup>.

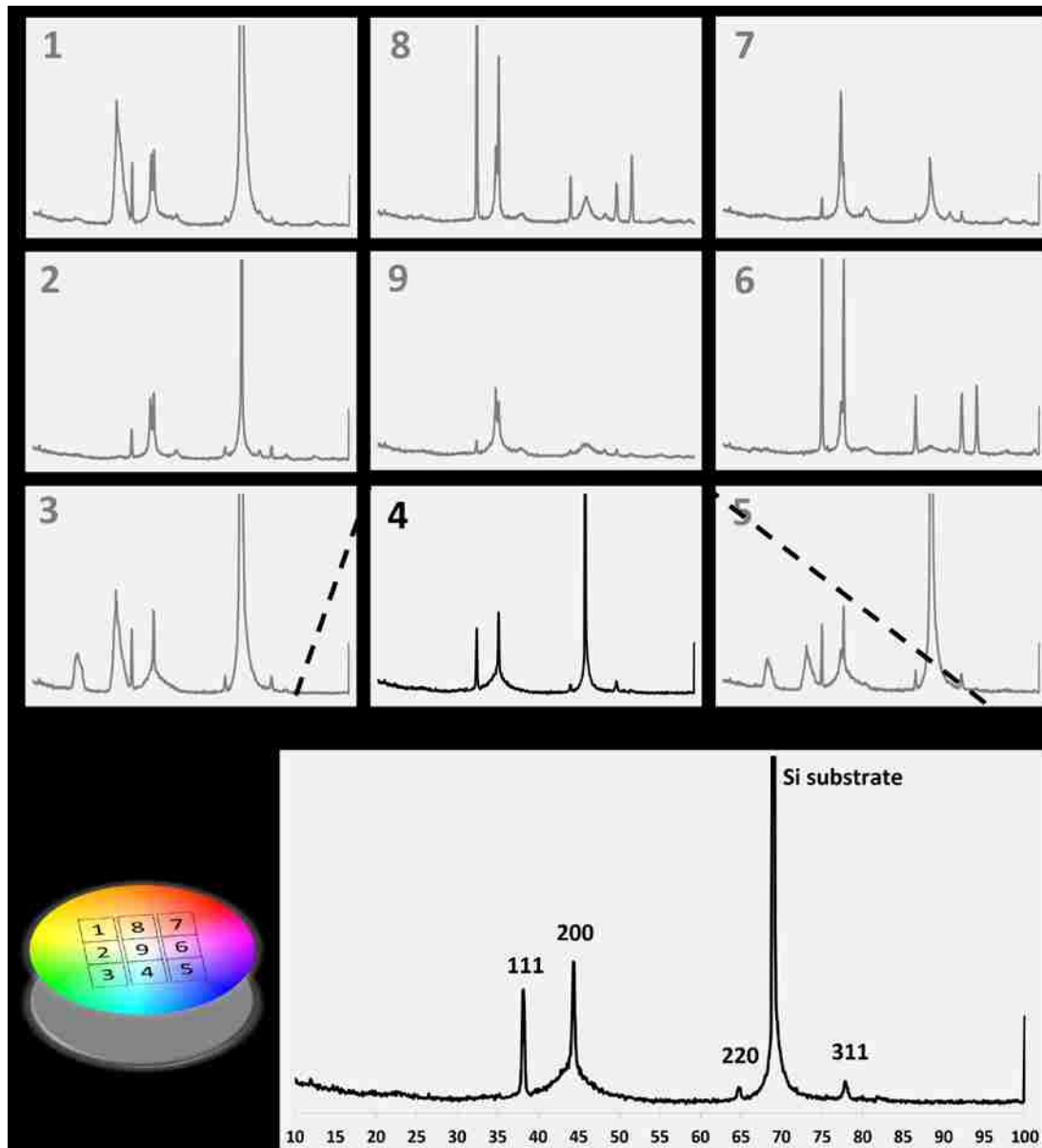


*Figure 4.2. XRD data collected from 9 different spots on the fabricated thin film sample; the approximate location of the spots on the Si wafer are marked in the schematic. Spot 4 on this sample exhibit a single phase FCC structure.*

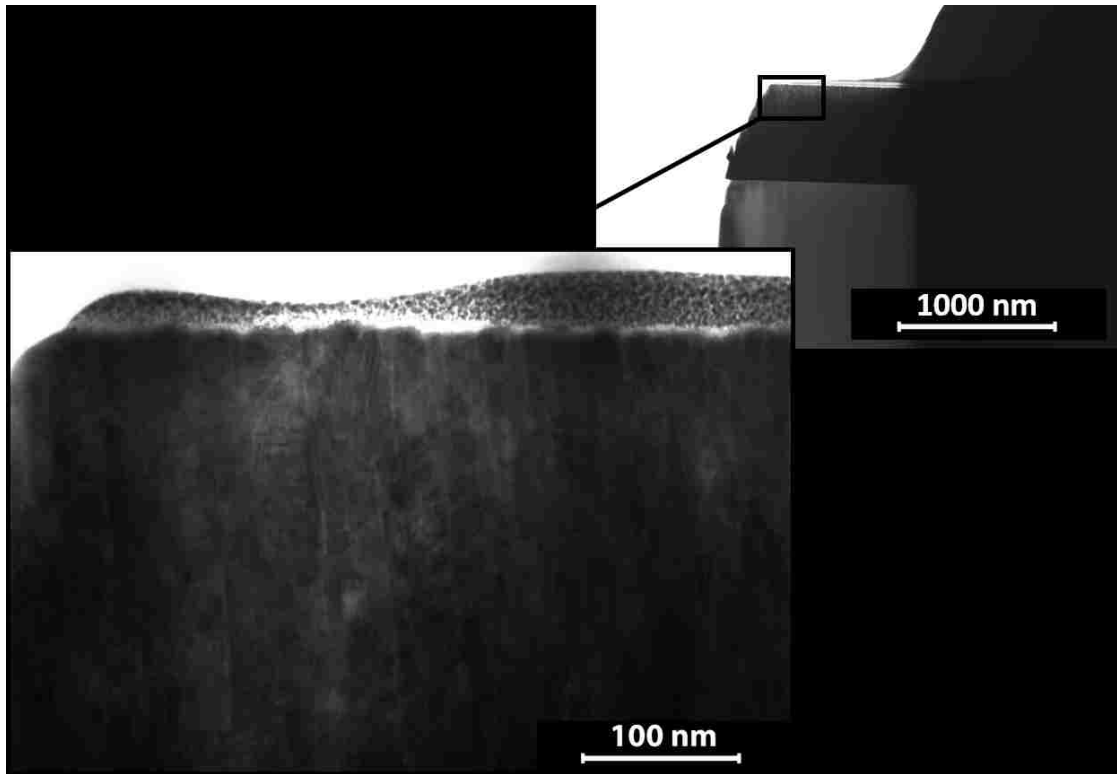


*Figure 4.3. STEM image of the spot 4 on the thin film sample; the lamella, fabricated by FIB, is presented in top right corner. The higher magnification STEM image shows a columnar grain structure in spot 4 on the thin film sample.*

As the EDS and XRD results from the thin films show, based on the chemical composition different phases may develop in bulk form of this alloy family. In this study we chose spot 4 as it formed a single phase FCC in the film, whereas the XRD results from the other spots suggested the formation of more than one phase. In addition to the single phase XRD pattern, the observed grain structure in the STEM images of the spot 4 made it an ideal candidate for the bulk fabrication. The chemical composition of spot 4 was cast in bulk form.

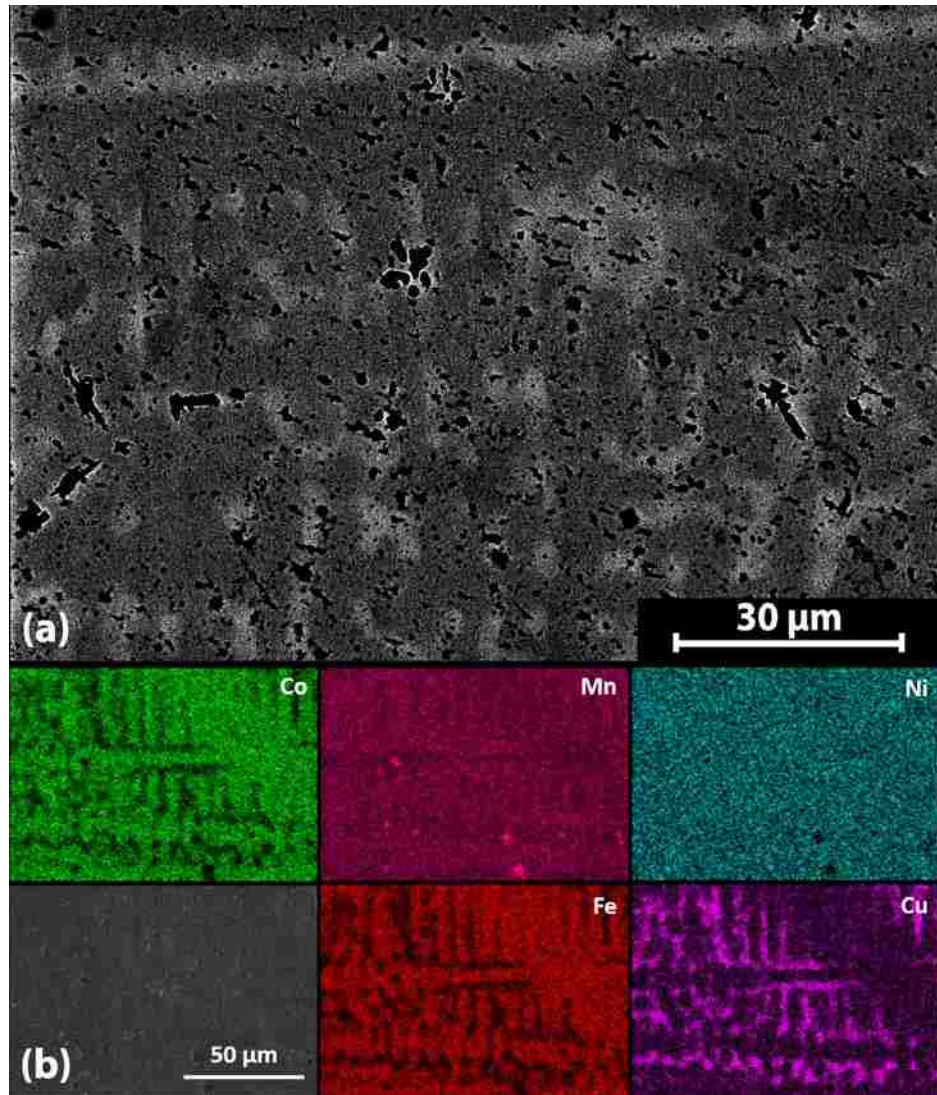


*Figure 4.4. (a) The SEM micrograph of the as-cast bulk sample showing the dendritic structure. (b) The EDS maps of another region on the same sample exhibits the segregation of the elements.*

The EDS technique was used to confirm the overall composition of the sample to be  $\text{Mn}_{30}\text{Fe}_{20}\text{Co}_{20}\text{Ni}_{15}\text{Cu}_{15}$  (at. %). Considering the standard error inherent to EDS quantification ( $\pm 1$  at. %), the chemical composition is equivalent to that of spot 4 on the film. Figure 4.4. presents the SEM micrograph of the as-cast sample after proper metallographic sample preparations. Both the SEM image and the EDS maps confirm

a dendritic structure. The dendrites seem to be richer in Cu, whereas the inter-dendritic phase is more Fe/Co rich. Mn and Ni seem to have a more uniform distribution within the as-cast material and did not segregate as much. As extensively discussed in the literature<sup>35</sup>, the dendritic structure is most probably due to the different melting points and diffusion rates of the elements within the alloy system. It should also be noted that due to the nature of the arc-melting fabrication process, the as-cast sample has a porous microstructure.

The as-cast samples went through a series of thermomechanical processing, as described above in the experimental methods section. This was done in order to achieve a similar grain structure to what we observed in the thin film sample. Figure 4.5. presents the SEM image of the same bulk sample post processing and metallographic preparation steps. The applied thermomechanical course successfully resulted in the equiaxed grain structure as observed all over the sample. However, some relatively large pores are still observed within the structure as well. Further thermomechanical processing or modifications to the casting process is required to reduce the size and number of the porous in this alloy.

The EBSD maps from the sample are presented in Figure 4.6. The data is collected from an area with no pores. The phase map confirms the single phase FCC equiaxed grain structure. Based on this EBSD data, the average grain size is  $\sim 71 \mu\text{m}$ . No significant preferential orientation or texture is observed in the orientation map, which is presented in this figure as well. This indicates that the thermomechanical

processing steps involving recrystallization and grain growth were successful in achieving a uniform microstructure.

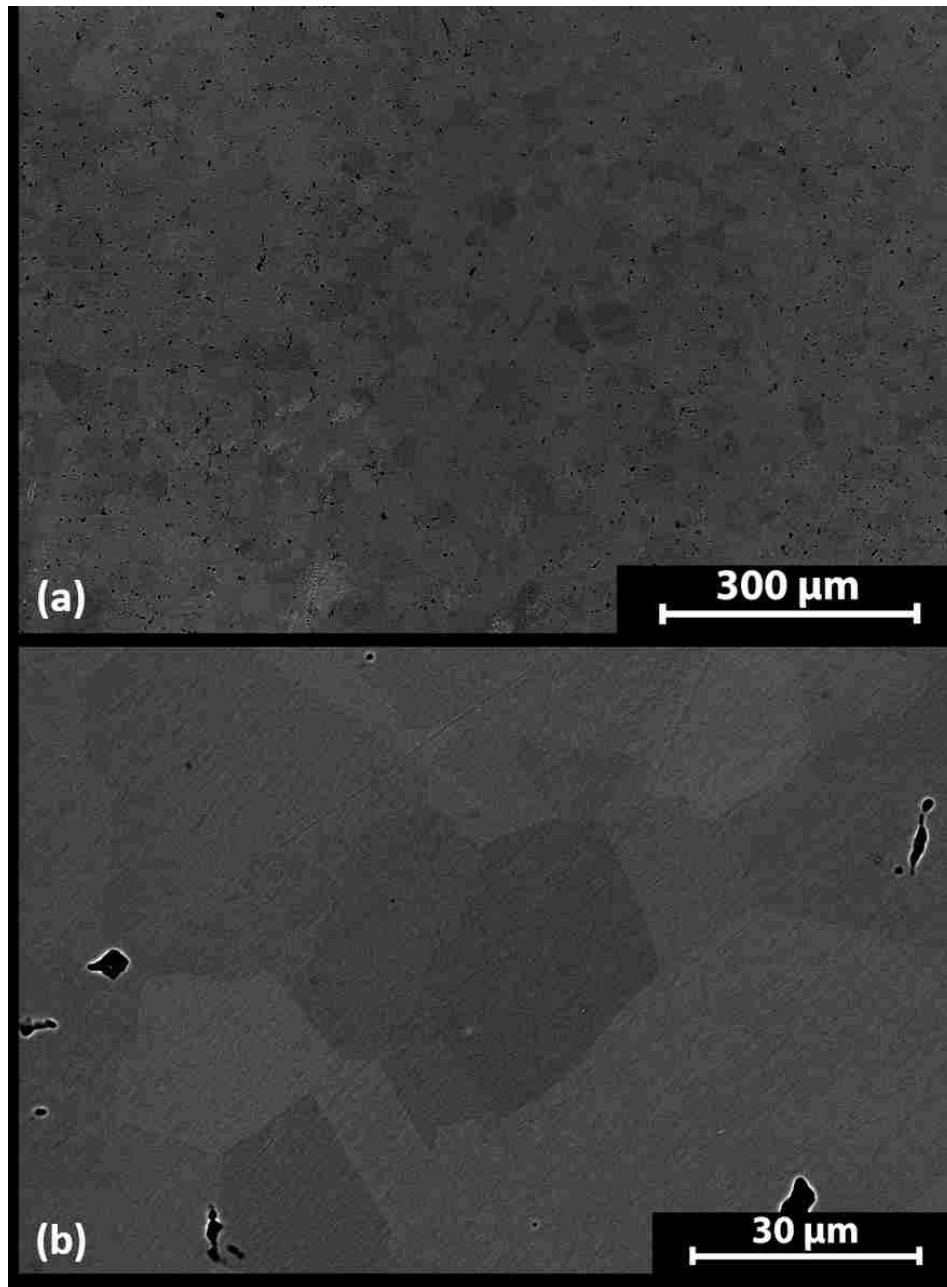


*Figure 4.5. The SEM micrographs of the bulk sample after the thermomechanical processing. The uniaxial grain structure of the sample can be observed in (a) low and (b) high magnifications.*

The nanoindentation results of the 9 spots of the thin film sample is presented in Table 4.2. The hardness value of the spot 4 is the lowest. We speculate that higher hardness values on the other spots are due to the formation of intermetallic phases on those areas of the film. The mechanical properties of ceramics, and intermetallics in particular, have been well studied in the literature<sup>26</sup>. They are known to have higher hardness and lower ductility compared to metallic materials and solid solutions. These phases usually have very complicated crystal structures with low angle x-ray diffractions. Some of the peaks that are observed at the lower angles of the XRD patterns support the speculation that intermetallic phases exist in these samples. (Figure 4.2.)

*Table 4.2. Hardness values from the nanoindentation of the 9 spots on the thin film sample*

<b>Spot</b>	<b>Hardness (GPa)</b>
<b>1</b>	$6.7 \pm 0.2$
<b>2</b>	$6.1 \pm 0.1$
<b>3</b>	$5.76 \pm 0.08$
<b>4</b>	$5.80 \pm 0.07$
<b>5</b>	$6.77 \pm 0.06$
<b>6</b>	$8.1 \pm 0.1$
<b>7</b>	$7.95 \pm 0.08$
<b>8</b>	$7.64 \pm 0.08$
<b>9</b>	$6.6 \pm 0.1$



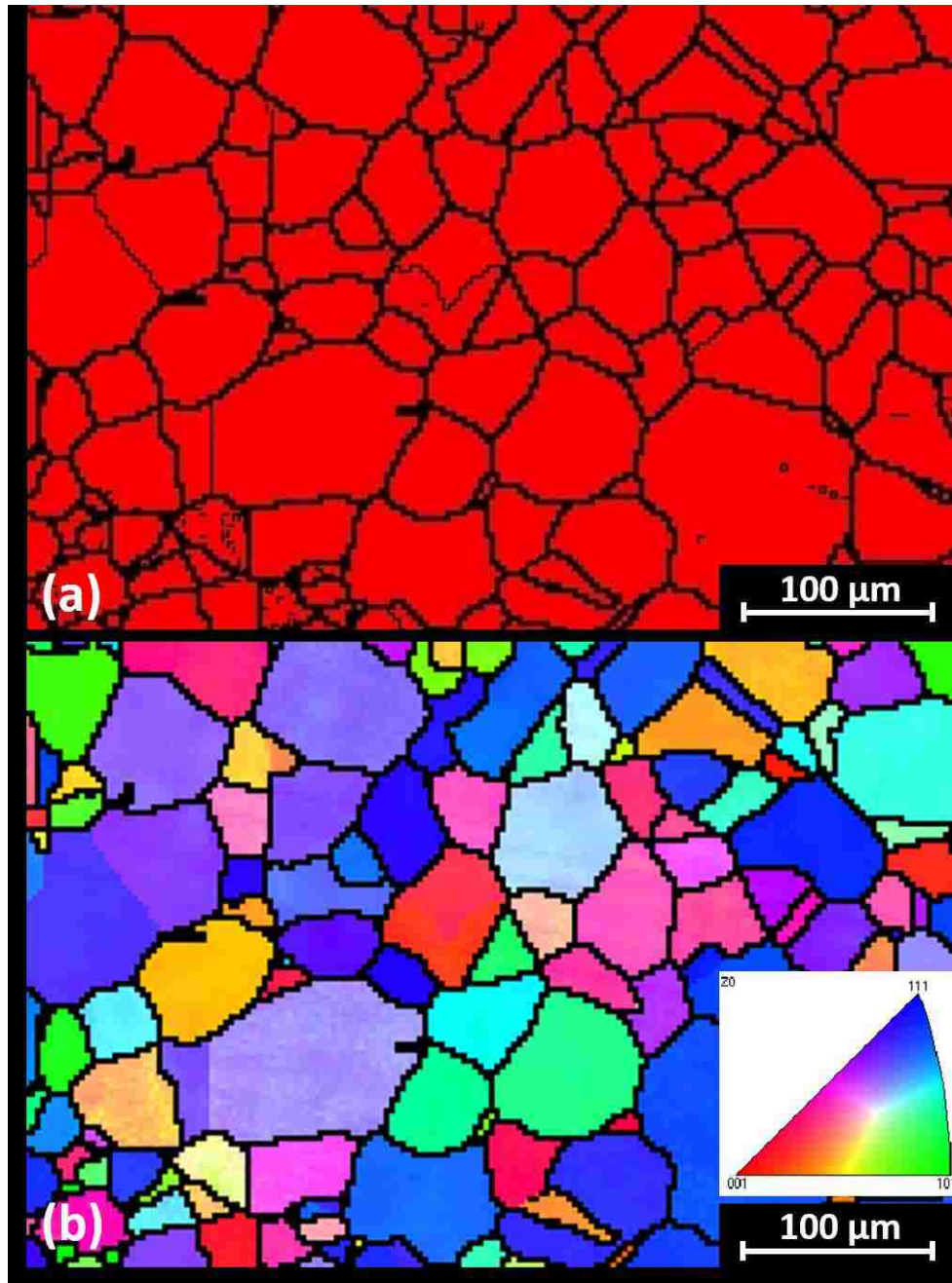


*Figure 4.6. The EBSD (a) phase and (b) orientation maps of the bulk sample post thermomechanical processing confirming the single phase structure in this sample.*

The hardness value of the bulk sample was found to be around 3 GPa. Spot 4 on the film has much higher hardness compared to the bulk sample even though they have almost identical chemical compositions. We hypothesize that there are two main



reasons for this difference in hardness values. The internal stresses in the as-deposited thin films contribute significantly to their mechanical behavior. The higher hardness value observed in spot 4 is most probably due to the residual stresses after the film deposition. Secondly, it should be noted that the nanoindentation technique is a rather localized method for hardness measurements. Therefore some strengthening mechanisms in the bulk sample, such as grain boundary effect, are not observable in this measurement particularly with larger grain size. The fabricated bulk sample has grains of  $\sim 37 \mu\text{m}$  in size which is much larger than the nanoindentation scale of measurement.

Applying the combinatorial thin film, we were able to successfully produce a single phase FCC HEA with a non-equiatomic composition with one casting attempt. This technique is more effective and efficient compared to more conventional alloy development methods. Due to the versatility of thin film fabrication this alloy development method can be applied to a variety of alloy combinations.

#### **4.4. Conclusions**

By fabricating gradient thin films of MnFeCoNiCu, we were able to study this alloy family over a wide compositional range. The composition and crystal structure of the film were screened across the substrate, using advanced characterization techniques including EDS and XRD. Applying this combinatorial thin film approach, a potential single phase FCC HEA composition was identified as

$\text{Mn}_{30}\text{Fe}_{20}\text{Co}_{22}\text{Ni}_{14}\text{Cu}_{14}$ . This composition was casted in bulk form via arc melting followed by thermomechanical processing. Characterization results (SEM, EDS and EBSD) confirmed the formation of the predicted single phase FCC HEA with equiaxed grain structure in the  $\text{Mn}_{30}\text{Fe}_{20}\text{Co}_{20}\text{Ni}_{15}\text{Cu}_{15}$  alloy system.

This combinatorial thin film approach can potentially be applied to any alloy system for a more efficient alloy development process by reducing the casting attempts compared to more conventional techniques. This approach may reduce the development costs as well by reducing the exploratory steps of identifying new alloy systems. Our team has utilized this method for identifying multiple principle element alloy systems with different crystal structures. The screening approach may be used to study various properties across a wide compositional gradient, such as mechanical properties via Nano indentation.

## **Chapter 5: Thin Film Combinatorial Approach in Development of a Hexagonal Closed Packed High Entropy Alloy**

### **5.1. Introduction**

The research community has been working on identifying single phase high entropy alloys (HEAs) in the past few years<sup>40</sup>. Most of the discussed alloy systems in the literature have either FCC or BCC crystal structures<sup>17</sup>. However, there has not been as much development in the research on HCP HEAs. Takeuchi et al. and others has worked on fabrication of HCP HEAs with high melting points for refractory applications such as YGdTbDyLu and GdTbDyTmLu<sup>64</sup>. Whereas most of these alloy systems contain lanthanide metals, the OsRuWMoRe alloy system studied in this chapter is one of the few HCP systems that contain only intrinsic metals.

As previously discussed, whereas most alloys have a base element as a solvent, HEAs contain multiple principle elements. This complicates the identification of new HEAs via conventional alloy development techniques. Literature suggests successful HEA developments by approaches of an exploratory nature<sup>19,65,66</sup>. Designing computational models is the other popular approach within the research community. These models are developed to predict the phase space of a potential HEA system<sup>32</sup>. Even though multiple HEAs have been successfully identified and fabricated by these techniques, in most cases they require extensive experimental data and are relatively time consuming and expensive.

In this chapter the efficient combinatorial thin film approach is applied to the development of new HCP HEAs. A 2D gradient of composition is created over a relatively large area. Different phases form within each unit of area on this gradient due to the variations in the chemical composition. Each of these phases exhibits a different crystal structure. Screening crystal structure over this wide gradient enables us to predict which phases will form given a certain chemical composition. A thorough understanding of the phase space will be achieved by this combinatorial screening approach.

## **5.2. Experimental Methods**

To investigate the applicability of the thin film method to HCP alloys, the OsRuWMoRe alloy system was chosen as a potential HCP HEA based on the previous work of our research group on OsRuW alloys<sup>67</sup>.

To fabricate the gradient thin films of the potential alloy systems, Magnetron sputtering (ORION system, AJA International) was used on single crystal Si wafers as substrates. Depositing from multiple sputtering targets oriented at different angles towards the immobile substrate (as shown in Figure 5.1.) results in compositional gradients in the films. A pure W target was used, whereas the Os/Ru and Mo/Re targets were pre-alloyed for convenience. The films were deposited during 20 mins of

sputtering using DC power supplies for W and Os/Ru targets at 60 Watts and a RF power supply for Mo/Re at 100 Watts.

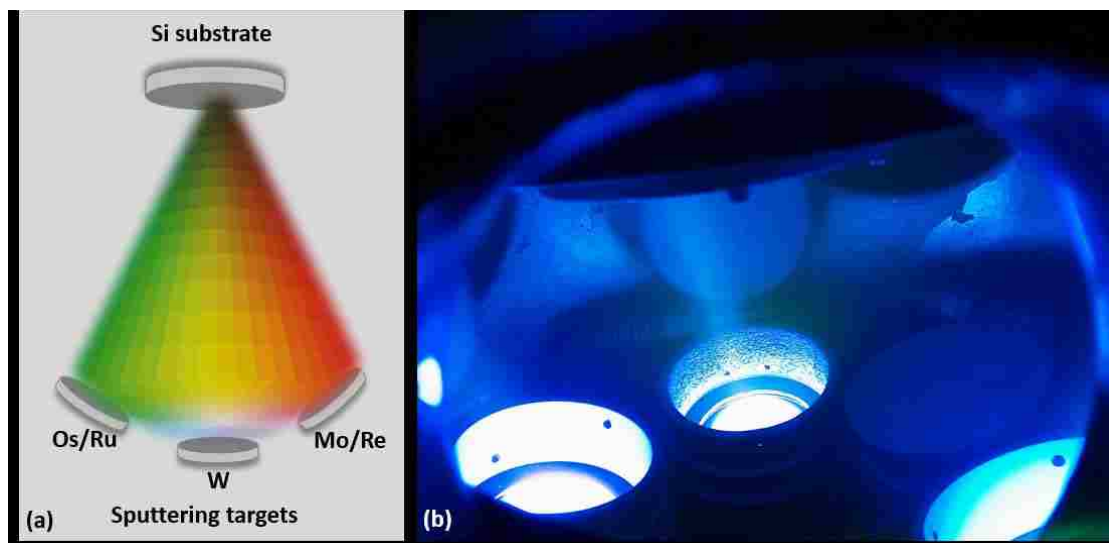


*Figure 5.1. (a) Schematic of the target arrangement set up and (b) the sputtering targets flowing with the plasma*

Smaller pieces of about 10 x10 mm in size were cut from each fabricated sample. The chemical composition of each unit sample was studied by an Oxford X-Max<sup>N</sup> energy dispersive x-ray spectroscopy (EDS) detector on a FEI Helios NanoLab 660. Additionally x-ray diffraction (XRD) technique was used to investigate the crystal structure of each unit sample (Siemens D500).

The focused ion beam (FIB) capability on the Helios was used to make thin lamellas of some of the spots on the films. Applying the lift-out technique enabled further investigation of the thin film structure and higher resolution scanning transmission electron microscopy (STEM) imaging.

Based on the results of the thin film approach, a chemical composition with single phase crystal structure was identified. This composition was casted in bulk form via Edmund Buhler compact arc-melter MAM-1. Several remelting steps were performed in order to attain a more chemically uniform sample.

The bulk sample was cut in half and studied with the scanning electron microscope (SEM), after sample preparation steps including: mounting in epoxy, grinding with SiC papers, polishing with fine diamond solutions and ultra-fine polishing with Buehler Vibromet. EDS technique was used to confirm the chemical composition of the sample. Electron backscatter diffraction (EBSD) data was collected from the sample using the Oxford NordlysMax<sup>2</sup> detector for a more thorough analysis of the crystal structure. The EBSD data was post-processed using the Channel 5 software package. Tango software applied about 20% noise reduction to the collected data and the grain boundary was defined as 10° of misorientation.

### **5.3. Results and Discussion**

XRD and EDS data is collected from each unit sample of the film. Based on the EDS data map, the composition of each element varies through the 76 mm (3 in) diameter of the Si substrate (~10 at. %). Figure 5.2. summarizes the data collected from 9 different spots on the film over the area of around 40 mm diameter in the center of the Si wafer. Each unit has a different chemical composition and therefore different phases may be formed. The unique X-ray diffraction pattern of each spot

confirms the formation of different phases with different crystal structure within each unit. Spot 1 with the chemical composition of  $\text{Os}_{24}\text{Ru}_{14}\text{W}_{25}\text{Mo}_{23}\text{Re}_{14}$  (at. %) exhibits a single phase HCP structure in the indexed XRD. This is a promising potential alloy for further investigation.

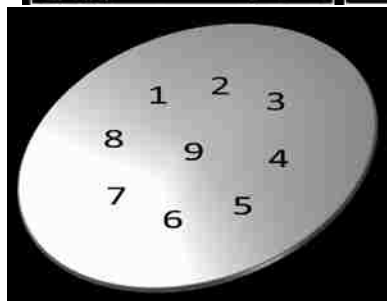
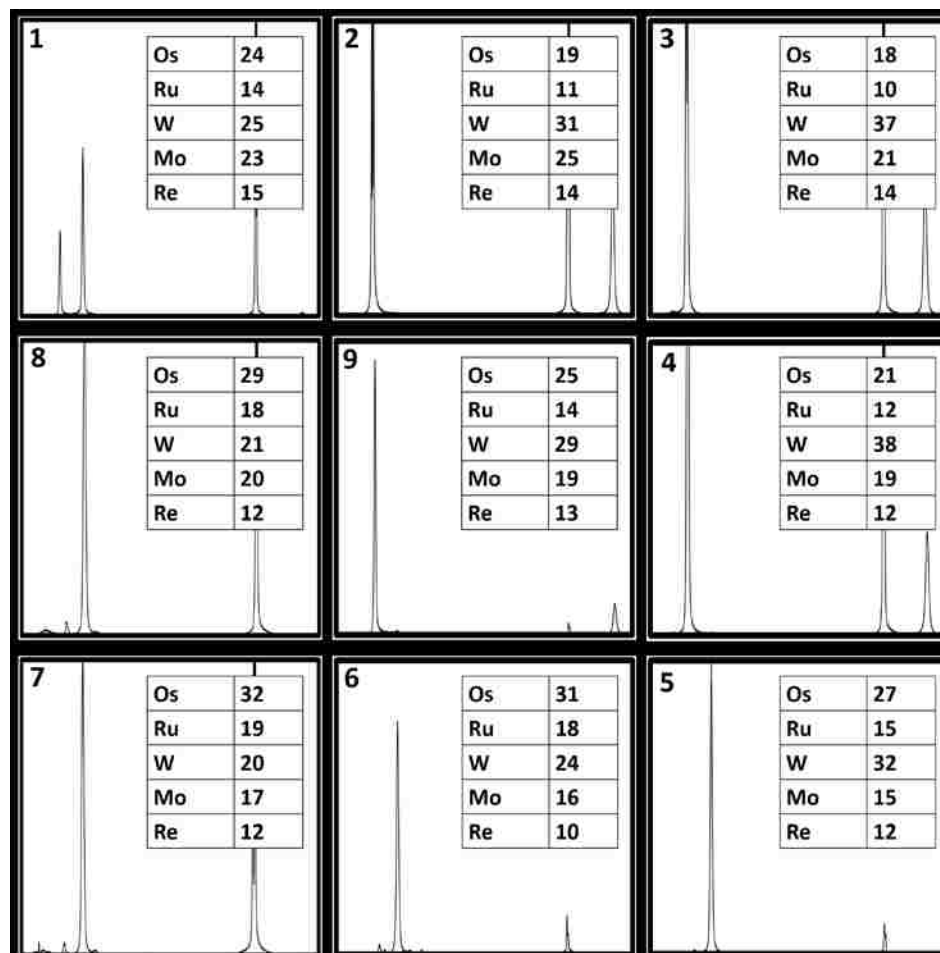


*Figure 5.2. The XRD patterns and EDS data collected from 9 different spots on the thin film sample and their approximate location on the Si wafer*

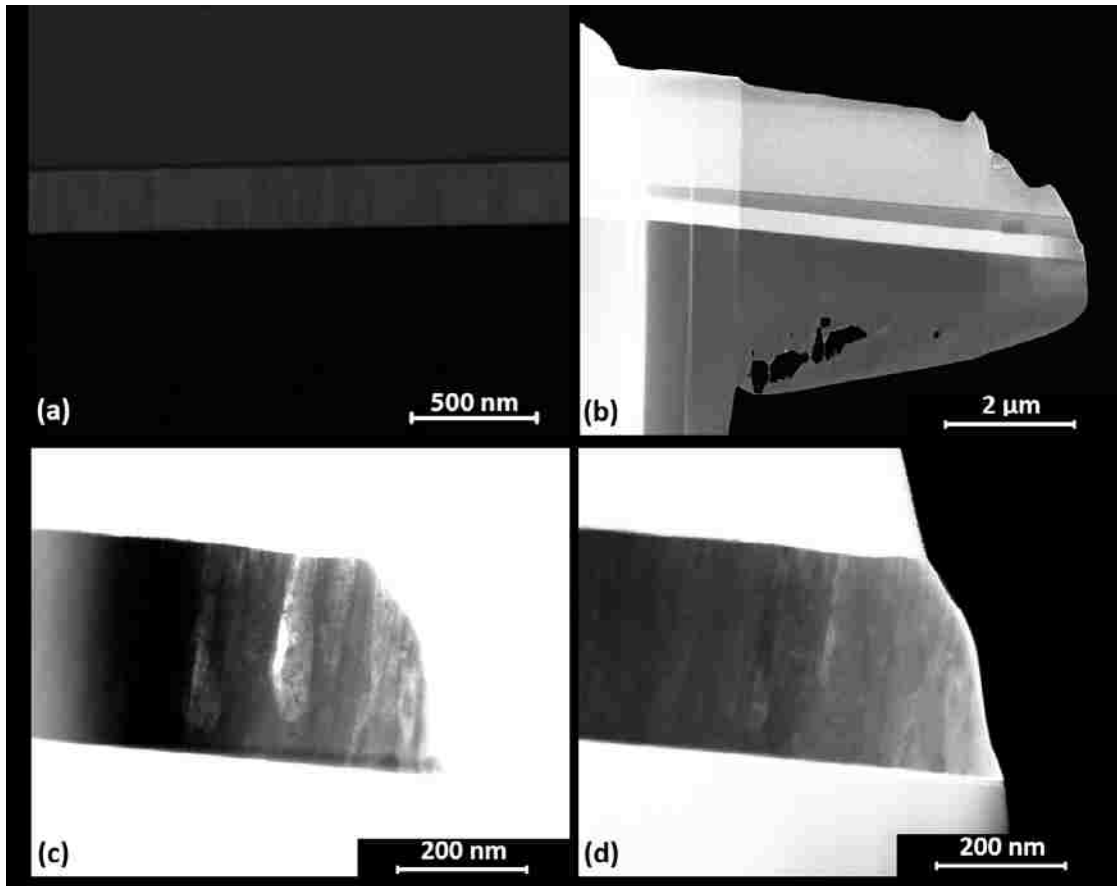


*Figure 5.3. (a) FIB cross section and (b) fabricated lamella of the spot 1 on the thin film sample; (c) and (d) STEM images of film in higher magnification, taken from the same lamella, exhibiting the columnar grain structure in this spot of the film*

In order to better study the structure of the thin film, a FIB lamella was made of spot 1. A FIB cross sectional image of the spot is presented in Figure 5.3.(a). The top layer is the Pt protective film and the bottom layer is the Si substrate. The sputtered film in the middle of the Pt and Si suggests a columnar grain structure, which is not uncommon in thin films fabricated via physical vapor deposition techniques<sup>63</sup>. The columnar grain structure and the single phase identification via XRD suggest that this composition is an ideal candidate for bulk fabrication. The



STEM image on the lamella, made from the same region, confirms the observation of the grain structure in higher magnifications as seen Figure 5.3.(b).

*Table 5.1. Chemical composition and crystal structure of the 2 phases observed in the bulk sample*

Phases	Composition (at. %)					Crystal Structure			
	Os	Ru	W	Mo	Re	a [Å]	b [Å]	c [Å]	
<b>Dendrites</b>	26	13	26	19	16	<b>HCP</b>	2.8	2.8	4.5
<b>Inter-dendrites</b>	19	11	30	27	13	<b>Orthorhombic</b>	7.3	25.3	3.8

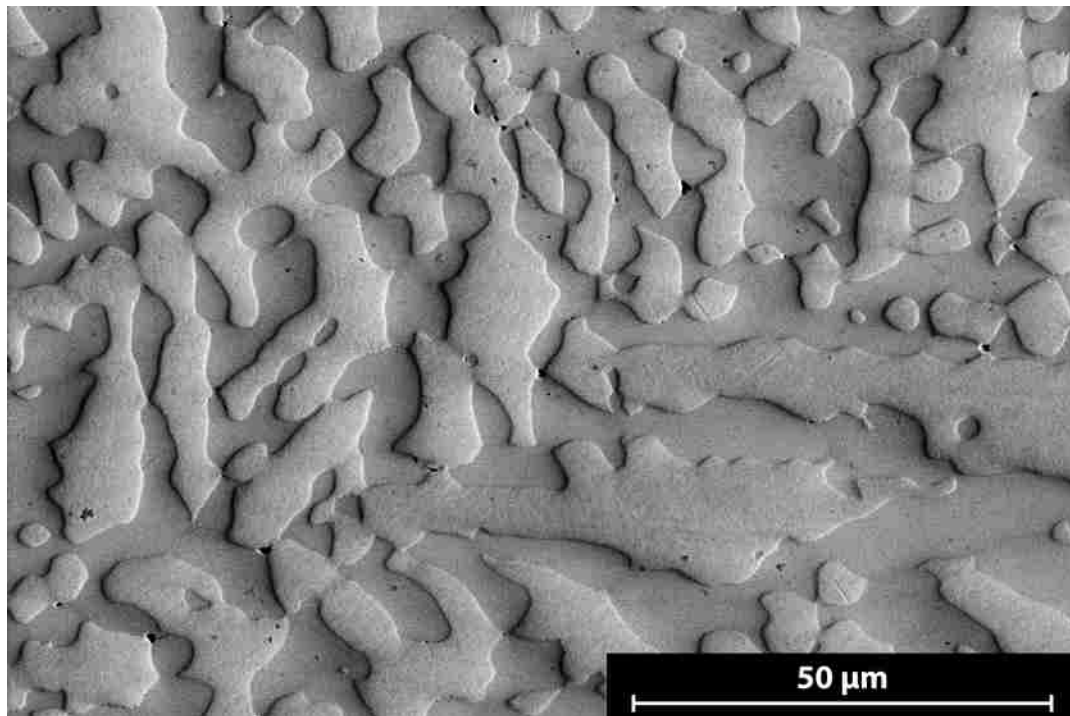


*Figure 5.4. Microstructure of the as-cast bulk sample, exhibiting a dendritic structure*

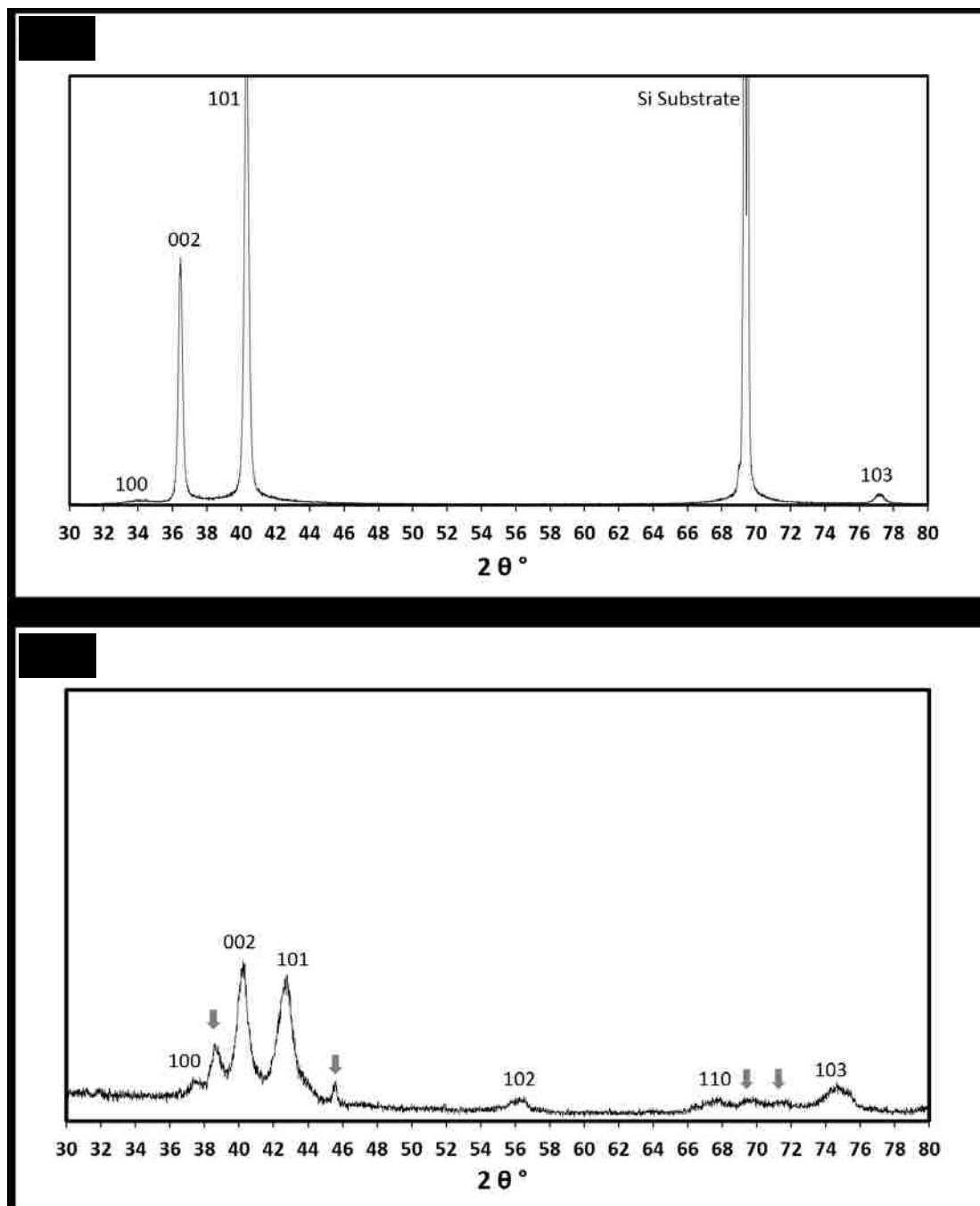
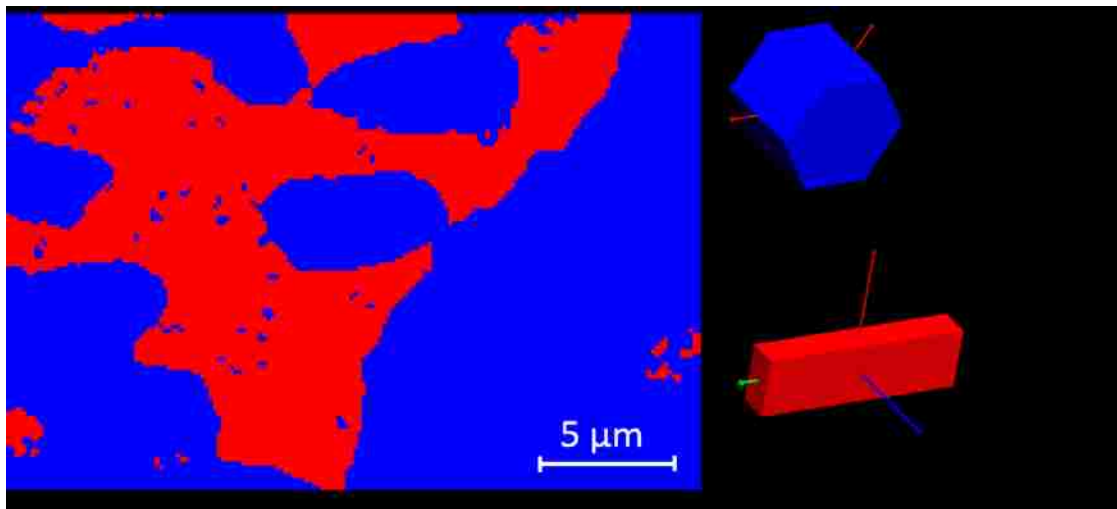


Figure 5.5. Indexed XRD patterns of (a) spot 1 on the thin film sample and (b) the as-cast bulk sample; the peaks marked with arrows represent the second phase in the bulk sample.

Based on the results from the thin film samples, the chemical composition of spot 1 was casted in bulk form via arc melting. The EDS technique was used to confirm the overall chemical composition of the sample to be  $\text{Os}_{23}\text{Ru}_{13}\text{W}_{27}\text{Mo}_{23}\text{Re}_{14}$  (at. %). Considering the precision of the EDS technique, this is similar to the chemical composition of the film. Figure 5.4. presents the SEM micrograph of the as-cast sample after proper metallography sample preparation steps. Even though the samples were not etched, we observed a dendritic structure with the atomic number contrast with indicates lack of chemical uniformity within this sample. Using the spot analysis mode in the EDS software, the chemical compositions of the two phases were analyzed, the results of which are presented in Table 5.1. It must be noted that, the X-ray signal is generated from a larger area than what appears in the 2D SEM image. Therefore, the EDS spot analysis values might vary from the true chemical composition of these two phases. Due to the dendrites' thickness, the x-ray signal might have been generated from a greater depth within the samples. Nevertheless, the 2 phases observed in this bulk sample have different chemical composition.

Figure 5.5. compares the XRD patterns of the spot 1 on the thin film and the corresponding bulk sample. A similar HCP phase was identified and indexed in both the thin film and the bulk sample. However, we also observe a second phase in the bulk sample, which we speculate to be the inter-dendritic phase. Further analysis of the crystal structure of the bulk sample was found to be necessary as we were unable to index the second phase peaks in the XRD pattern. Therefore EBSD data was collected from the 2 phases. Based these results, the dendrites are in fact the HCP

phase with lattice parameters  $a = 2.8 \text{ \AA}$  and  $c = 4.5 \text{ \AA}$ . These crystal structure parameters are the same as the ones calculated from the XRD data. The inter-dendritic region, however, exhibits an orthorhombic crystal structure. (Figure 5.6.) The unindexed peaks in the XRD pattern are due to the x-ray diffraction crystal planes of the secondary orthorhombic phase. Table 5.1. summarizes the chemical composition and structural information of the existing phases in the bulk sample.



*Figure 5.6. EBSD phase map of the as-cast bulk sample showing the multi-phase nature of this sample*

In order to achieve a single-phase structure, further processing is needed in most as-cast alloys<sup>35</sup>. However, for this particular alloy, performing heat treatments is more challenging. The weighted average melting point of this alloy is around 2981 °C based on the melting points of the involved elements. With an assumption that the melting point of this alloy mixture is around the average, for annealing this alloy, temperatures of at least 1800 °C is required. Providing such high temperatures in

controlled atmosphere and over long periods of time was not available in our research group facilities.

#### **5.4. Conclusions**

By fabricating gradient thin films of OsRuWMoRe, we were able to study this alloy family over a wide compositional range. The composition and crystal structure of the film were screened across the substrate, using advanced characterization techniques including EDS and XRD. The single-phase grain structure of the film was confirmed by further characterization of the thin film with the Helios dual beam system. The potential single phase HCP HEA composition was identified as  $\text{Os}_{24}\text{Ru}_{14}\text{W}_{25}\text{Mo}_{23}\text{Re}_{14}$ .

The bulk sample made with the same composition ( $\text{Os}_{23}\text{Ru}_{13}\text{W}_{27}\text{Mo}_{23}\text{Re}_{14}$ ) as the thin film sample was made via arc melting. It exhibited a dendritic structure with HCP dendrites and orthorhombic inter-dendritic phase. Further thermomechanical processing is required to fabricate the predicted single phase HCP HEA in bulk form. Unfortunately, such high temperature equipment was not available in our research lab at the time and we were not able to fabricate a single phase HCP HEA at this time.

## **Chapter 6: Thin Film Combinatorial Approach in Development of a Body Centered Cubic High Entropy Alloy**

### **6.1. Introduction**

High entropy alloys (HEAs) with the body centered cubic (BCC) crystal structure have been an interest to the research community due to their refractory properties<sup>17,18</sup>. Low ductility of the BCC alloys has been well studied in the mechanical behavior research community. However recent literature in the HEA field has observed more ductility in some of the HEAs with BCC crystal structure<sup>58,68,69</sup>. A prospective ductile refractory alloy has potential for promising applications in the industry.

The BCC HEAs usually contain five or six different principle elements of intrinsic metals in the periodic table, with chemical composition of each component in the range of 5-35 at. %. This study focuses on the VNbMoTaW alloy system in order to screen it for potential single phase BCC HEAs. This alloy system has been recognized in the literature by multiple computational researchers<sup>41</sup> to form a single phase solid solution in the equiatomic chemical composition. This composition has been made successfully in bulk form<sup>70</sup>. Minor additions of Ti and Al to this alloy have been explored by the community as well<sup>70</sup>. However, the formation of a non-equiatomic solid solution phase has not been explored, computationally or otherwise.

By screening the gradient film of the VNbMoTaW we would be able to identify potential HEAs with either equiatomic or non-equiatomic chemical compositions.

As previously mentioned in chapter 2, unlike conventional alloys, the HEAs do not have a base element as a solvent, which will complicate the application of conventional development techniques to HEAs. Development techniques of both an exploratory and computational nature have been used to develop new HEAs<sup>7</sup>. However, such techniques require extensive experimental data and are relatively time consuming and expensive.

The combinatorial thin film alloy development process proposed in this project was applied in identification of new BCC HEAs. The idea is to create a 2D gradient of composition in a relatively large area. Each unit of area on this gradient has a different composition, hence a different phase (or phases) which might have a different crystal structure. Therefore, by screening crystal structure over this wide range, one would be able to predict which phases will form at a certain chemical composition. By screening the properties in a similar manner, a thorough understanding of the composition-phase-property relations will be achieved.

## **6.2. Experimental Methods**

In the present work, magnetron sputtering (ORION system, AJA International) was used to fabricate gradient thin films of the VNbMoTaW as a potential alloy

system on single crystal Si wafers. The gradient in composition was achieved by depositing from different sputtering targets orientated at different angles towards the substrate as shown in Figure 6.1. 100, 45, 40, 50 and 100 Watts was used to deposit V, Nb, Mo, Ta and W respectively for 15 mins.

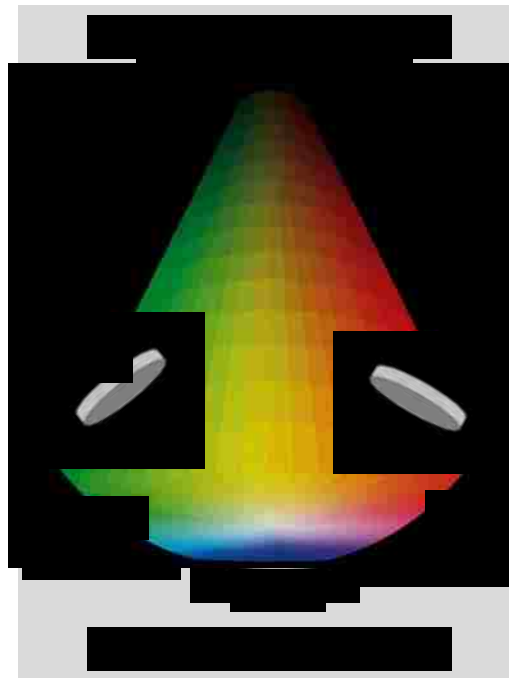


*Figure 6.1. Sputtering target arrangement set-up resulting in a compositional gradient in the fabricated thin films*

Each fabricated specimen was cut into smaller pieces of about 10 x10 mm in size. The chemical composition of each sample was studied by an Oxford X-Max<sup>N</sup> energy dispersive X-ray spectroscopy (EDS) detector on a FEI Helios dual-beam NanoLab 660. In order to investigate the crystal structure of each sample, X-ray diffraction (XRD) technique was used (Siemens D500).



Two set of bulk samples were cast via Edmund Buhler compact arc-melter MAM-1. Each set contain 2 family of alloys: VNbMoTaW and VNbTaW. First set of the samples were 5 g each and the second set were 2.5 g. In order to attain a more uniform sample, the as-cast pieces were flipped and re-melted several times.

The bulk samples were cut in half and studied with scanning electron microscope (SEM), after sample preparation steps including: mounting in epoxy, grinding with SiC paper, polishing with fine diamond solutions and ultra-fine polishing with Buehler Vibromet. The chemical compositions of the samples were confirmed with the EDS technique.

### **6.3. Results and Discussion**

The collected XRD and EDS data from each unit sample of the film is summarized in Figure 6.2. The chemical composition of each element varies through the 76 mm (3 in) diameter of the Si substrate (~10 at. %). Each unit has a different chemical composition and therefore different phases may have been formed. The unique X-ray diffraction pattern of each spot confirms the formation of different phases with different crystal structure within each unit. Multiple spots on this gradient film exhibit a single phase BCC crystal structure in their indexed XRD pattern. It should be noted that the [200] peak does not appear in the XRD patterns of the film due to the highly textured nature of as-deposited thin films. This preferred crystal orientation is also observed in the relative higher intensity of the [110] peak.

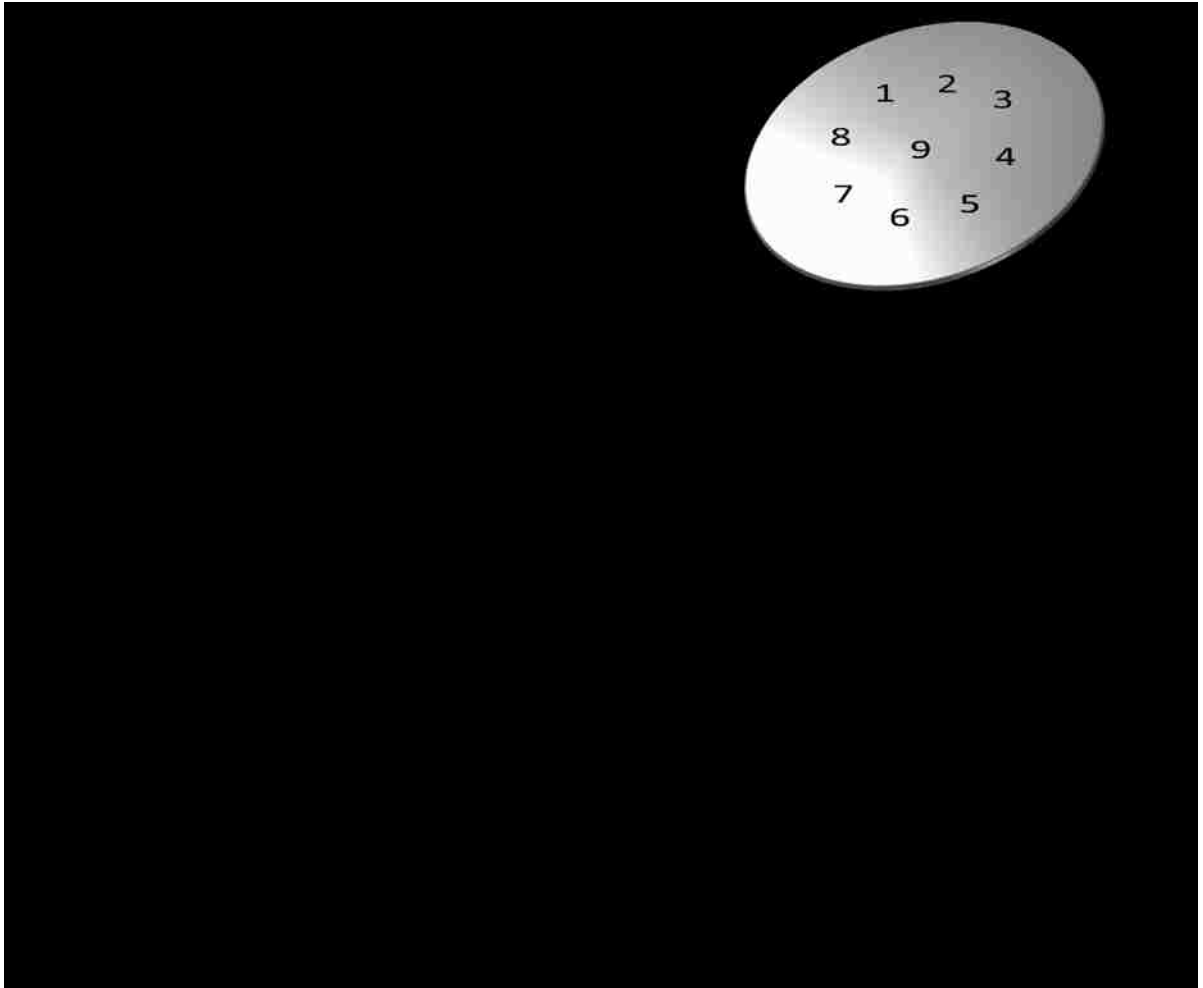


*Figure 6.2. XRD data collected from 9 different spots and their approximate location on the thin film sample*

For the study of VNbMoTaW alloy system we decided to fabricate a bulk sample with chemical composition closer to the equiatomic. The EDS confirmed the composition of the as-cast 5 g sample to be  $V_{21}Nb_{17}Mo_{22}Ta_{21}W_{19}$  (at. %). The deviation from equiatomic chemical composition is most probably due to the nature of mixing process in arc-melting and unavoidable oxidation. The weighting error should not be neglected as well. Figure 6.3. presents the microstructure and the EDS chemical

maps collected from the sample. As the SEM micrograph and EDS maps suggest, the observed structure is not chemically uniform. Some of the Mo, V and Nb contents of the alloy have segregated out of the W-rich phase. V has the lowest melting point among these elements and therefore, unsurprisingly, it has segregated the most compared to the other components. Ta, however, seems to have a more uniform distribution across the sample.

*Table 6.1. The chemical composition (at. %) of 9 different spots on the thin film sample*

<b>Spot</b>	<b>V</b>	<b>Nb</b>	<b>Mo</b>	<b>Ta</b>	<b>W</b>
<b>1</b>	15	14	20	23	28
<b>2</b>	15	17	15	29	24
<b>3</b>	17	16	15	31	20
<b>4</b>	20	14	16	33	17
<b>5</b>	21	11	20	29	19
<b>6</b>	21	9	25	23	23
<b>7</b>	19	10	25	21	26
<b>8</b>	16	11	23	19	31
<b>9</b>	18	13	20	26	24

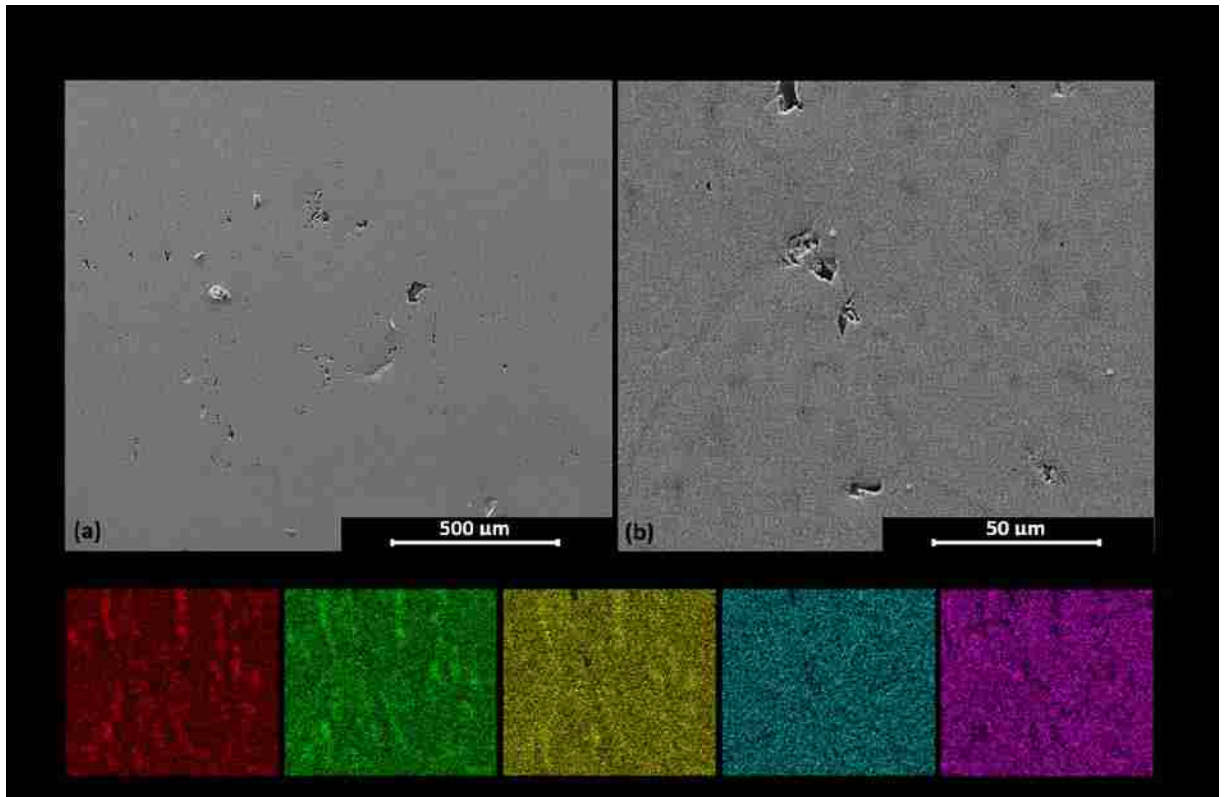


*Figure 6.3. (a) Low, (b) high magnification micrograph of the VNbMoTaW bulk sample and the EDS maps of the same region*

In order to decrease the cooling rate during the solidification process, the second set of samples were made in a smaller scale. The smaller bulk sample of VNbMoTaW weighted around half of the first sample (2.5 g). Figure 6.4. presents the SEM micrographs of this sample at low and high magnifications. The samples were not chemically or otherwise etched, however a grain looking structure is observed across the sample. It should be noted that there are some contamination on the surface of the sample due to the insufficient sample cleaning set. Long ultrasonic bath in ethanol is suggested to avoid such contaminations from the lab environment in the future.

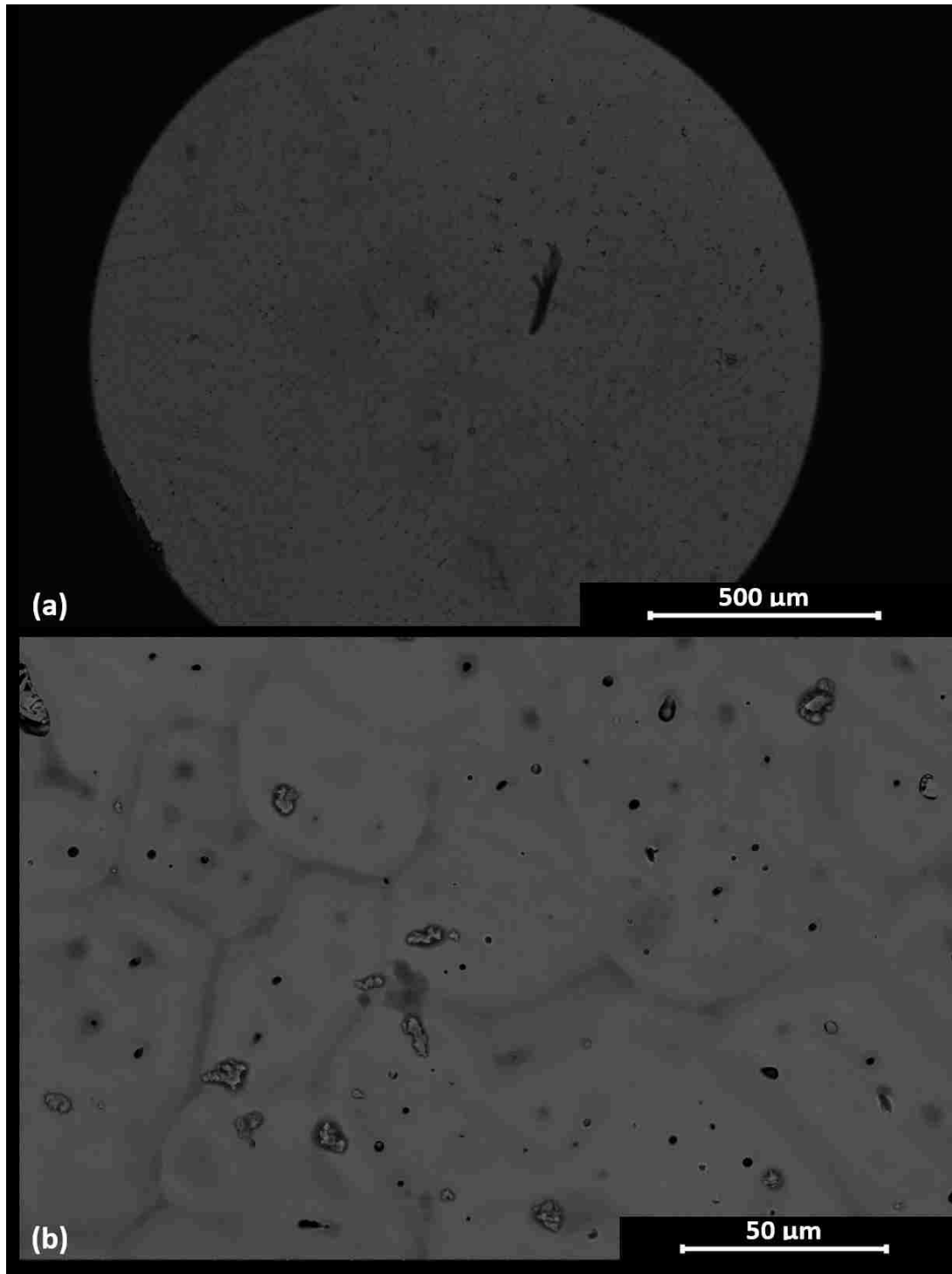


*Figure 6.4. (a) Low and (b) high magnification micrographs of the 2.5 g VNbMoTaW bulk sample after hot rolling*

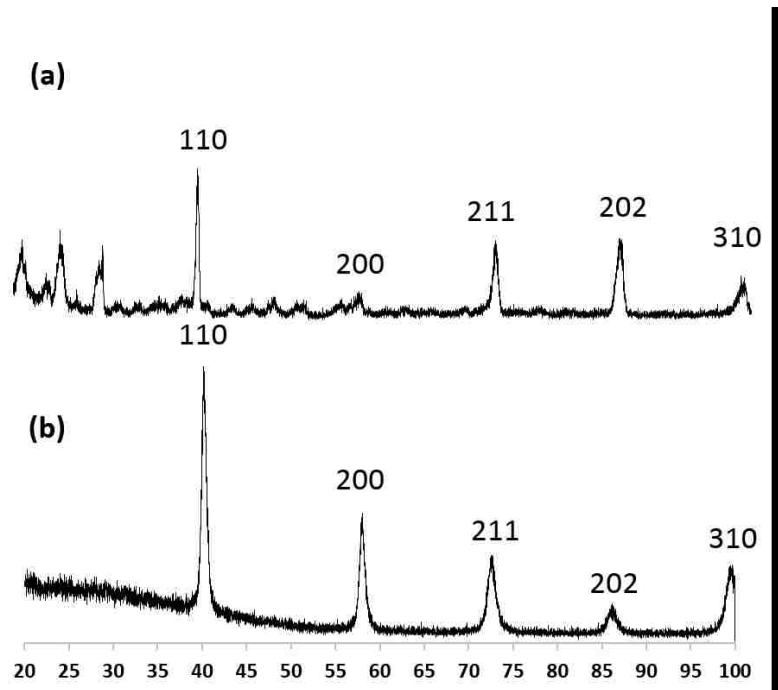


*Figure 6.5. XRD data collected from (a) 5 g as-cast and (b) 2.5 g VNbMoTaW samples*

The XRD pattern of both of the bulk samples is presented in Figure 5.5. Even before indexing, an experienced eye would recognize the existence of multiple phases in the XRD pattern of the 5 g as-cast sample. One BCC phase was identified and indexed as seen in the figure. Due to the low angle peaks of the secondary phase, it might be an intermetallic or an oxide phase. The XRD pattern (b) (the 2.5 g sample), in the other hand, confirms the existence of a BCC phase in the sample. There is no evidence of a secondary phase in this XRD pattern in this angle range.

EDS maps were collected from the 2.5 g VNbMoTaW bulk sample. (Figure 6.6.) Even though the XRD data confirmed the formation of a single phase BCC alloy, the EDS maps shows lack of chemical homogeneity. Similar to the 5 g sample,

chemical segregation is observed in this sample. V, Nb and Mo are segregating in the grain boundary areas. In order to achieve a chemically uniform structure for this alloy, further thermomechanical processing or modification to the casting process is recommended.

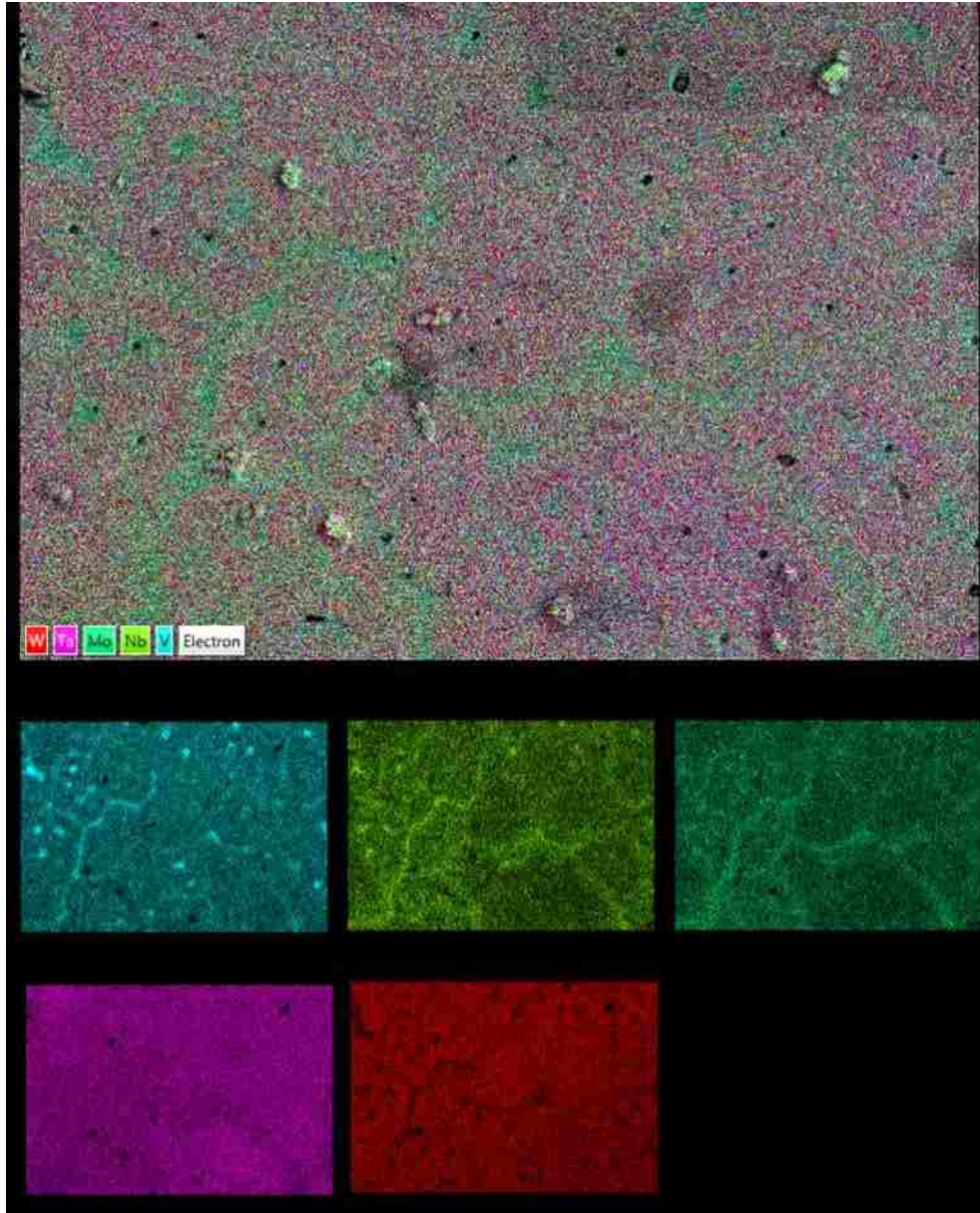


*Figure 6.6. EDS maps of the 2.5 g VNbMoTaW bulk sample*

The VNbTaW alloy system was studied in this project as well. We fabricated a bulk sample with no Mo and twice Nb compared to the VNbMoTaW samples. A similar crystal structure is expected in these alloys as we speculate that the Nb atoms would replace the Mo atoms in the crystal structure. The EDS confirmed the chemical composition of both of the fabricated bulk samples (5 and 2.5 g) as  $V_{21}Nb_{40}Ta_{20}W_{19}$ .

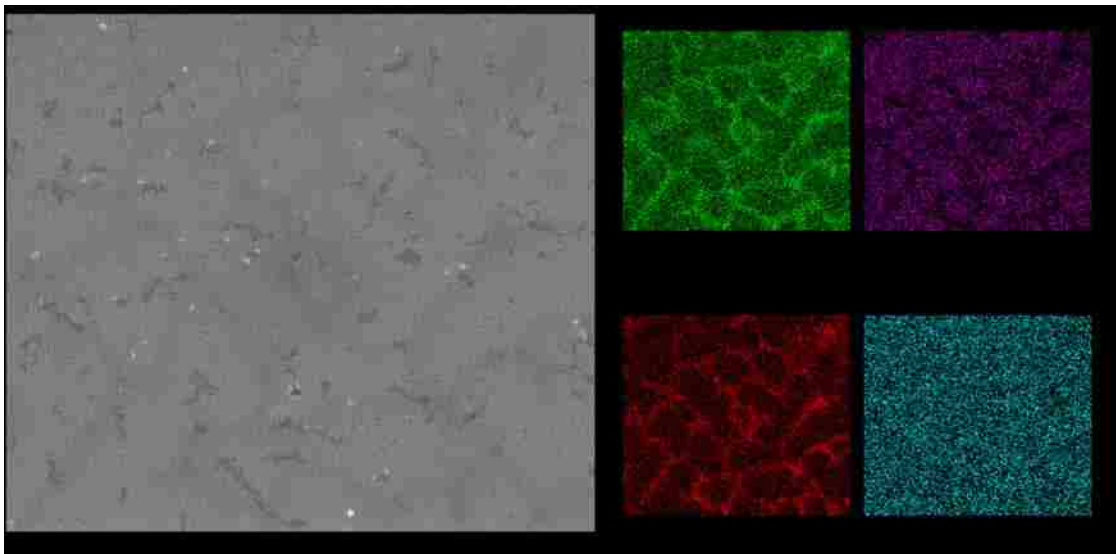


*Figure 6.7. EDS maps of the as-cast 5 g VNbTaW sample*

The EDS map of the as-cast 5 g bulk sample show a dendritic structure with an inhomogeneous chemical composition. (Figure 6.7.) On other hand, the 2.5 g sample shows a single phase BCC crystal structure in both the XRD and the SEM images in Figure 6.83 and 6.9. However, similar to the 5 component sample, EDS maps show segregation of the atoms close to the grain boundaries.



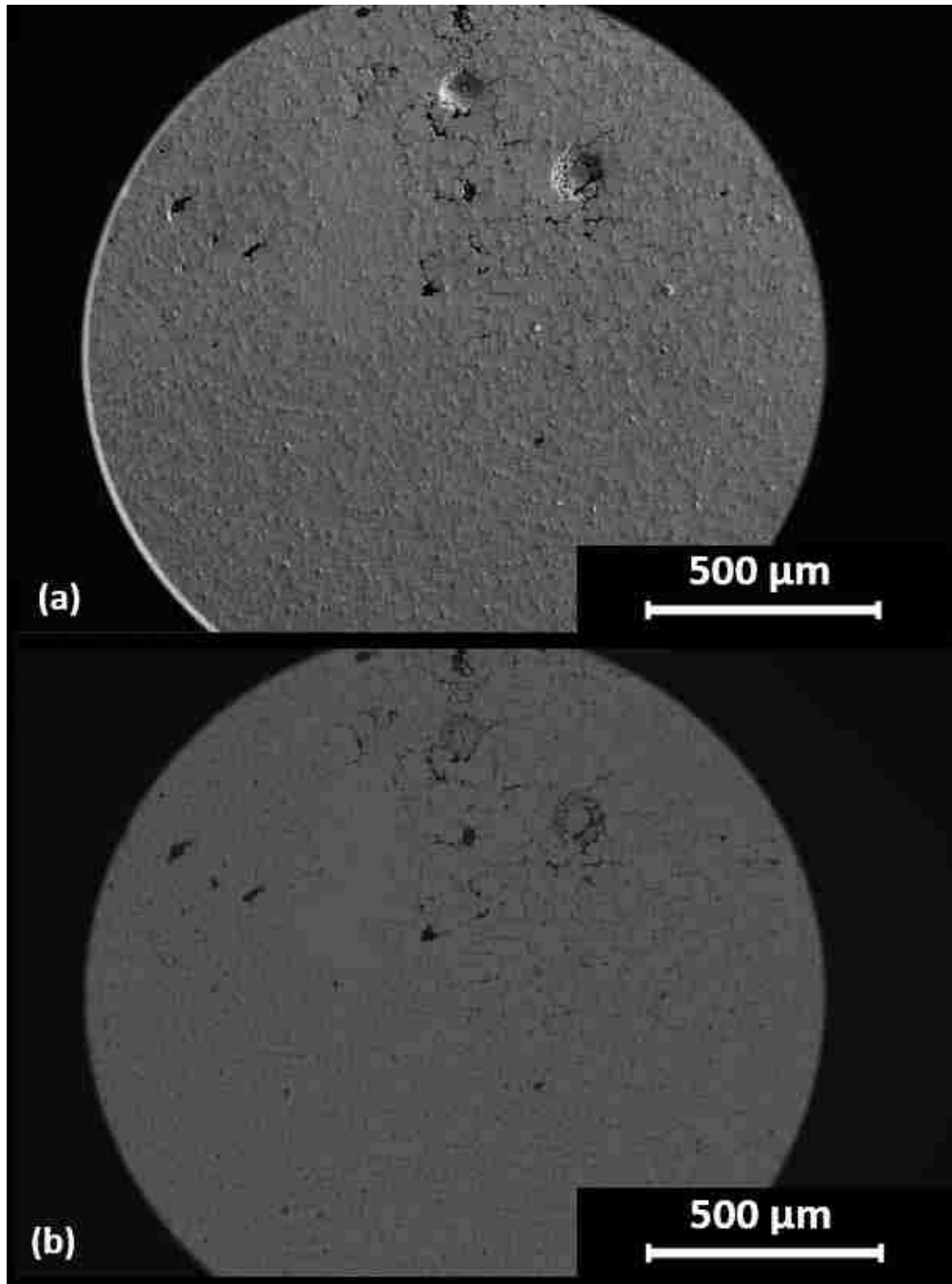


*Figure 6.8. Micrographs of the VNbTaW sample post thermomechanical processing*

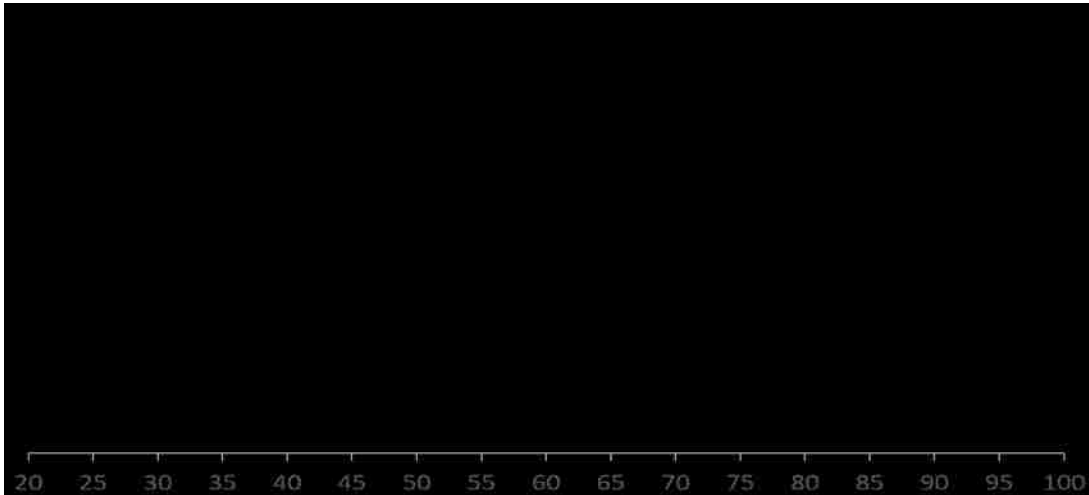


*Figure 6.9. XRD data collected from (a) 5 g as-cast and (b) 2.5 g VNbTaW samples*

#### **6.4. Conclusions**

By applying the combinatorial thin film approach to the VNbMoTaW alloy system, multiple non-equiatomic potential BCC HEAs were identified. Bulk samples of  $V_{21}Nb_{17}Mo_{22}Ta_{21}W_{19}$  and  $V_{21}Nb_{40}Ta_{20}W_{19}$  were fabricated via arc-melting. Even though a single phase BCC was observed via XRD in both alloys, further processing of the fabricated  $V_{21}Nb_{17}Mo_{22}Ta_{21}W_{19}$  and  $V_{21}Nb_{40}Ta_{20}W_{19}$  alloy systems is necessary to achieve a homogenous uniaxial grain structure. Heat treatments that involve isotactic pressure at high temperatures are recommended. Ongoing research in Dr. Balk's research group will attempt this step for this group of alloys as well as other alloy systems with high melting point elements.

## **Chapter 7: Multilayer Thin Film Approach in Development of a Face Centered Cubic Alloys**

### **7.1. Introduction**

Magnetron sputtering is a physical vapor deposition (PVD) technique that is commonly used to fabricate metallic thin films<sup>63</sup>. However, such film fabrication set ups usually have only a few number of target placements from which the alloying components are sputtered. This limited number of sputtering targets introduces challenges in sputtering multicomponent alloy films and in particular high entropy alloys (HEAs), which usually contain 5 or more alloying elements.

This chapter suggests the multilayer fabrication technique as a promising solution to the challenges of sputtering alloys with higher numbers of components. In this method, each element is individually sputtered as a layer onto the substrate, followed by high temperature annealing of the layered film. The goal is to achieve a uniform alloy across the film thickness. The higher temperatures and appropriate annealing times provide an ideal diffusion space for the atoms of the elements to form an alloyed film<sup>35,63</sup>.

A CrFeCoCuNi alloy system is a promising candidate for application of the multilayer alloy technique. For this project, Cu, Co, Fe and Cr were deposited on a Ni substrate in that order. This order of deposition was decided based on the binary phase


diagrams of the elements. Cu and Ni form a single-phase solid solution over a wide compositional range. Co and Fe tend to form a solid solution as well. Cr was chosen to be the top surface layer due to its better oxidation resistivity. This multilayer thin film technique applied to CrFeCoCuNi alloy system may result in identification of HEAs with both equiatomic and non-equiatomic chemical composition.

## **7.2. Experimental Methods**

The thin films were fabricated by Magnetron sputtering (ORION AJA International) from pure elemental targets of Cr, Fe, Co and Cu on a Ni substrate. The base pressure was around  $10^{-6}$  Pa and the sputtering was done over Ar flow of around 0.3 Pa. In the first set of the samples, in order to achieve the layered structure, we sputtered about 15 to 20 min from each elemental target with 100 Watts power for each target. For annealing, some of the samples were kept in the high vacuum and the temperature was raised to 500 °C at the rate of 50 °C/min. After 2 hours of annealing, the temperature was decreased to room temperature with the same rate. During both the deposition and the annealing processes the substrate was rotating in order to maintain the uniformity. For the second set of the samples Fe, Co, Ni and Cu sputtering targets were used at 100 Watts power to fabricate the samples. In this series of samples, multiple layers were deposited from each target on to Si wafers as substrate. Base on the previously measured sputtering rates, the sputtering time for each layer was adjusted to have 20 nm thick layers in the first set and 100 nm thick

layers in the second set. Table 7.1. summarized the deposition steps for these samples. The sputtering was followed by the same annealing processes.

*Table 7.1. Order of deposition in the second set or the thin film samples*

In order of deposition 	<b>Cu</b>	<b>Ni</b>	<b>Co</b>	<b>Fe</b>	
First set of layers	1' 30"	3' 45"	2'	3' 45"	Repeated 3 times
Second set of layers	7' 30"	18' 10"	10'	18' 10"	

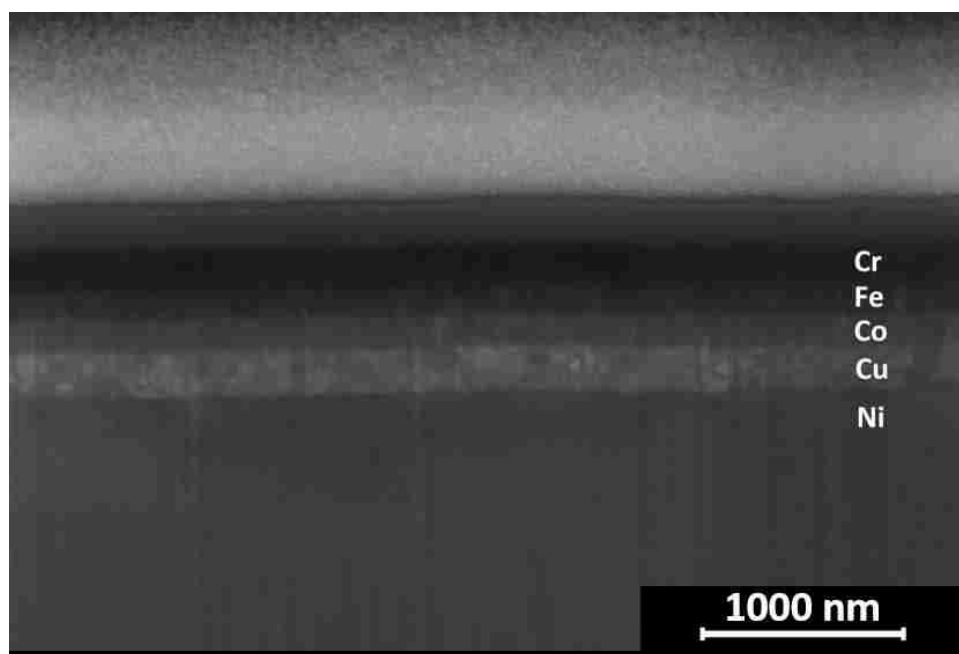
Both sets of the samples were then cut into 10x10 mm pieces for further analysis with the FEI Helios NanoLab 660 before and after annealing. Using the focused ion beam (FIB) capabilities on the system, a protective Pt layer was deposited, followed by a cross sectional cut into the sample to expose the layered film. For the annealed films, the other side of the Pt-protected area was milled as well. Using the micro-manipulator, the fabricated lamella was lifted out and reattached to a Cu grid by Pt welding. After performing some low voltage cleaning steps with the FIB, more images and energy dispersive spectroscopy (EDS) data was collected from the lamella using the Oxford X-Max<sup>N</sup> detector.

The lamella was further milled using the FIB to a thickness transparent to the electron beam. The sample was sent to the FEI research center to be characterized by FEI Talos transmission electron microscopy (TEM). Bright field (BF) and dark field

(DF) images as well as a diffraction pattern and EDS maps was collected from the sample.

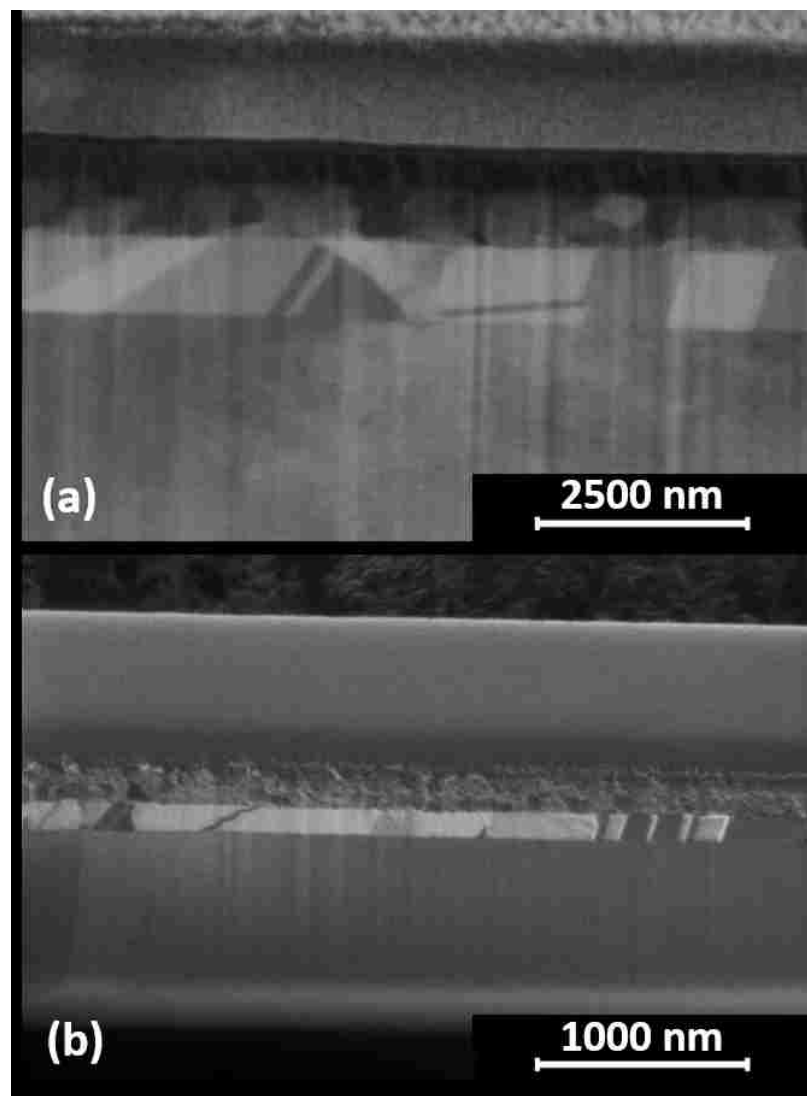
### 7.3. Results and Discussion:

Figure 7.1. presents an electron image of the FIB cross section of the first set of the thin film samples. The top 2 layer in the figure are the protective Pt deposited in the Helios with electron beam and the ion beam. The 4 deposited layers of Cr, Fe, Co and Cu are clearly distinguishable on the Ni substrate. The thickness of each layer is around 200 nm.



*Figure 7.1. The FIB cross section of the as-deposited layered thin film.*

An identical sample was annealed at 500 °C in the vacuum. As a result it formed 3 new layers as shown in Figure 7.2. In this figure 2 different contrast of the sample is presented collected with electron beam and the ion beam. In both of the images, a clear grain structure is observed in all the layers which suggest formation of new alloy systems as a result of annealing processing of the deposited layers.



*Figure 7.2. FIB cross sectional images of the post annealing sample via (a) electron beam and (b) ion beam*

A thin lamella of the same region was fabricated using the FIB. EDS data was collected from the lamella. The collected x-rays from the lamella are generated from a much smaller volume compared to the bulk sample. By collecting the EDS from a lamella rather than the bulk, we were able to increase the spatial resolution of the technique through reducing the size of the electron beam interaction volume with the sample material.

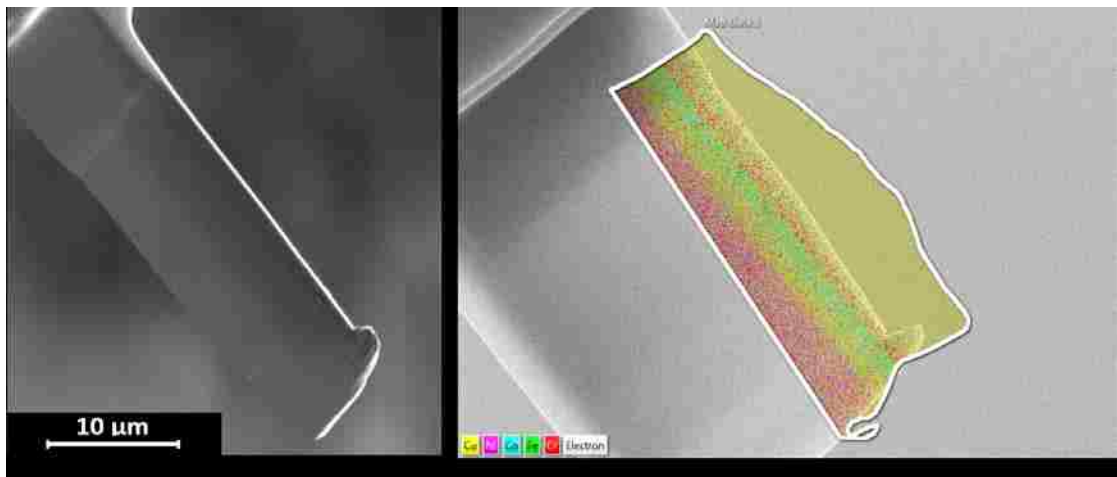


*Figure 7.3. Thin lamella of the annealed film and the EDS map collected by the Helios*

Based on the EDS results from the Helios in Figure 7.3. the top Cr layer did not diffuse within the film after the annealing process. However, the other 2 layers, which formed post annealing, show signs of significant diffusion. Even by collecting the EDS data from the lamella, the spatial resolution is insufficient to distinguish the chemical composition of the alloyed layers with high precision. Therefore further investigation with TEM was found to be necessary to have a better understanding of the alloying process of the multilayer film.



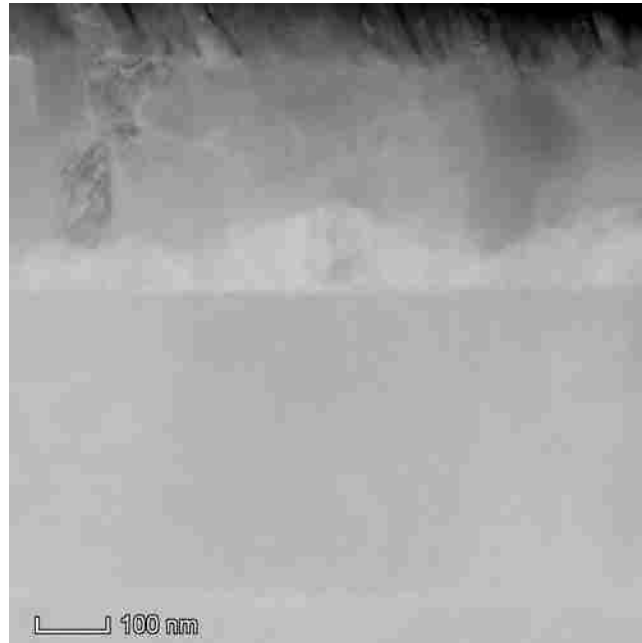


*Figure 7.4. Electron image and the EDS map collected from the alloyed sample by the Talos TEM*

Figure 7.4. presents a more detailed EDS maps collected by the Talos. The top Cr layer is observed clearly in this map similar to the map collected by the Helios.

However, the non cr-containing layers do not appear to be as well alloyed as previously thought. Due to the higher resolution of these maps, we can observe the diffusion of the Fe and Co layer into one another post alloying. The Ni substrate in the other hand has not diffused as much in to the deposited layers.

A high resolution BF TEM image and the corresponding selected area diffraction pattern (SDP) of the alloyed Fe/Co layer is presented in Figure 7.5. The SDP is indexed as  $[1\bar{1}1]$ . Considering the Fe-Co phase diagram and Co solubility in BCC Fe over a wide compositional range, we speculate that the crystal structure resulting from this mixture is in fact a BCC.

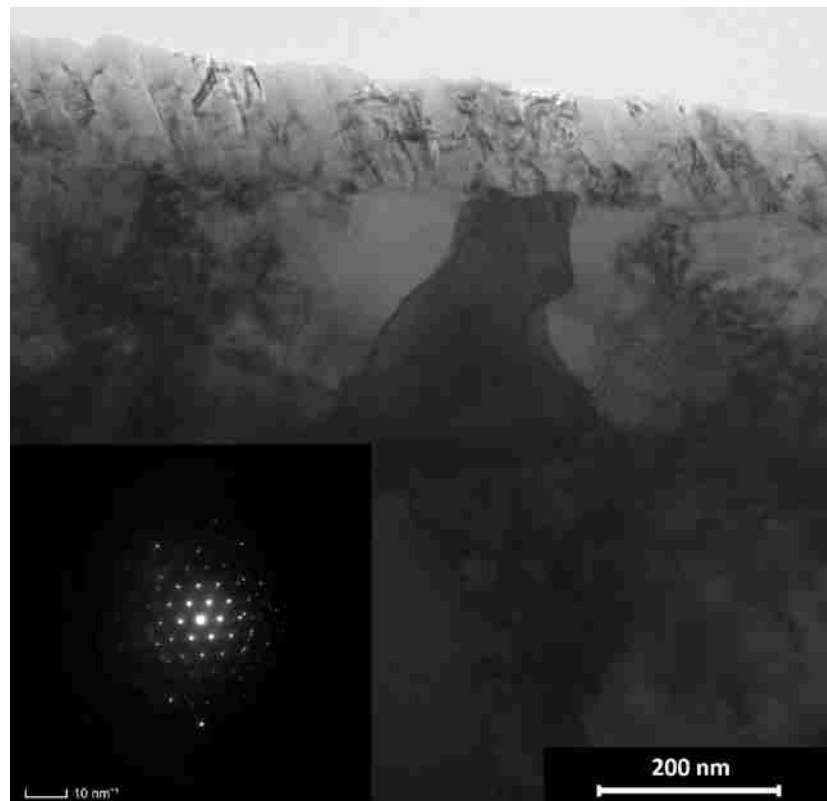


*Figure 7.5. BF TEM image of the post annealing sample and the SDP*

Figure 7.6. presents the FIB cross sectional images of both as-deposited and post annealed samples from the second set of thin film samples. The distinctive layers of the deposited film are observed in the images similar to the first set of the samples. The deposition time for each layer was reduced which resulted in layers with decreased thicknesses. However, by repeating the sputtering multiple times, we were able to achieve a similar overall thickness to the first set of the samples.

The diffusion distance for the atoms in these samples are significantly decreased as the thickness of each layered is reduced. Therefore, a more homogenous structure was expected after annealing. The Figure 7.6. (b) shows the post annealing FIB cross sectional image. The grain growth, observed in the top layers of the film, makes this annealed film a promising alloy sample. However, it can be observed from the figure that the overall thickness of the film has increased. In some areas the film has diffused into the substrate and we speculate that some material from the substrate has diffused into the film. This unexpected phenomenon can be explained by the Si-Cu phase diagram. For a relatively wide composition range, Cu and Si form a solid solution. This tendency of mixing in Si and Cu has affected the results of this study and this film is no longer a FeCoNiCu alloy.

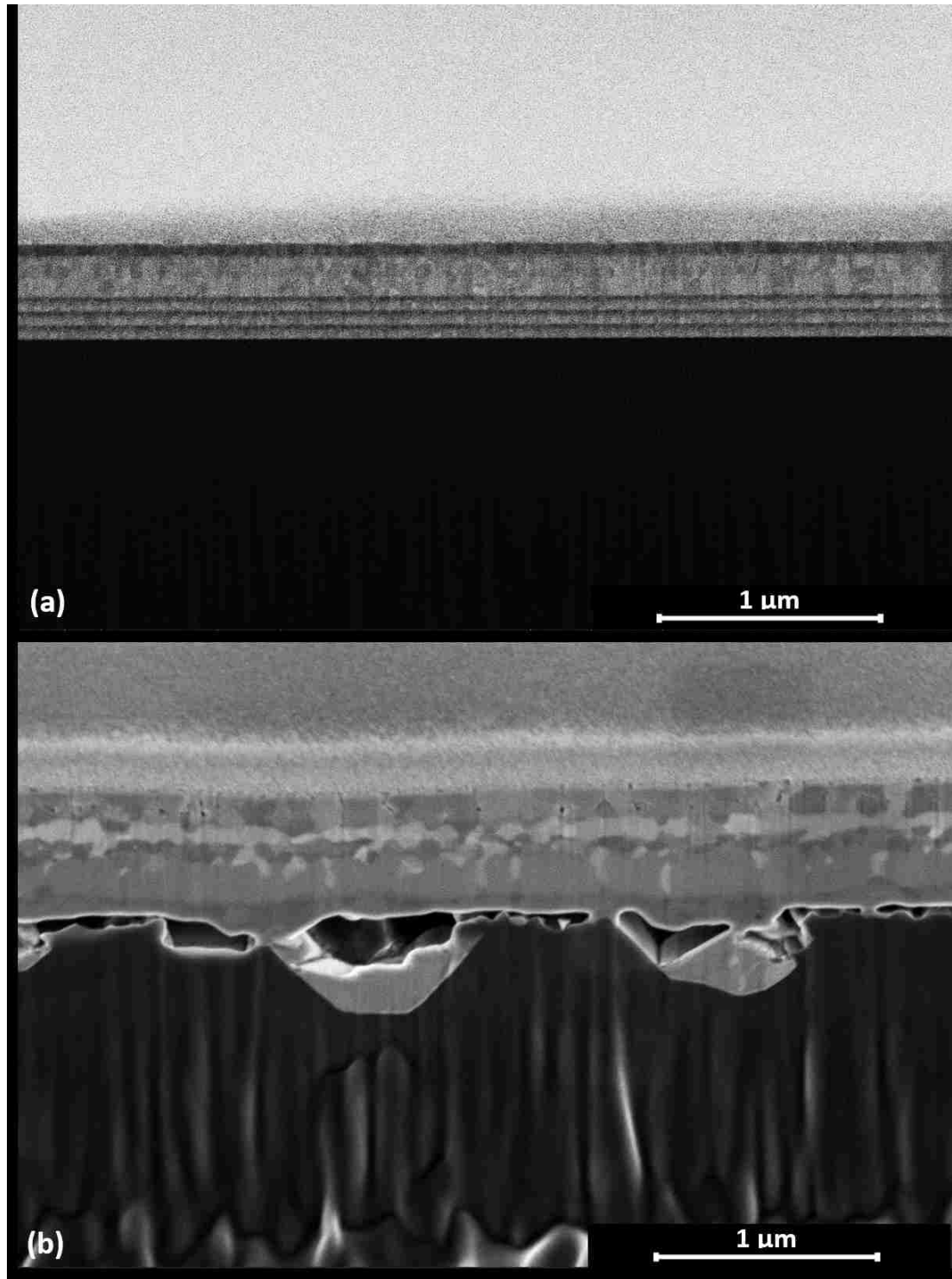


*Figure 7.6. Multilayer sample (a) before and (b) after annealing*

#### **7.4. Conclusions**

While this multilayer technique failed to achieve a single-phase multicomponent alloy, it provided base for investigation of similar layering alloying techniques. For instance, depositing thinner individual layers repetitively will provide a smaller diffusion distance for the atoms of the involved elements. This would potentially enable us to fabricate a well-mixed and relatively more homogenized alloy film post annealing.

## Chapter 8: Conclusions and Continuing Work

This project successfully applied a thin film combinatorial approach as a more efficient experimental method to developing new high entropy alloy (HEA) alloy systems. In order to study HEA systems with different crystal structures, nominal HEA compositions were selected, including: OsRuWMoRe to obtain hexagonal closed packed (HCP), CoFeMnNiCu in order to achieve face centered cubic (FCC) HEA and VNbMoTaW in an attempt to form a body centered cubic (BCC) crystal structure. Thin film samples were fabricated by simultaneous magnetron sputtering of the elements onto silicon wafer substrates. This arrangement yielded a chemical composition gradient in the films which ultimately resulted in the formation of various phases. Some of these phases exhibited the desired single-phase HEA, albeit with non-equiatomical chemical compositions. Bulk samples of the identified HEA compositions were prepared by arc melting mixtures of the metals. Microstructure of both thin film samples and bulk samples were characterized via scanning electron microscopy (SEM), focused ion beam (FIB) and energy dispersive x-ray spectroscopy (EDX). The crystal structures of the samples were studied by X-ray diffraction (XRD) and electron backscattered diffraction (EBSD) technique. Applying Nano-indentation technique, the mechanical properties of some of the samples were screened over the composition gradient as well.

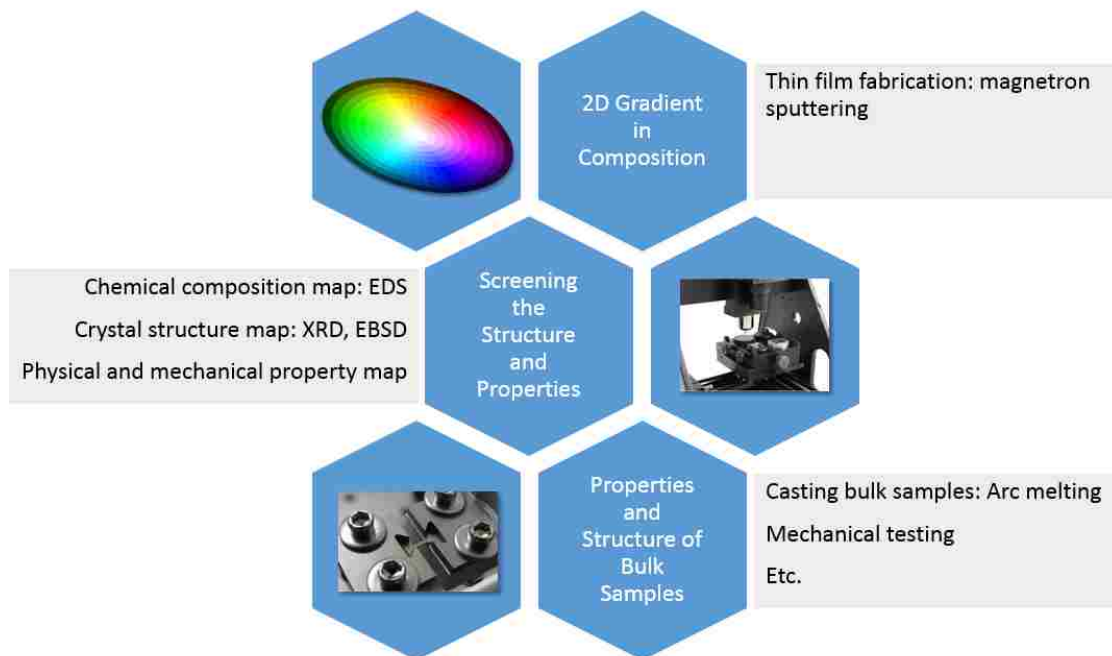


*Figure 8.1. Illustration summarizing the combinatorial thin film approach*

By applying this combinatorial thin film approach to the MnFeNiCoCu alloy system, a single-phase FCC HEA was identified as  $\text{Mn}_{30}\text{Fe}_{20}\text{Co}_{20}\text{Ni}_{15}\text{Cu}_{15}$ . The alloy was fabricated in bulk form via arc-melting. In order to achieve the desired uniaxial grain structure, the casting procedure was followed by thermomechanical processing.

Similarly, a potential HCP HEA was identified from the application of the thin film approach to the OsRuWMoRe alloy system. The  $\text{Os}_{23}\text{Ru}_{13}\text{W}_{27}\text{Mo}_{23}\text{Re}_{14}$  was successfully casted in bulk form; however, we were not able to thermomechanically processes it due to the higher melting points of its components. Therefore, the ideal grain structure was not achieved for this alloy.

After applying the combinatorial thin film approach to the VNbMoTaW alloy system, multiple single phase BCC alloys were identified. The  $V_{21}Nb_{17}Mo_{22}Ta_{21}W_{19}$  and  $V_{21}Nb_{40}Ta_{20}W_{19}$  alloy systems were fabricated in bulk form via arc-melting. Performing the thermomechanical processing, we were able to achieve a single phase BCC structure in both alloys, however, the EDS maps showed chemical segregation. Further processing is required to obtain a chemically uniform structure for these alloys.

The bulk samples of the identified alloys can be used for further investigation of their properties. For instance, dog bone specimens of the fabricated samples can be machined to be used in tensile testing set up for a more in depth study of the mechanical properties of the alloys. Due to the size of the arc-melted samples, micro tensile testing is recommended. Such equipment is available in Dr Balk's research group at the University of Kentucky. (Figure 8.2.) The properties of the materials in thin film form may be vary from those of the bulk form due to the size effect. Therefore, the collected data from bulk samples are particularly important in predicting the material's behavior in the actual applications.

Multiple HEAs were detected and successfully produced in bulk form applying the combinatorial thin film approach. This experimental approach proved to be more efficient in identifying new alloy systems than conventional exploratory development methods. The combinatorial thin film approach can potentially be applied in the development of alloy systems of various natures. Using this approach, the



development process can be modified to be more efficient and reduce the costs of research and development in alloy industries. Additionally, by screening the properties of the compositionally gradient thin films, more in depth information about the alloy candidates can be provided. For instance, the mechanical and/or environmental properties can be screened over the chemical composition of the alloy system.

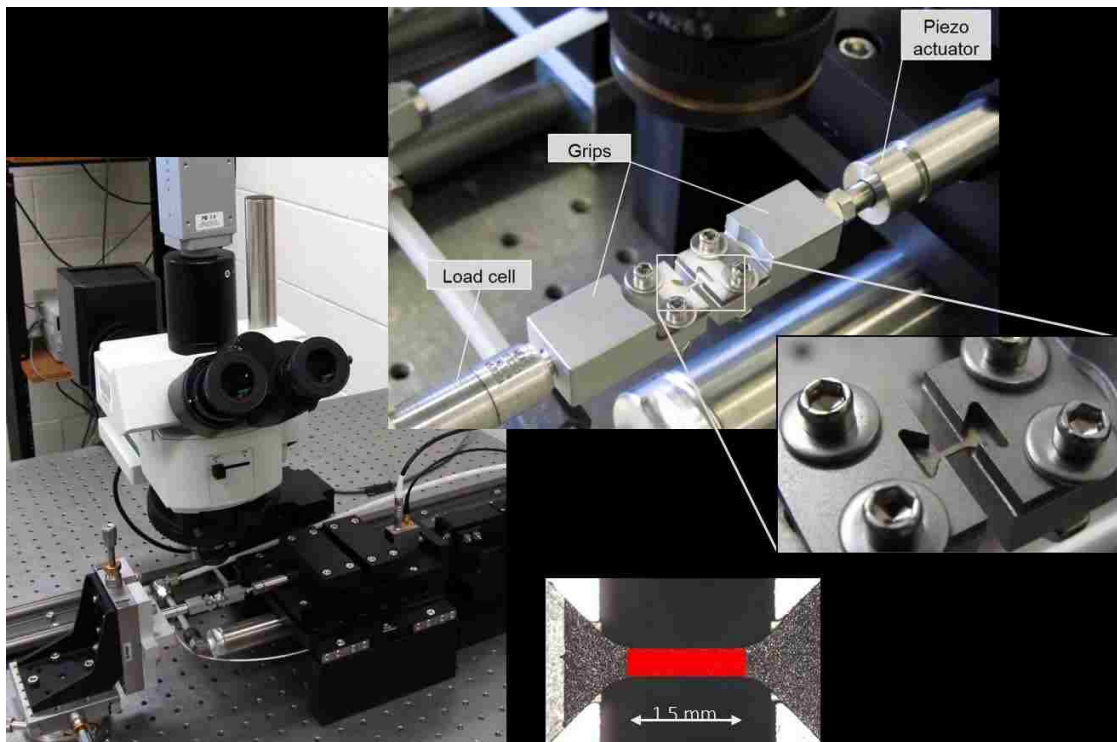


*Figure 8.2. Micro specimen test set-up available in Dr. Balk's research group at the University of Kentucky<sup>11</sup>*

As suggested in chapter 4, Nano indentation is a great tool in screening the mechanical properties of materials in thin film form. The environmental properties, such as corrosion and oxidation resistance, can be screened as well over the thin film gradient by a simple corrosion test. This additional screening step was recommended

by Dr Dan Miracle in the U.S. air force laboratory. This complimentary information provides a thorough understanding of the relationship between the chemical composition, crystal structure and properties of the alloy system, which is very valuable in the process of designing materials for specific applications.

## **Appendix A**

### **Muti-component thin film samples fabricated for this project in Dr Balk's Research Group**

#### **Alloy with HCP crystal structure:**

OsRuWCo

OsRuWMoRe

OsRuWNb

OsRuWIr

OsRuMoRe

#### **Alloys with FCC crystal structure:**

CrMnFeCoNi

CrMnFeCoNi

CrFeCoNiCu

MnFeCoNi

FeCoNiCu

#### **Alloys with BCC crystal structure:**

TiZrNbHfTa

TiZrNbHfTa

TiVNbMoTa

VNbMoTaW

VMoTaW

VNbTaW

## Appendix B

	Atomic Number	Atomic Weight	Crystal	$\rho$ (g/cm <sup>3</sup> )	$T_m$ (C°)
	(Z)	(A)	Structure		
<b>V</b>	23	51	BCC	6.11	1910
<b>Mn</b>	25	55	BCC	7.47	1246
<b>Fe</b>	26	56	BCC	7.87	1538
<b>Co</b>	27	59	HCP	8.9	1495
<b>Ni</b>	28	59	FCC	8.9	1455
<b>Cu</b>	29	64	FCC	8.96	1084
<b>Nb</b>	41	93	BCC	8.57	2477
<b>Mo</b>	42	96	BCC	10.28	2623
<b>Ru</b>	44	101	HCP	12.45	2334
<b>Ta</b>	73	181	BCC	16.65	3017
<b>W</b>	74	184	BCC	19.25	3422
<b>Re</b>	75	186	HCP	21.2	3182
<b>Os</b>	76	190	HCP	22.59	3072

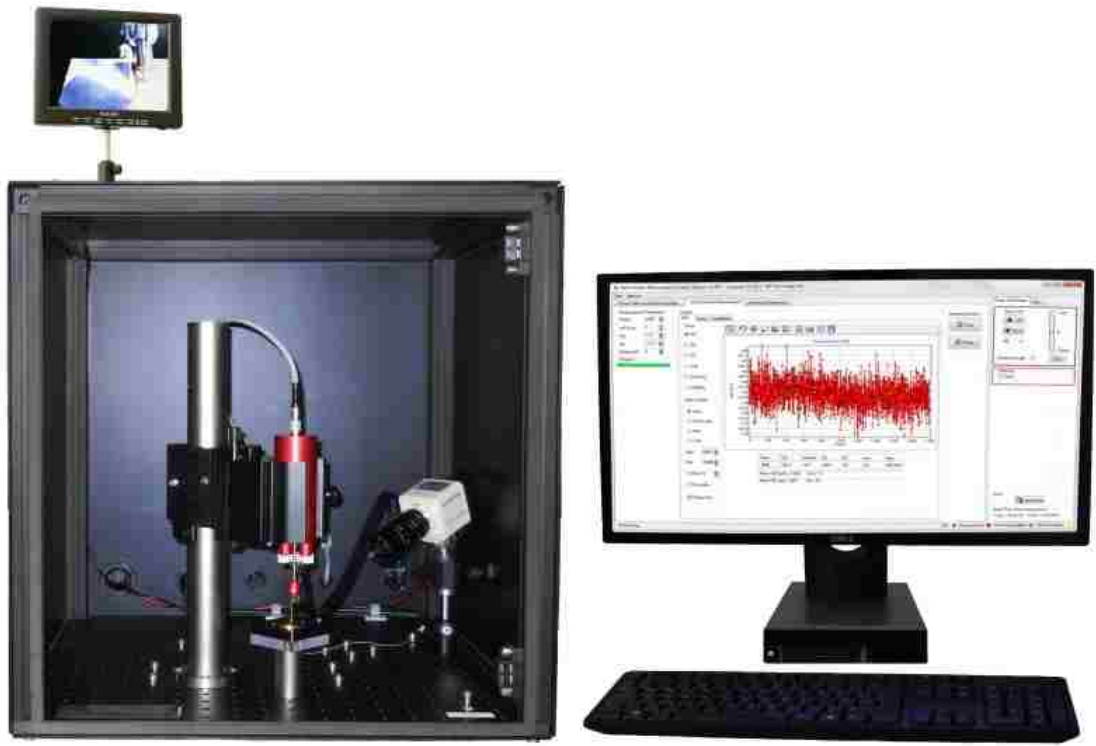
## **Appendix C**

### **Screening Work Function across Gradient Thin Film**

Work function is defined as the minimum amount of energy needed to remove an electron from a solid material in vacuum just outside the surface. It should be noted that work function is a physical property of the surface and even though it strongly depends on the material, it is not a characteristic of the bulk material.

The Kelvin Probe system can provide precise and localized measurements of the work function. The figure presents the system that we have in our research lab. This technique is very surface sensitive, which makes it ideal for thin film samples. Considering that it is also very localized, it could potentially screen the work function across a compositionally gradient film.

The MnCoFeNiCu thin film gradient was screened across 9 spots using the Kelvin Probe. However, no significant changes were observed in the measurements of these 9 spots. We speculate that contamination on the film's surface is the reasoning behind these results. Further investigation of work function measurements is outside the scope of this project, but is strongly recommended for future work.



## References

1. Murty, B. S., Yeh, J. W. & Ranganathan, S. A Brief History of Alloys and the Birth of High-Entropy Alloys. *High Entropy Alloy*. 1–12 (2014). doi:10.1016/B978-0-12-800251-3.00001-8
2. Zhang, Y. *et al.* Microstructures and properties of high-entropy alloys. *Prog. Mater. Sci.* **61**, 1–93 (2014).
3. Paul, A. Comments on “Sluggish diffusion in Co–Cr–Fe–Mn–Ni high-entropy alloys” by K.Y. Tsai, M.H. Tsai and J.W. Yeh, *Acta Materialia* 61 (2013) 4887–4897. *Scr. Mater.* **135**, 153–157 (2017).
4. Dean, S. W., Zhang, Y., Chen, G. L. & Gan, C. L. Phase Change and Mechanical Behaviors of  $Ti_xCoCrFeNiCu_{1-y}Al_y$  High Entropy Alloys. *J. ASTM Int.* **7**, 102527 (2010).
5. Murty, B. S., Yeh, J. W. & Ranganathan, S. High-Entropy Alloys. *High Entropy Alloy*. **5**, 13–35 (2014).
6. Yeh, B. J. *et al.* Nanostructured High-Entropy Alloys with Multiple Principal Elements: Novel Alloy Design Concepts and Outcomes \*\*. 299–303 (2004). doi:10.1002/adem.200300567
7. Zhang, Y., Yang, X. & Liaw, P. K. Alloy design and properties optimization of high-entropy alloys. *JOM* (2012). doi:10.1007/s11837-012-0366-5
8. No Title. *Oxford Instruments* at <<http://ebbsd.com/ebbsd-explained/principle-components-of-an-ebbsd-system>>
9. Thermo Fisher Scientific FEI. No Title. at <<https://www.fei.com/>>



10. No Title. *Nano Science Instruments* at  
<<https://www.nanoscience.com/products/nanoindenters/>>
11. Briot, N. Nanomechanical and scaling behavior of nanoporous gold. (2015).
12. Cantor, B., Chang, I. T. H., Knight, P. & Vincent, A. J. B. Microstructural development in equiatomic multicomponent alloys. *Mater. Sci. Eng. A* **375**, 213–218 (2004).
13. Sonkusare, R. *et al.* Phase equilibria in equiatomic CoCuFeMnNi high entropy alloy. *Mater. Chem. Phys.* **210**, 269–278 (2018).
14. He, F. *et al.* Phase separation of metastable CoCrFeNi high entropy alloy at intermediate temperatures. *Scr. Mater.* **126**, 15–19 (2017).
15. Singh, S., Wanderka, N., Murty, B. S., Glatzel, U. & Banhart, J. Decomposition in multi-component AlCoCrCuFeNi high-entropy alloy. *Acta Mater.* **59**, 182–190 (2011).
16. Manzoni, A., Daoud, H., Völkl, R., Glatzel, U. & Wanderka, N. Phase separation in equiatomic AlCoCrFeNi high-entropy alloy. *Ultramicroscopy* **132**, 212–215 (2013).
17. Miracle, D. B. & Senkov, O. N. A critical review of high entropy alloys and related concepts. *Acta Mater.* **122**, 448–511 (2016).
18. Senkov, O. N., Wilks, G. B., Miracle, D. B., Chuang, C. P. & Liaw, P. K. Refractory high-entropy alloys. *Intermetallics* **18**, 1758–1765 (2010).
19. Lilensten, L., Curie, M. & Bourgon, J. New structure in refractory high-entropy alloys. *Mater. Lett.* **132**, 123–125 (2014).
20. Soni, V. *et al.* Phase stability as a function of temperature in a refractory high-

- entropy alloy. *J. Mater. Res.* 1–12 (2018). doi:10.1557/jmr.2018.223
21. Senkov, O., Isheim, D., Seidman, D. & Pilchak, A. Development of a Refractory High Entropy Superalloy. *Entropy* **18**, 102 (2016).
  22. Ye, Y. F., Wang, Q., Lu, J., Liu, C. T. & Yang, Y. High-entropy alloy: challenges and prospects. *Mater. Today* (2015). doi:10.1016/j.mattod.2015.11.026
  23. Thurston, K. V. S. *et al.* Effect of temperature on the fatigue-crack growth behavior of the high-entropy alloy CrMnFeCoNi. *Intermetallics* **88**, 65–72 (2017).
  24. Gludovatz, B., George, E. P. & Ritchie, R. O. Processing, Microstructure and Mechanical Properties of the CrMnFeCoNi High-Entropy Alloy. *JOM* **67**, 2262–2270 (2015).
  25. Youssef, K. M. *et al.* A Novel Low-Density , High-Hardness , High- entropy Alloy with Close-packed Single-phase Nanocrystalline Structures. **3831**, (2015).
  26. Murty, B. S., Yeh, J. W. & Ranganathan, S. *Intermetallics, Interstitial Compounds and Metallic Glasses in High-Entropy Alloys. High Entropy Alloy.* 119–131 (2014). doi:10.1016/B978-0-12-800251-3.00007-9
  27. Pickering, E. J., Muñoz-Moreno, R., Stone, H. J. & Jones, N. G. Precipitation in the equiatomic high-entropy alloy CrMnFeCoNi. *Scr. Mater.* **113**, 106–109 (2016).
  28. Ridge, O. & Ridge, O. Temperature dependence of the mechanical properties of equiatomic solid solution alloys with face-centered cubic crystal structures solid

- solution alloys with face-centered cubic crystal structures. *ActaMaterialia*, (2014). doi:10.1016/j.actamat.2014.08.026
29. Otto, F. *et al.* The influences of temperature and microstructure on the tensile properties of a CoCrFeMnNi high-entropy alloy. *Acta Mater.* **61**, 5743–5755 (2013).
  30. Otto, F., Yang, Y., Bei, H. & George, E. P. Relative effects of enthalpy and entropy on the phase stability of equiatomic high-entropy alloys. *Acta Mater.* **61**, 2628–2638 (2013).
  31. Tsai, M.-H. Three Strategies for the Design of Advanced High-Entropy Alloys. *Entropy* **18**, 252 (2016).
  32. Gao, M. C., Zhang, B., Guo, S. M., Qiao, J. W. & Hawk, J. A. High-Entropy Alloys in Hexagonal Close-Packed Structure. *Metall. Mater. Trans. A* doi:10.1007/s11661-015-3091-1
  33. Jablonski, P. D., Licavoli, J. J., Gao, M. C. & Hawk, J. A. Manufacturing of High Entropy Alloys. **67**, 2278–2288 (2015).
  34. Pickering, E. J. & Jones, N. G. founding principles and future prospects High-entropy alloys : a critical assessment of their founding principles and future prospects. **6608**, (2016).
  35. DeHoff, R. T. *Thermodynamics in materials science*. (McGraw-Hill Higher Education, 1993). at <<https://books.google.com/books?id=EZgQAQAAMAAJ>>
  36. Yeh, J. W. No Title. in *Recent progress in high entropy alloys. Presentation at Changsha meeting* (2011).
  37. Tracy, C. L. *et al.* High pressure synthesis of a hexagonal close-packed phase of

- the high-entropy alloy CrMnFeCoNi. *Nat. Commun.* **8**, 15634 (2017).
38. Soler, R. *et al.* Microstructural and mechanical characterization of an equiatomic YGdTbDyHo high entropy alloy with hexagonal close-packed structure. *Acta Mater.* **156**, 86–96 (2018).
  39. Zou, Y., Ma, H. & Spolenak, R. ARTICLE Ultrastrong ductile and stable high-entropy alloys at small scales. *Nat. Commun.* **6**, (2015).
  40. Kozak, R., Sologubenko, A. & Steurer, W. Single-phase high-entropy alloys - An overview. *Zeitschrift für Kristallographie* **230**, 55–68 (2015).
  41. Wu, Z. *et al.* Phase stability, physical properties and strengthening mechanisms of concentrated solid solution alloys. *Current Opinion in Solid State and Materials Science* **21**, (2017).
  42. Troparevsky, M. C., Morris, J. R., Kent, P. R. C., Lupini, A. R. & Stocks, G. M. Criteria for Predicting the Formation of Single-Phase High-Entropy Alloys. doi:10.1103/PhysRevX.5.011041
  43. Rogal, L. *et al.* Computationally-driven engineering of sublattice ordering in a hexagonal AlHfScTiZr high entropy alloy. *Sci. Rep.* **7**, 2209 (2017).
  44. Li, Z., Körmann, F., Grabowski, B., Neugebauer, J. & Raabe, D. Ab initio assisted design of quinary dual-phase high-entropy alloys with transformation-induced plasticity. *Acta Mater.* **136**, 262–270 (2017).
  45. Sharma, A., Singh, R., Liaw, P. K. & Balasubramanian, G. Cuckoo searching optimal composition of multicomponent alloys by molecular simulations. *Scr. Mater.* **130**, 292–296 (2017).
  46. Critical review of analysis and interpretation of nanoindentation test data. **200**,

- 4153–4165 (2006).
47. Laplanche, G., Kostka, A., Horst, O. M., Eggeler, G. & George, E. P. Microstructure evolution and critical stress for twinning in the CrMnFeCoNi high-entropy alloy. *Acta Mater.* **118**, 152–163 (2016).
  48. Okamoto, N. L., Fujimoto, S., Kambara, Y., Kawamura, M. & George, E. P. Size effect , critical resolved shear stress , stacking fault energy , and solid solution strengthening in the CrMnFeCoNi high-entropy alloy. *Nat. Publ. Gr.* 1–10 (2016). doi:10.1038/srep35863
  49. Li, D. *et al.* High-entropy Al<sub>0.3</sub>CoCrFeNi alloy fibers with high tensile strength and ductility at ambient and cryogenic temperatures. *Acta Mater.* **123**, 285–294 (2017).
  50. Fu, X., Schuh, C. A. & Olivetti, E. A. Materials selection considerations for high entropy alloys. *Scr. Mater.* **138**, 145–150 (2017).
  51. Li, Z., Zhao, S., Diao, H., Liaw, P. K. & Meyers, M. A. High-velocity deformation of Al<sub>0.3</sub>CoCrFeNi high-entropy alloy: Remarkable resistance to shear failure. *Sci. Rep.* **7**, 42742 (2017).
  52. Fazakas, É. *et al.* Comparative microstructural and corrosion development of VCrNiCoFeCu equiatomic multicomponent alloy produced by induction melting and spark plasma sintering. *IOP Conf. Ser. Mater. Sci. Eng.* **329**, 012016 (2018).
  53. Csaki, Ioana *et al.* Microstructural Study of the Corrosion Effect on AlCrFeNiMn Multicomponent Alloy Tested in Geothermal Environment. (2017). at <<https://www.onepetro.org/conference-paper/NACE-2017-8916>>

54. Tsai, M.-H. & Yeh, J.-W. High-Entropy Alloys: A Critical Review. *Mater. Res. Lett.* **2**, 107–123 (2014).
55. Glatzel, U. & Wanderka, N. Ultramicroscopy Phase separation in equiatomic AlCoCrFeNi high-entropy alloy. **132**, 212–215 (2013).
56. Li, C. *et al.* Microstructure and mechanical properties of Al<sub>x</sub>Si<sub>0.2</sub>CrFeCoNiCu<sub>1-x</sub> high-entropy alloys. *Mater. Des.* **90**, 601–609 (2016).
57. Sriharitha, R., Murty, B. S. & Kottada, R. S. Alloying, thermal stability and strengthening in spark plasma sintered Al<sub>x</sub>CoCrCuFeNi high entropy alloys. *J. Alloys Compd.* **583**, 419–426 (2014).
58. Kao, Y.-F., Chen, T.-J., Chen, S.-K. & Yeh, J.-W. Microstructure and mechanical property of as-cast, -homogenized, and -deformed Al<sub>x</sub>CoCrFeNi ( $0 \leq x \leq 2$ ) high-entropy alloys. *J. Alloys Compd.* **488**, 57–64 (2009).
59. Reddy, T. S. *et al.* Severe plastic deformation driven nanostructure and phase evolution in a Al<sub>0.5</sub>CoCrFeMnNi dual phase high entropy alloy. *Intermetallics* **91**, 150–157 (2017).
60. Chang, Y.-J. & Yeh, A.-C. The evolution of microstructures and high temperature properties of Al<sub>x</sub>Co<sub>1.5</sub>CrFeNi<sub>1.5</sub>Ti<sub>y</sub> high entropy alloys. *J. Alloys Compd.* **653**, 379–385 (2015).
61. Chen, C., Pang, S., Cheng, Y. & Zhang, T. Microstructure and mechanical properties of Al<sub>20-x</sub>Cr<sub>20+0.5x</sub>Fe<sub>20</sub>Co<sub>20</sub>Ni<sub>20+0.5x</sub> high entropy alloys. *J. Alloys Compd.* **659**, 279–287 (2016).
62. Rao, S. I., Woodward, C., Parthasarathy, T. A. & Senkov, O. Atomistic

- simulations of dislocation behavior in a model FCC multicomponent concentrated solid solution alloy. *Acta Mater.* **134**, 188–194 (2017).
63. Ohring, M. in *Materials Science of Thin Films (Second Edition)* (ed. Ohring, M.) 495–558 (Academic Press, 2002). doi:<https://doi.org/10.1016/B978-012524975-1/50012-4>
  64. Takeuchi, A., Amiya, K., Wada, T., Yubuta, K. & Zhang, W. High-Entropy Alloys with a Hexagonal Close-Packed Structure Designed by Equi-Atomic Alloy Strategy and Binary Phase Diagrams. *JOM* **66**, 1984–1992 (2014).
  65. Stepanov, N. D., Yurchenko, N. Y., Zhrebtsov, S. V., Tikhonovsky, M. A. & Salishchev, G. A. Aging behavior of the HfNbTaTiZr high entropy alloy. *Mater. Lett.* **211**, 87–90 (2018).
  66. Yusenko, K. V. *et al.* First hexagonal close packed high-entropy alloy with outstanding stability under extreme conditions and electrocatalytic activity for methanol oxidation. *Scr. Mater.* **138**, 22–27 (2017).
  67. Swartzentruber, P. D. *et al.* Composition and work function relationship in Os – Ru – W ternary alloys Composition and work function relationship in Os – Ru – W ternary alloys. **021405**, (2017).
  68. Ye, Y. X., Lu, Z. P. & Nieh, T. G. Dislocation nucleation during nanoindentation in a body-centered cubic TiZrHfNb high-entropy alloy. *Scr. Mater.* **130**, 64–68 (2017).
  69. Lilensten, L. *et al.* Design and tensile properties of a bcc Ti-rich high-entropy alloy with transformation-induced plasticity. *Mater. Res. Lett.* **5**, 110–116 (2017).

70. Liu, C. M., Wang, H. M., Zhang, S. Q., Tang, H. B. & Zhang, A. L. Microstructure and oxidation behavior of new refractory high entropy alloys. *J. Alloys Compd.* **583**, 162–169 (2014).



## Vita

### AZIN AKBARI

#### EDUCATION

- 2015-2018 | University of Kentucky, USA | PhD | Materials Science and Engineering
- 2011-2013 | Tampere University of Technology, Finland | MS | Major: Materials Research, Minor: Metallic Materials | Awarded “Graduation with Distinction” award from Industrial Research Fund in Finland
- 2007-2011 | University of Tehran, Iran | BS | Major: Metallurgy and Materials Science Engineering | Awarded Scholarship from Ministry of Science and Technology in Iran

#### EXPERIENCE

- May 2015-Aug 2018 | University of Kentucky, USA | Staff at Electron Microscopy Center
- Aug 2015-May 2016 | University of Kentucky, USA | Teaching Assistant
- Aug 2013-Dec 2015 | Case Western Reserve University, USA | Research Assistant
- May 2013-Aug 2013 | Tampere University of Technology, Finland | Researcher
- July-Sep 2012 | Clausthal University of Technology, Germany | Researcher
- July-Sep 2010 | Turbine Blade Engineering and Manufacturing co., Iran | Intern

#### INTERNATIONAL CONFERENCES

- AADR/CADR 2018, Fort Lauderdale, FL, Oral Presentation: “Hydroxyapatite Crystal Production by Epithelial Keratinocytes in vitro”
- TMS 2018, Phoenix, AR, Oral Presentation: “Screening of Structure and Properties of FCC Thin Film High Entropy Alloys Using Compositional Gradient Samples”
- TMS 2017, San Diego, CA, Poster Presentation : “Development of Non-Equiatomic MnFeCoNiCu High Entropy Alloy with Single-Phase Stability”
- MRS 2016, Boston, MA, Oral Presentation: “Thin Film Combinatorial Approach to Screen Structure, Composition and Properties of High Entropy Alloys” and “High Entropy Alloy Matrix Composite from Equilibrium Solidification”
- TMS 2016, Nashville, TN, Oral Presentation: “Thin Film Approach to Screen Structure and Composition of High Entropy Alloys”
- MS&T 2105, Pittsburgh, PA, Poster Presentation: “Fatigue Crack Propagation of Unfilled PEEK Material”
- TMS 2015, Orlando, FL, Poster Presentation: “Microstructure and Mechanical Properties of high Mg Content Al-Si Alloy”
- MSNO 2014, Cleveland, OH, Poster Presentation: “Compositionally Dependent Structure of Metallic Glasses, Quantified by XAFS”
- ShowCase 2014, Cleveland, OH, Poster Presentation: “Quantitative XAFS Structural analysis of Metallic Glasses”